Methodology for development of smart epoxy coatings incorporated with Ethylenediamine-N, N'-disuccinic ac-id (EDDS) layered double hydroxides (LDHs) for corrosion protection of XC38 carbon steel

Gata Joseph Ayemi

N°d'ordre NNT : **2023ISAL0038**

THESE de DOCTORAT DE L'INSA LYON, Membre de l'Université de Lyon

Ecole Doctorale N° 34
(L'École Doctorale Matériaux de Lyon)

Spécialité/ discipline de doctorat : Science et génie des matériaux

Soutenue publiquement le 03/07/2023, par :
(Gata Joseph AYEMI)

Methodology for development of smart epoxy coatings incorporated with Ethylenediamine-N, N'-disuccinic acid (EDDS) layered double hydroxides (LDHs) for corrosion protection of XC38 carbon steel

Devant le jury composé de :

Nom, prénom	Grade/qualité	Établissement/entreprise	Rôle du membre
MOL Arjan	Professeur des Universités	Delft University of Technology Netherlands	Rapporteur
ZHELUDKEVICH Mikhail	Professeur des Universités	Kiel University Kiel, Germany	Rapporteur
PEBERE Nadine	Directrice de Recherche	Université de Toulouse Toulouse, France	Examinatrice
THERIAS Sandrine	Directrice de Recherche	Institut de Chimie de Clermont-Ferrand, France	Examinatrice
NORMAND Bernard	Professeur des Universités	INSA de Lyon Villeurbanne, France	Directeur de thèse
MARCELIN Sabrina	Ingénieure de recherche	INSA de Lyon, Villeurbanne, France	Co-directrice de thèse

INSTITUT NATIONAL DES SCIENCES APPLIQUÉES LYON

Département de la Formation par la Recherche et des Études Doctorales (**FEDORA**)

Bâtiment INSA direction, 1er étage
37, av. J. Capelle
69621 Villeurbanne Cédex
fedora@insa-lyon.fr

Référence : TH0968_Gata Joseph AYEMI

L'INSA Lyon a mis en place une procédure de contrôle systématique via un outil de détection de similitudes (logiciel Compilatio). Après le dépôt du manuscrit de thèse, celui-ci est analysé par l'outil. Pour tout taux de similarité supérieur à 10%, le manuscrit est vérifié par l'équipe de FEDORA. Il s'agit notamment d'exclure les auto-citations, à condition qu'elles soient correctement référencées avec citation expresse dans le manuscrit.

Par ce document, il est attesté que ce manuscrit, dans la forme communiquée par la personne doctorante à l'INSA Lyon, satisfait aux exigences de l'Etablissement concernant le taux maximal de similitude admissible.

INSA LYON
Campus LyonTech La Doua
20, avenue Albert Einstein - 69621 Villeurbanne cedex - France
Tél. +33 (0)4 72 43 83 83 - Fax +33 (0)4 72 43 85 00
www.insa-lyon.fr

membre de

Département FEDORA – INSA Lyon - Ecoles Doctorales

SIGLE	ECOLEDOCTORALE	NOM ET COORDONNEES DU RESPONSABLE
CHIMIE	**CHIMIE DE LYON** **https://www.edchimie-lyon.fr** Sec. : Renée EL MELHEM Bât. Blaise PASCAL, 3e étage secretariat@edchimie-lyon.fr	**M. Stéphane DANIELE** C2P2-CPE LYON-UMR 5265 Bâtiment F308, BP 2077 43 Boulevard du 11 novembre 1918 69616 Villeurbanne **directeur@edchimie-lyon.fr**
E.E.A.	**ÉLECTRONIQUE, ÉLECTROTECHNIQUE, AUTOMATIQUE** **https://edeea.universite-lyon.fr** Sec. : Stéphanie CAUVIN Bâtiment Direction INSA Lyon Tél : 04.72.43.71.70 secretariat.edeea@insa-lyon.fr	**M. Philippe DELACHARTRE** INSA LYON Laboratoire CREATIS Bâtiment Blaise Pascal, 7 avenue Jean Capelle 69621 Villeurbanne CEDEX Tél : 04.72.43.88.63 **philippe.delachartre@insa-lyon.fr**
E2M2	**ÉVOLUTION, ÉCOSYSTÈME, MICROBIOLOGIE, MODÉLISATION** **http://e2m2.universite-lyon.fr** Sec. : Bénédicte LANZA Bât. Atrium, UCB Lyon 1 Tél : 04.72.44.83.62 secretariat.ediss@univ-lyon1.fr	**Mme Sandrine CHARLES** Université Claude Bernard Lyon 1 UFR Biosciences Bâtiment Mendel 43 Boulevard du 11 novembre 1918 69622 Villeurbanne Cedex **sandrine.charles@univ-lyon1.fr**
EDISS	**INTERDISCIPLINAIRE SCIENCES-SANTÉ** **http://ediss.universite-lyon.fr** Sec. : Bénédicte LANZA Bât. Atrium, UCB Lyon 1 Tél : 04.72.44.83.62 secretariat.ediss@univ-lyon1.fr	**Mme Sylvie RICARD-BLUM** Institut de Chimie et Biochimie Moléculaires et Supramoléculaires (ICBMS) - UMR 5246 CNRS - Université Lyon 1 Bâtiment Raulin - 2ème étage Nord 43 Boulevard du 11 novembre 1918 69622 Villeurbanne Cedex Tél : +33(0)4 72 44 82 32 **sylvie.ricard-blum@univ-lyon1.fr**
INFOMATHS	**INFORMATIQUE ET MATHÉMATIQUES** http://edinfomaths.universite-lyon.fr Sec. : Renée EL MELHEM Bât. Blaise PASCAL, 3e étage Tél : 04.72.43.80.46 infomaths@univ-lyon1.fr	**M. Hamamache KHEDDOUCI** Université Claude Bernard Lyon 1 Bât. Nautibus 43 Boulevard du 11 novembre 1918 69622 Villeurbanne Cedex France Tél : 04.72.44.83.69 **hamamache.kheddouci@univ-lyon1.fr**
Matériaux	**MATÉRIAUX DE LYON** **http://ed34.universite-lyon.fr** Sec. : Yann DE ORDENANA Tél : 04.72.18.62.44 yann.de-ordenana@ec-lyon.fr	**M. Stéphane BENAYOUN** Ecole Centrale de Lyon Laboratoire LTDS 36 avenue Guy de Collongue 69134 Ecully CEDEX **stephane.benayoun@ec-lyon.fr**
MEGA	**MÉCANIQUE, ÉNERGÉTIQUE, GÉNIE CIVIL, ACOUSTIQUE** **http://edmega.universite-lyon.fr** Sec. : Stéphanie CAUVIN Tél : 04.72.43.71.70 Bâtiment Direction INSA Lyon mega@insa-lyon.fr	**M. Jocelyn BONJOUR** INSA Lyon Laboratoire CETHIL Bâtiment Sadi-Carnot 9, rue de la Physique 69621 Villeurbanne CEDEX **jocelyn.bonjour@insa-lyon.fr**
ScSo	**ScSo*** **https://edsciencessociales.universite-lyon.fr** Sec. : Mélina FAVETON INSA : J.Y. TOUSSAINT Tél : 04.78.69.77.79 melina.faveton@univ-lyon2.fr	**M. Bruno MILLY** Université Lumière Lyon 2 86 Rue Pasteur 69365 Lyon CEDEX 07 **bruno.milly@univ-lyon2.fr**

*ScSo : Histoire, Géographie, Aménagement, Urbanisme, Archéologie, Science politique, Sociologie, Anthropologie

Abstract

Layered double hydroxides (LDHs) are interesting candidates as corrosion inhibitor reservoirs for the protection of metals. Indeed, these species present a strong capacity to release the inhibitor contained between their hydroxide lamellae, and based on the principle of anions exchange, they simultaneously allow the capturing of aggressive species such as chloride ion present in the solution. Due to their aforementioned properties, they represent interesting fillers that can be incorporated into epoxy coatings matrix for improvement of barrier properties. The design of an intelligent corrosion inhibition system using this material, could significantly increase the durability and efficiency of the coated system by providing active corrosion protection.

The objective of this thesis is to investigate the effectiveness of the Zn-Al LDH system as a smart reservoir of ethylenediamine-N,N'-disuccinic acid (EDDS). The $[Zn_2Al(OH)_6]^+$ $[EDDS]^{4-}_{0.25}$ $2H_2O$ LDH (Zn_2Al-$EDDS^{4-}$ LDH) is then incorporated into the matrix of epoxy coating for active corrosion protection of XC38 carbon steel in sodium chloride media. The choice of non-toxic and biodegradable EDDS as inhibitor is to replace ethylenediaminetetraacetic acid (EDTA), which is harmful and difficult to biodegrade. In addition, EDDS has the ability to form stable complexes with iron, which is the main component of carbon steel, has a passivation capacity and synergistic effects with other inhibitors. The first part of the results, present a methodology for characterizing the effectiveness of Zn_2Al-$EDDS^{4-}$ LDH essentially based on electrochemical measurements. This part allows to highlight a synergistic effect between the $EDDS^{4-}$ anions and the Zn^{2+} cations constituting the LDH skeleton. The second part of the results is devoted to the characterization of epoxy coatings containing different amount of Zn_2Al-$EDDS^{4-}$ LDH to determine the optimum content needed to achieve better corrosion protection properties. The best candidate coating is then selected for further characterization in terms of water absorption and barrier properties. The study is conducted by using electrochemical techniques, such as current-potential curves, electrochemical impedance spectroscopy (EIS). The impedance data of the coated system obtained from EIS is interpreted in detail using an improved graphical method and power law resistivity distribution profiles along the thickness of the coatings. These results provide a better interpretation and understanding of the presence of LDH in the epoxy matrix on water-uptake.

***Keywords**: Corrosion inhibition, Carbon Steel, Epoxy coating, Layered Double Hydroxides (LDH), Electrochemical impedance spectroscopy (EIS.)*

Résumé

Les hydroxydes doubles stratifiés (LDH) sont des candidats intéressants comme réservoirs d'inhibiteurs de corrosion pour la protection des métaux. En effet, ces espèces présentent une forte capacité à libérer l'inhibiteur contenu entre leurs lamelles d'hydroxyde, et selon le principe de l'échange d'anions, elles permettent simultanément la capture d'espèces agressives telles que l'ion chlorure présent dans la solution. En raison de leurs propriétés susmentionnées, ils représentent des charges intéressantes qui peuvent être incorporées dans la matrice des revêtements époxy pour améliorer les propriétés de barrière. La conception d'un système intelligent d'inhibition de la corrosion utilisant ce matériau, pourrait augmenter de manière significative la durabilité et l'efficacité du système revêtu en fournissant une protection active contre la corrosion.

L'objectif de cette thèse est d'étudier l'efficacité du système LDH Zn-Al comme réservoir intelligent d'acide éthylènediamine-N,N'-disuccinique (EDDS). Les $[Zn_2Al(OH)_6]^+$ $[EDDS]^{4-}{}_{0.25}$ $2H_2O$ HDL (Zn_2Al-$EDDS^{4-}$ HDL) sont ensuite incorporés dans la matrice d'un revêtement époxy pour une protection active contre la corrosion de l'acier au carbone XC38 en milieu chlorure de sodium. L'EDDS est une molécule non toxique et biodégradable est intéressante à utiliser comme inhibiteur pour remplacer l'acide éthylènediaminetétraacétique (EDTA), qui est nocif et non respectueux de l'environnement. De plus, l'$EDDS^{4-}$ a la capacité de former des complexes stables avec les ions métalliques du fer, qui est le principal composant de l'acier au carbone pour apporter une protection du substrat et peu interagir en synergie avec d'autres inhibiteurs de corrosion. La première partie des résultats, présente une méthodologie de caractérisation de l'efficacité du Zn_2Al-$EDDS^{4-}$ HDL essentiellement basée sur des mesures électrochimiques. Cette partie permet de mettre en évidence un effet synergique entre les anions $EDDS^{4-}$ et les cations Zn^{2+} constituant le squelette du LDH. La deuxième partie des résultats est consacrée à la caractérisation de revêtements époxy contenant différentes quantités de Zn_2Al-$EDDS^{4-}$ HDL afin de déterminer la teneur optimale nécessaire pour obtenir de meilleures propriétés de protection contre la corrosion. Le meilleur revêtement candidat est ensuite sélectionné pour une caractérisation plus poussée en termes d'absorption d'eau et de propriétés barrière. L'étude est menée en utilisant des techniques électrochimiques, telles que le tracé des courbes courant-potentiel, la spectroscopie d'impédance électrochimique (SIE). Les données d'impédance du système revêtu obtenues par SIE sont interprétées en détail à l'aide d'une méthode graphique améliorée et par l'utilisation du modèle en loi de puissance qui permet d'obtenir des profils de résistivité dans l'épaisseur des revêtements. Ces résultats permettent une meilleure compréhension des différentes prises en eau lorsque le revêtement des HDL que lorsqu'il n'en contient pas.

Mots-clés : Inhibition de la corrosion, acier au carbone, revêtement époxy, hydroxydes doubles stratifiés (LDH), spectroscopie d'impédance électrochimique (SIE).

Acknowledgements

First of all, I would like to give thanks to the Almighty God, the giver of life, wisdom and understanding and for seeing me throughout the PhD programme alive and healthy.

Many thanks to my thesis supervisor, Professor Bernard Normand and co-thesis supervisor, Dr. Sabrina Marcelin who, in collaboration with Institut de Chimie de Clermont-Ferrand (ICCF), structured the project for this research. They dedicated their time and energy tirelessly so shape my scientific skills. Thank you for taking your time diligently to proof read my manuscripts, the entire thesis and making concrete comments and suggestions. I am indeed grateful for all your inputs in life and God bless you for making me a better researcher.

I would also like to thank Dr. Sandrine Therias, Professor Fabrice Leroux and from ICCF for their great collaboration in this PhD work. Thanks to Dr. Camille Blivet who devoted her time to produce most of the coated samples used in this research.

I would like to mention the following wonderful people and/or friends I met in the laboratory, Dr. Quentin Lemarie, Dr. Ying Hou, Dr. Dwaipayan Mallick, Dr. Elizaveta Lapushkina, Dr. Yu Shi, Dr. Chloé Comas, Dr. Zhiheng Zhang, Dr. Kathleen Jaffre, Dr. Jung-Eun Lee, Dr. Hugo Klinklin, Dr. Jonathan Quibel, Mr. Yohan Douest, Mr. Romain Haeffele, Dr. Liliana Zarazua Villalobos, Dr. Kevin Perrin, Dr. Gabriella Aristia and Mr. Zhixin Dong. I am grateful to some of you who contributed in helping me in one way or the other, it was nice time been among you. For all other members of CorrIS team, Thank you.

I would like to specially thank my beloved parents, Mr. and Mrs. Joseph Gbedanya, my lovely family Ruth Kali Bulus Ayemi (Wife), Divinefavour Eliana Ayemi (Daughter), and David Shekwonugaza Ayemi Bernard (Son) who have stood prayerfully with me for the success of this research, I love you all.

Thanks to Petroleum Technology Development Fund (PTDF) Nigeria for the 4 years sponsorship of this research. Thanks again to my thesis director, Professor Bernard Normand for the additional extension of the financial support. I have faith that, the time and resources invested in this research will bear fruits.

God bless you All,

Gata Joseph AYEMI.

Table of Contents

Introduction

Carbon steels are the most preferred construction and structural materials globally across many industries. This is due to their excellent mechanical properties, high availability, low cost and economy compared with other corrosion-resistant alloys [1]. However, carbon steels are generally prone to corrosion and therefore need high level of corrosion protection for their cost-effective and safe operations [1,2].

All-natural processes tend to return to their lowest energy states. Similarly, finished metallic products such as iron and steel possess the natural ability to return to their original lowest possible energy state when they are in contact with aqueous environment [3]. Corrosion is known to be an unavoidable phenomenon and a major treat to most industries and human's life around the world as it can lead to sudden failure and/or damage of structures [2,4]. Its negative impact on the economic and GDP of industrialized countries is huge. The annual global cost of corrosion is estimated to be about 3-4% of the Global Domestic Product (GDP) in developed and industrialized countries which amount to 2.5 trillion US dollar [5,6]. As long as metals are always in contact with aggressive environment during service, their corrosion is inevitable. Therefore, corrosion protection of metallic structures while in service cannot be overemphasized. The high cost of corrosion which affects the investment products of many industries and nations, call for improved corrosion protection counter measures. The environmental hazards and health risks associated to corrosion failures especially in the oil and gas sector has also driven the need for the development of improved corrosion resistant materials [7]. In order to extend the service-life of a material and/or prevent its failure while in service, an efficient anti-corrosion strategy is required [8]. Passive and/or active methods are been currently employed for corrosion protection of carbon steel [9,10].

Organic coatings, inhibitors, and cathodic protection among others methods have been employed for corrosion protection of carbon steel [2,11,12]. Organic coatings are chosen for their barrier effect to protect the metallic substrate from corrosive environment. Epoxy resins are most widely used in a variety of applications which include aerospace, oil and gas, marine, electronic packing, food and can industries due to their excellent anti-corrosive properties, excellent mechanical properties, low shrinkage, good adhesion, excellent solvent and chemical resistance, high dimensional and thermal stabilities [13,14]. However, despite the above-mentioned remarkable properties, organic coatings are generally prone to water uptake and their

protection is considered as passive [15,16]. Furthermore, organic coatings may encounter intrinsic defects such as free volume, porosities, cavities during deposition on the substrate or mechanical/physical damage while in service [17]. As a consequence, aggressive species such as water, oxygen and chloride ions take advantage of these defects and diffuse through the polymer intermolecular network thereby causing dipolar relaxation and de-bonding of the polymer, reaching the coating/metal interface to initiate corrosion and subsequently causing coating barrier failure [18].

To overcome these limitations, inhibitors are introduced into the polymer matrix to obtain smart-coatings which possess self-healing properties [9,19,20]. Corrosion inhibitor can be added into coatings formulation at either primer or pretreatment stage of preparation. However, it cannot be added directly as the inhibitor could interact with the polymer and also to avoid quick leaching out, therefore, a reservoir containing the inhibitor could be used instead of direct addition. Special attention must be paid to the compatibility between the inhibitors and the organic matrix to ensure the protective character of the new protection system. The solubility of the inhibitive species is very important to optimize inhibition efficiency. High solubility will result in short-time protection as the inhibitor will leach out quickly from its reservoir and could cause osmotic pressure leading to blistering and delamination of coating from the substrate while low solubility might result to inadequate of active inhibitive species and then poor inhibition of the substrate. Therefore, an optimum solubility of the inhibitor is required to maximized the inhibition efficiency [21]. More importantly, the interaction of the inhibitor with the environment must be considered to avoid environmental hazards. There is a greater demand to develop green or smart inhibition system to effectively protect metals from corrosion.

A recent strategy widely used to develop smart-coating is by incorporating a “guest host” assembly as a corrosion inhibitor reservoir with an ability to respond to certain external stimuli such as changes in local pH, temperature, and aqueous environment [22–27]. The corrosion reservoir should have the potential to accommodate proper amount of an inhibitive compound, controlled or on-demand release of the inhibitive species and simultaneous capturing of the harmful corrosive species [28]. Examples of corrosion reservoirs that have been incorporated into epoxy coatings to protect carbon steel from corrosion are hydrotalcites, layered double hydroxides (LDHs), polymeric capsules, halloysite, etc [9,12,29–31]. LDHs among others have recently show a more promising potential for the development of anticorrosive performance coated systems due to their anion-exchange ability, self-healing and barrier effect mechanisms

[6,21,26,32–34]. Organic inhibitors such as Ethylenediaminetetraacetic (EDTA) [35,36], Benzothiazolylthio-succinic acid (BTSA) [37–39], benzotriazole (BTA) [40–42], 8-hydroxyquinoline (8HQ) [43], Indole-3 butyric acid (IBA) [44] intercalated into LDHs have been studied for carbon steel corrosion protection. The inhibitor-loaded layered doubled hydroxide is an on-demand release system with the aim of delivering an inhibitive specie to a targeted corrosion sites of the metallic substrate when exposed to electrolyte. As water, oxygen and chloride ions diffused through micropores towards the metal/coating interface, the change in the pH of the surrounding environment trigger the release of inhibitor out of the LDH interlayer galleries. The inhibitive species released adsorb on the substrate to form a protective barrier (chelate) or oxide film which could block either of the anodic or cathodic or both reactions thereby protect the substrate from corrosion. The formed chelate could also provide self-healing to the coating at the damage site [28,32]. Moreover, the homogenous dispersion of functionalized LDH particles into organic coating matrix could cause labyrinth effect which increases the tortuosity of the coating network thereby decreases the diffusion pathways and then limits or delays the diffusion of water and/or arrival of the aggressive species at the coating/substrate interface [33,45]. The releasing of inhibitive species from LDHs is accompanied by a simultaneous capturing of chloride ions from electrolyte environment. Therefore, LDHs play a double inhibition role as a reservoir for corrosion inhibitor and also as a trap for aggressive species [38].

The main goal of this present work is to develop and characterize smart epoxy coatings using Ethylenediamine-N,N'-disuccinic acid (EDDS) intercalated Zn-Al LDHs for protection of XC38 carbon steel from corrosion. The beneficial effects of EDDS, including its environmentally friendly nature, complexation with metal ions, passivation capabilities, synergistic effects with other inhibitors, and high-temperature stability make it a promising choice as a corrosion inhibitor for carbon steel. Zn-Al cations combination were chosen due the easy synthesis, specialty with this type of hybrids LDH, their inherent corrosion resistance properties, couple with the fact that Zn^{2+} cation has an inhibition influence on cathodic process, hence, it partial release could be an added advantage in the corrosion inhibition process [46]. In this study, the following aspects are considered: *(i)* the inhibition effect of Zn_2Al-$EDDS^{4-}$ LDH and *(ii)* the barrier and self-healing of epoxy coating with and without Zn_2Al-$EDDS^{4-}$ LDH. To achieve these goals, we first synthesized and characterized intrinsic properties of EDDS-intercalated Zn_2Al LDH by studying the role of additive elements such as EDDS, Zn^{2+} and Al^{3+} alone or combine, in a chloride environment. This was to establish the inhibitive role of the parent Zn_2Al-$EDDS^{4-}$ LDH

and synergistic effect between its components. To validate the concept of inhibition, the functionalized LDH was then incorporated into an epoxy matrix to investigate the barrier and inhibitive effect of LDH by monitoring the water uptake of the coating and corrosion process. This work illustrates a methodology for the development of smart coatings for corrosion and surface engineering application.

This work was financially supported by the Petroleum Technology Development Fund (PTDF) Nigeria. It was also the opportunity for a fruitful collaboration between the Clermont Ferrand Institute of Chemistry, represented by Sandrine Therias of the Polymer, Photochemistry, Properties and Interfaces team, and Fabrice Leroux of the Layered Double Hydroxide team.

Structure of thesis contents

The document is articulated in a classical way which include a bibliographic chapter, then a chapter dedicated to the experimental methods and finally, two chapters of results. These last two chapters are largely inspired by articles published (chapter 3) and submitted (chapter 4) in international journals.

The chapter 1, discussed bibliographical review of layered double hydroxides (LDHs), their role as corrosion inhibitor reservoirs and, their corrosion protection mechanisms and applications in a coated system.

The chapter 2 is dedicated to the presentation of the adopted methodologies and techniques used for the whole work, with specific techniques or methodologies for each of the chapters 3 and 4 being presented in their respective chapter.

The chapter 3, discusses in details the characterization of EDDS (corrosion inhibitor) intercalated into LDH (reservoir). The electrochemical behavior of the carbon steel in a sodium chloride electrolyte containing the hybrid Zn_2Al-$EDDS^{4-}$ LDH is addressed. To further understand the inhibition mechanism, offer by this type of hybrid material, the electrochemical results obtained for each element (Zn^{2+}, or Al^{3+}, or $EDDS^{4-}$) alone or in combination in the aqueous electrolyte are discussed.

The chapter 4 is dedicated to the characterization of barrier properties and active protection functionalities of epoxy coatings incorporated with Zn_2Al-$EDDS^{4-}$ LDH for corrosion protection of XC38 carbon steel. The EIS measurements coupled with microscopic observations allowed the selection of the best candidate coating. The barrier properties evolutions correlated to the water-uptake are properly addressed in this chapter.

All these chapters are supported by an introduction and a conclusion/perspective.

Chapter 1 Bibliographical review

1.1 Introduction to layered double hydroxides (LDHs)

Layered double hydroxides, named also hydrotalcite or anionic clay materials are hydrate lamellar structures. They are composed of positively-charged hydroxide layers of mixed metals cations, with negatively-charged exchangeable anions and water molecules present within their interlayer gallery spacing. Due to their unique characteristics such as anion-exchange potential, barrier resistance and structure memory effect, their application cut across many disciplines including corrosion and surface engineering [32]. In the recent years, they have been widely developed and used in the field of corrosion science based on the afore mentioned characteristics. They have a general formula as thus $\left[M^{2+}_{(1-x)}M^{3+}_{x}(OH)_2\right]^{+}\left[A_{x/n}\right]^{n-}.yH_2O$, where M^{2+} and M^{3+} are the divalent (Zn^{2+}, Mg^{2+}, Ca^{2+}, Ni^{2+}, Fe^{2+}, Co^{2+}, Cd^{2+} etc.) and trivalent (Al^{3+}, Cr^{3+}, Fe^{3+}, Co^{3+} etc.) metal cations respectively, A^{n-} is the exchangeable charge-balancing anion with a valence of n, which is located between the interlayer spacing, x is the ratio of $[M^{3+}]/([M^{3+}]+[M^{2+}])$ which is usually between $0.25 \leq x \leq 0.33$ range and y is number of water molecule [47]. Couple of scientific journals on this subject have been published in corrosion science for corrosion protection of carbon steel [12,13,38,39,43,44].

1.2 Structure and bonding of LDHs

The structure of LDHs is similar to that of brucite, $Mg(OH)_2$, because of their layered sheet-like structural morphology. A unit cell of both brucite and LDHs have an octahedral symmetrical structure in which the metallic cation (M^{2+} or M^{3+}) located at the central of the unit cell is ionically bonded to six hydroxides group [48]. Each hydroxide groups are located perpendicular to the plane of the unit cell that are stacked on top of each other forming a three-dimensional layer structure[49]. These linked octahedral units formed a positively-charged hydroxide layers due to partial substitution of divalent (M^{2+}) cations by trivalent (M^{3+}) cations. The positively-charged hydroxide layers can be charge-balanced by "guest" anions to obtained a neutral LDHs. It has also been reported that the compensation of the positive charge by anions has resonance effect characteristics [41,42,50]. The typical structure of LDHs is shown in Figure 1.1. The charge density of the positive-charged layers is directly proportional to M^{3+} / (M^{2+} + M^{3+}) ratio. The higher the charge density of the hydroxide layers, the more anions that can be accommodated within the interlayer spacing [39] which is beneficial for entrapment of chloride anions.

The electrostatic bond does not exist between the intercalated anion and mixed-cations, however, there exist hydrogen bond between the anions and the hydroxides layers. The larger the ionic radius of the metals, the more the octahedral structure of the LDH will be compressed.

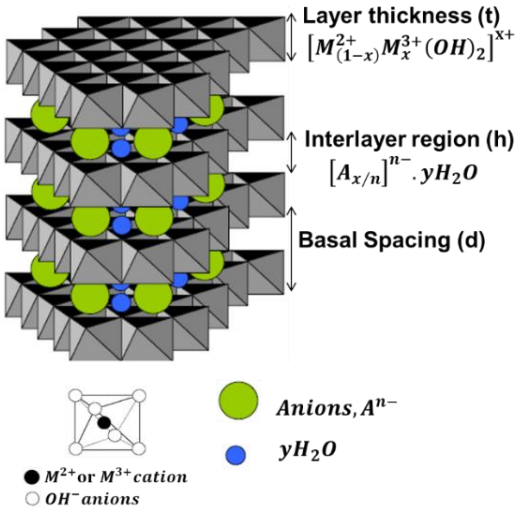

Figure 1.1: The typical structure of LDHs [48,49]

The increasing in stacking, lowers the hydroxide layer thickness and increases the ionic distance between the metallic cations. LDHs commonly exhibit two major sequence; hexagonal or rhombohedral stacking sequence. It is possible to have both sequence in the similar material at different proportion [28]. LDHs have wide range of cation combinations which includes monovalent-trivalent combination [51], divalent-trivalent combination, and divalent-tetravalent combination but the most commonly synthesized LDHs are the divalent-trivalent LDH. Binary LDHs have been widely reported. However, ternary LDHs which consist in three different metal cations such as ZnMgAl, ZnAlCu, ZnAlCe, MgAlCe, ZnLaAl, MgFeAl, NiCoRu FeCoNi for example, are recently developed [52,53]. The ionic radius of the third metal cation determines the possibility of obtaining a ternary LDH [53].

1.3 Thermodynamic Stability of LDHs

Three methods are employed to establish the thermodynamic stability of LDHs.

(i) Solubility product

LDHs are usually synthesized by alkali coprecipitation from mixed-metals (M^{2+} + M^{3+}) salts solution. The solubility products of LDHs was related to their thermodynamic stability and

reported that; the lower the solubility product, the greater thermodynamic stability of the LDH [54,55].

(ii) Enthalpy of formation Measurement

This is a direct method which involves the calorimetric enthalpy of formation measurement. It was adopted by Navrotsky and coworkers [55,56].

(iii) Electronic structure

An electronic structure method can be employed to determine the thermodynamic stability of LDH by considering the following factors: (a) The octahedral crystal field stabilization energies of the metal ions (b) The coordination mode of the interlayer's anions [55].

1.4 Mechanism of LDHs formation

Discussions on how LDHs are formed during their synthesis have been reported. However, the ion-substitution theory and dissociation-deposition-diffusion are the two main mechanisms of LDHs formation discussed in the literature [32].

1.4.1 Ion substitution theory

The ion substitution theory has two types of hypotheses[32]:

The first hypothesis said that during the synthesis of LDH, hydroxides of divalent metals are formed first as the LDH precursor such as $Mg(OH)_2$ where the divalent cation ($M^{2+)}$ is replaced by trivalent cation (M^{3+}).

The second hypothesis said, it is hydroxides of M^{3+} that are formed first as the LDH precursor such as $Al(OH)_3$ where the trivalent cation (M^{3+}) is replaced by divalent cation (M^{2+})

Based on the first hypothesis, LDHs were synthesized by reacting $Zn(OH)_2$ as the precursor with $Al(NO_3)_3$ or $Cr(NO_3)_3$ where Al^{3+} or Cr^{3+} cations react with $Zn(OH)_2$ and successfully replaced Zn^{2+} cation in the octahedral sheet to obtain ZnAl-LDH and ZnCr-LDH phases [57]. The second hypothesis of ion substitution theory is usually more accepted. The growth behavior of nitrate intercalated Zn-Al LDH film was studied by electrochemical quartz crystal microbalance (EQCM) and open circuit potential (OCP). The results show four stages of growth processes which include Al substrate dissolution, $Al(OH)_3$ formation, ZnAl-NO_3 LDH nucleation and the growth as shown below.

$$Al_2O_3 + 3H_2O + 2OH^- \rightarrow 2Al(OH)_4^- \quad \text{(eq. 1.1)}$$

$$Al \rightarrow Al^{3+} + 3e^- \quad \text{(eq. 1.2)}$$

$$O_2 + 2H_2O + 4e^- \rightarrow 4OH^- \quad \text{(eq. 1.3)}$$

$Al_2O_3 + 3H_2O \rightarrow 2Al(OH)_3$ (eq. 1.4)

$Zn^{2+} + OH^- \rightarrow Zn(OH)^+$ (eq. 1.5)

$Al(OH)_3 + 2Zn(OH)^+ + OH^- + NO_3^- \rightarrow ZnAl\text{-}NO_3$ LDH (eq. 1.6)

It was assumed that Zn^{2+} from $Zn(OH)^+$ replaces Al^{3+} position in $Al(OH)_3$ to form Zn-Al LDH while the nitrate anion migrates into interlayer gallery space to balance the charge. The phase transformations of $Al(OH)_3$ into LDH in the four stages was based on the XPS, XRD and SEM detailed analysis of data. These results suggested that, $Al(OH)_3$ could be considered as the ZnAl-LDH precursor [58]. Although it had been reported by XRD and XPS analyst that, the replacement of both divalent ion (Mg^{2+}) from $Mg(OH)_2$ by trivalent ion ($Al^{3+)}$ and Al^{3+} ion from $Al(OH)_3$ by Mg^{2+} co-existed [59]. However, it was still yet unclear how the ion substitution occurs.

1.4.2 Dissociation/deposition/diffusion mechanism

This mechanism is reported to follow two possible pathways. MgAl LDH was synthesis in both neutral and basic solution. Based on the results, a general dissociation−deposition−diffusion mechanism was proposed to explained the LDH formation. For nearly neutral solution, $Mg(OH)_2$ from MgO hydration was reported to have dissociated into Mg^{2+} and OH^- ions, and then deposited on $Al(OH)_3/Al_2O_3$ surface to form the pre-LDH phase. On the other hand, ionization of $Al(OH)_3$ in the basic solution produced $Al(OH)_4^-$ ions which deposit on $Mg(OH)_2$ surface to form pre-LDH phase. The bilateral diffusion of metal ions in the crystal resulted in the formation of uniform and well-crystallized LDHs [60]. Other researchers reported the chemical dissociation-deposition-diffusion mechanism with $Al(OH)_4^-$ and $Zn(OH)^+$ species considered as the main building blocks of ZnAl-LDH formation mechanism [61–63].

The LDH formation in the aqueous solution is influenced by factors such as temperature, solution pH and concentration, alkali source etc., which makes the processes more complicated [60,61] . More research is needed to understand the mechanism behind LDH formation.

1.5 LDHs as corrosion inhibitors reservoir

LDHs themselves are not corrosion inhibitors but reservoir for corrosion inhibitor. Due to their charged balanced structure and/or anion-exchanged potentials, they possess the ability to accommodate wide variety of “guest” anions ranging from inorganic anions to organic anions. It is for these reasons that LDHs are widely employed as reservoirs of different inhibitive anions

for corrosion protection. Studies have shown that LDHs have strong affinity for carbonate anions, that is, carbonate anions are easily intercalated but very hard to be exchange by other anions from the LDHs gallery. While, Nitrates and halides ions are not only easily intercalated but also exchange easily [64]. Therefore, LDHs loaded with nitrates are usually used as precursor for the synthesis of LDHs intercalated with more complex anions through ion-exchange reactions. On the other hand, carbonate loaded LDHs could be use as blank LDH for reference purposes. The ease of intercalation of the anion into the interlayer spacing of the LDH have been reported to follow the following sequence $OH^- > F^- > Cl^- > Br^- > NO_3^- > I^-$ for the monovalent anions and $CO_3^{2-} > MoO_4^{2-} > SO_4^{2-}$ for the divalent anions. The affinity of these anions to LDHs depend on the charge density and ionic radius of the anions. The affinity order of these anions is reported as $I^- < NO_3^- < Br^- < Cl^- < HPO_4^{2-} < F^- < OH^- < SO_4^{2-} < C_{10}H_4N_2O_8S^{2-} < CO_3^{2-}$. This implies that, anions on the left of the sequence are easily replace by anions on the right in the interlayer structure of LDH but not vice versa [65]. Therefore, it is required that, an anion is less stable than Cl^- ion for a successful anion-exchange in a chloride environment [66]. Factors such as nature of hydroxide layers, type of divalent (M^{2+}) cations, anions charges, pH, concentration, temperature etc. usually influence the equilibrium dynamic of the anion-exchange mechanism of LDHs.

1.6 Nature of layered hydroxides and divalent metallic cations

The nature of hydroxides layers and the type divalent metallic cations (M^{2+}) could influence the releasing of anions from LDHs which could be beneficial in corrosion protection. Chen *et al.*, studied the chloride binding capacity of Mg-Al, Ca-Al, Zn-Al LDHs intercalated with nitrate anions. Their results reveal that, Zn-Al LDH exhibited the highest chloride entrapment capacity attributed to its largest interlayers basal spacing compared to other LDHs. The chloride entrapment capacity was reported to increase with decease in M^{2+}/M^{3+} cationic ratio which ranges from 2 to 4. Zn-Al LDHs have been reported to have high anion-exchange potential which make it an effective chloride adsorbents [67]. Zheludkevich *et al*. studied divanadate anions as a corrosion inhibitor intercalated into hydroxides layers of Zn-Al and Mg-Al and reported that, coatings incorporated with divanadate intercalated Zn-Al LDHs exhibited a superior corrosion protection of aluminum alloy substrate and a well-defined self-healing effect compared to that of Mg-Al LDHs and chromate-based coatings [68]. Hang *et al*. performed a similar study but with an organic molecule of 2-benzothiazolythio-succinic acid (BTSA) and using carbon steel as the substrate [39]. The authors explore the inhibition efficiency of BTSA, Zn-Al, Mg-Al, Zn-

Al-BTSA, and Mg-Al-BTSA and the found that: The BTSA release into the three different electrolytes solution (ethanol/water, 3 wt.% NaCl, and 3 wt.% Na_2SO_4) from Mg-Al-BSTA LDHs and Zn-Al-BTSA LDHs was (81.3%, 61.2%, 19.7%) and (60.6%, 55.0%, 17.3%) respectively. The BTSA released from Mg-Al-BTSA LDHs was higher than that from Zn-Al-BTSA LDHs irrespective of the electrolytes used. This was attributed to higher electrostatic interactions between positively charged hydroxide layers of Zn-Al and BTSA anions compared to that in Mg-Al-BTSA LDHs. The releasing of BTSA which was based on anion-exchange, involves the breaking-up of the electrostatic bonds between the positively charge hydroxides layers and the outgoing (BTSA) anions, and the reformation of these bonds with the incoming (Cl^- or SO_4^{2-}) anions [69]. The polarization curves obtained of a bare carbon steel after 2 h immersion in 0.1 M of NaCl containing 1mM BTSA or 3 g/l (Mg-Al, Zn-Al, Mg-Al, Zn-Al-BTSA, Mg-Al-BTSA) LDHs revealed a shift in the corrosion potential toward a more positive values with a decrease in anodic current densities when compared with the curve obtained without inhibitor. The corrosion potentials for Mg-Al and Zn-Al were less positive, similar and very close to that of Mg-Al-BTSA while that of BTSA and Zn-Al-BTSA were similar and more positive. However, the anodic current densities: in the presence of BTSA was lower than that obtained for Mg-Al, Zn-Al, Mg-Al, Zn-Al-BTSA, and Mg-Al-BTSA, in the presence of Zn-Al-BTSA or Mg-Al-BTSA were very close but lower than that obtained for Zn-Al or Mg-Al. The shift in the corrosion potential to nobler values with a decrease in anodic current densities suggested anodic inhibition mechanism. The inhibition efficiency calculated from the polarization resistances of a bare carbon steel in the presence and absence of inhibitive species above are presented in Table 1.1.

Table 1.1: Polarization resistance and inhibition efficiency obtained for carbon steel substrate after 2 h of immersion in 0.1 M NaCl solution (without inhibitor), with 1 mM BTSA concentration and with 3 g/l LDHs concentration [70].

Sample	R_p (Ω cm^2)	E (%)
Without inhibitor	200	–
BTSA	4850	96
MgAl-LDH	430	53
ZnAl-LDH	800	75
MgAl(BTSA)-LDH	1600	88
ZnAl(BTSA)-LDH	6600	97

Although the release of BTSA from Mg-Al-BTSA LDHs was higher than that of Zn-Al-BTSA LDHs, the inhibition performance of Zn-Al-BTSA was higher than that of Mg-Al-BTSA. This

could be attributed to the influence of hydroxides layers nature and probably suggest the beneficial effect of Zn^{2+} cation in the corrosion protection of carbon steel.

Hang *et al* also investigate the inhibition efficiency of BTSA intercalated Mg-Al LDHs, and Mg-Al-BTSA incorporated into epoxy coating for carbon steel corrosion protection. The polarization curves of the bare carbon steel obtained at the corrosion potential after 2 h immersion in 0.1 M NaCl (blank solution) containing 1 g/l, 3 g/l and 5 g/l Mg-Al-LDHs revealed that: *i)* for 1 g/l, the corrosion potential shifted toward a positive value with lower anodic current densities compare to the blank solution, *ii)* for 3 g/l, the corrosion potential shifted further with lowest anodic current densities, *iii)* for 5 g/l, the corrosion potential was more negative with higher anodic current densities compare to 1 g/l and 3 g/l. These results showed that the optimum concentration of Mg-Al-BTSA LDHs was 3 g/l. The graphically determined polarization resistance from the impedance diagrams was found to increase with, increase in concentration of Mg-Al-BTSA from 1 g/l to 3 g/l and the inhibition efficiency was about 90% for 3 g/l. The incorporation of 3 wt.% of Mg-Al-BTSA into epoxy coating gave a high impedance modulus value of about $10^{10}\ \Omega\ cm^2$ at low frequency domain which decreases rapidly after 2 days of immersion to about $10^{9}\ \Omega\ cm^2$ and then remains stable at this value during 35 days of immersion. These could be probably due to the fact that, there was diffusion of electrolyte and chloride ions through the epoxy coating during the 2 days of immersion, however, the releasing of BTSA and the entrapment of chloride ions delayed the corrosion initiation process. On the other hand, the coating without Mg-Al-BTSA LDHs also exhibited high impedance modulus values at low frequency but after 2 days, it decreases continuously with time of immersion to a value of about $10^{8}\ \Omega\ cm^2$ for 35 days. This could be attributed to the diffusion of water and chloride ion through the coating without any hindrances due to the absence of inhibitive species. There results revealed that Mg-Al-BTSA is an anodic inhibitor and its presence in epoxy coating improved the corrosion protection of carbon steel [38].

The study of Zn-Al-BTSA LDHs incorporated into an epoxy coating matrix for corrosion of carbon steel have also been reported [37]. The low frequency impedance modulus which normally corresponds to the reactions occurring at the coating/substrate interface was approximately $10^{9}\ \Omega\ cm^2$, $10^{7}\ \Omega\ cm^2$, and $10^{6}\ \Omega\ cm^2$ for the epoxy coatings containing 3 wt% Zn-Al-BTSA, 3 wt% Zn-Al and 0 wt% LDHs respectively. The low barrier performance of the pure epoxy coating was attributed to the absence of LDHs, the improved barriers in the presence of Zn-Al or Zn-Al-BTSA LDHs was attributed to increase in the tortuosity of water, oxygen and Cl^- diffusion pathways by the dispersed LDHs in the epoxy matrix, and the superior protection offered by Zn-Al-BTSA LDHs was ascribed to a better dispersion of LDHs in the epoxy matrix

due to its modification with BTSA, coupled with releasing of BTSA as corrosion inhibitor of carbon steel and simultaneous entrapment of Cl^- ions. Alibakhshi *et al* studied Zn-Al-NO_3^-, Zn-Al-PO_4^{3-}, Mg-Al-NO_3^-, and Mg-Al-PO_4^{3-} LDHs incorporated into epoxy coating for corrosion protection of mild steel [71,72]. They reported the corrosion inhibition efficiency calculated from the polarization curves of a bare mild steel after 24h of immersion in 3.5 % NaCl containing 1 g of each Zn-Al-NO_3^-, Zn-Al-PO_4^{3-} and Mg-Al-NO_3^-, and Mg-Al-PO_4^{3-} as 68 %, 96 %, 47.3 %, and 57.1 %, respectively. When these LDHs are in epoxy coating, the coating containing Zn-Al-NO_3^- or Zn-Al-PO_4^{3-} demonstrates a better corrosion protection of mild steel with Zn-Al-PO_4^{3-} LDHs coating been superior. Based on the above studies, the nature of the hydroxide layers and the type of divalent metallic cations of LDHs have positive influence in the corrosion protection.

1.7 Corrosion protection mechanisms by LDHs coatings

As mentioned earlier, LDHs themselves are not corrosion inhibitors, but reservoirs of corrosion inhibitor due to their unique chemical structure and characteristics [18,34,38]. They possess some positive effects such as anion-exchange, self-healing, labyrinth/physical barrier, and hydrophobicity which make them attractive and relevant in field of corrosion science and protection [32].

1.7.1 Anion-exchange (chloride entrapment) mechanism

Anion exchange of the LDHs is the ability of the LDHs to donate its interlayer anion to the metallic substrate and then accept the chloride anion from the electrolyte. Their large accessible positively-charged hydroxide surface area allows them to attract negatively charge ions such as chloride from corrosive environment. The chloride trapping occurs in parallel with the inhibitor releasing. These attributes are highly beneficial in corrosion protection. The anion-exchange potential of LDHs material, make them an important subject in corrosion science [42,73,74].
The external part or edges of LDHs is believe to be the first place where the entrapment of chloride ions begins follow by interlayer gallery space. That is, the anions are easily exchange and starts at the edges of LDHs and then the internal interlayer space [75]. The rapid initial exchange of anions at the edges or external part of LDHs is described as the “burst effect”[32]. The proposed anion exchange mechanism is presented in Figure 1.2. During the anion-exchange reaction, anions such as Cl^- from the external corrosive environment are first adsorbed on the LDHs edges and exchange rapidly with the intercalated inhibitive anions at the edges of LDHs.

The exchanged Cl^- anions diffuse gradually into the LDHs interlayer gallery space until an equilibrium is attained. Therefore, the anion-exchange occur basically by entrapment of Cl^- ions into the LDHs and simultaneous releasing of inhibitive ions from the LDHs. This mechanism renders the electrolyte solution less aggressive. An anion-exchange equilibrium could be attained when Cl^- anions fully occupy the interlayers galleries of LDHs and inhibitive anions are completely leach out of the LDHs into the electrolyte solution as shown in Figure 1.2. A dynamic anion exchange equilibrium is reached when both anions entrapped and anion released are equal.

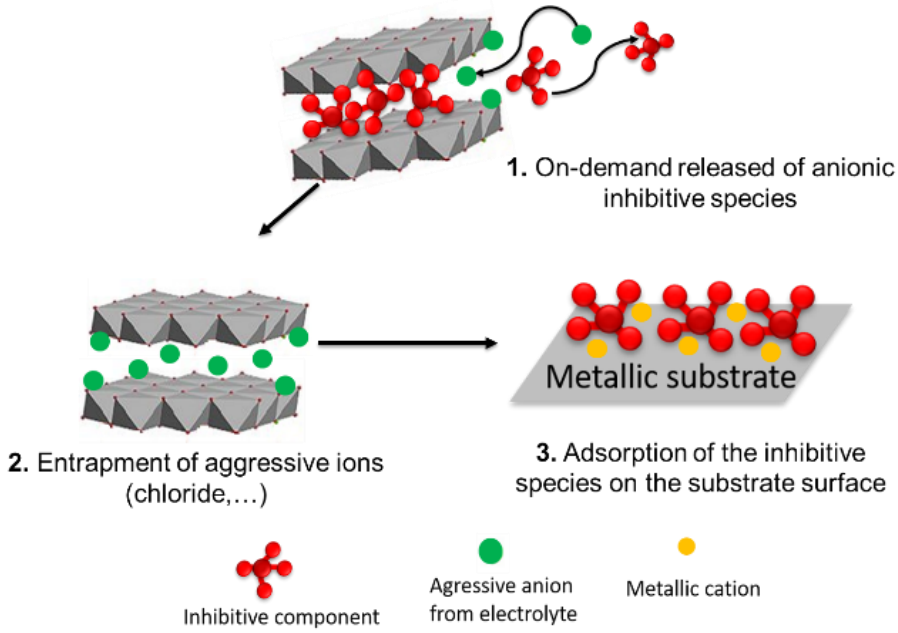

Figure 1.2: Schematic representation of aggressive species entrapment into LDH framework [45].

It was reported that at low Cl^- ions concentration, anion-exchange is the predominant mechanism while at high Cl^- ions concentration, either anion-exchange or adsorption are dominant [32]. Several factors such as charge density, anion size, ions concentration in the electrolyte solution, pH and temperature of the electrolyte solution can influence the anion-exchange mechanism [38,39,65,76]. The increase in the concentration of chloride ions in an electrolyte solution trigger an increase in the amount of inhibitor released from LDHs. That is, the rate of anion-exchange increases as the concentration of NaCl in the electrolyte solution increases. Hang *et al*. confirmed this by studying the BTSA releasing as corrosion inhibitor of carbon steel from Mg-Al-BTSA layered double hydroxide at different concentrations of sodium chloride.

They found that, the releasing of BTSA from LDH depends on the concentration of NaCl in the electrolyte as shown in Figure 1.3 [38].

The amount of inhibitor released from LDH could be influenced by charges of both intercalated anions and aggressive species presences in the corrosive environments. BTSA was found to be released more in 3wt % Na_2SO_4 compare to 3wt % NaCl due to the higher electrostatic interactions between SO_4^{2-} anions and positively charged hydroxide layers. Higher charges anions would prefer to stay in the interlayers of LDH due their strong electrostatic interactions [32,39,64].

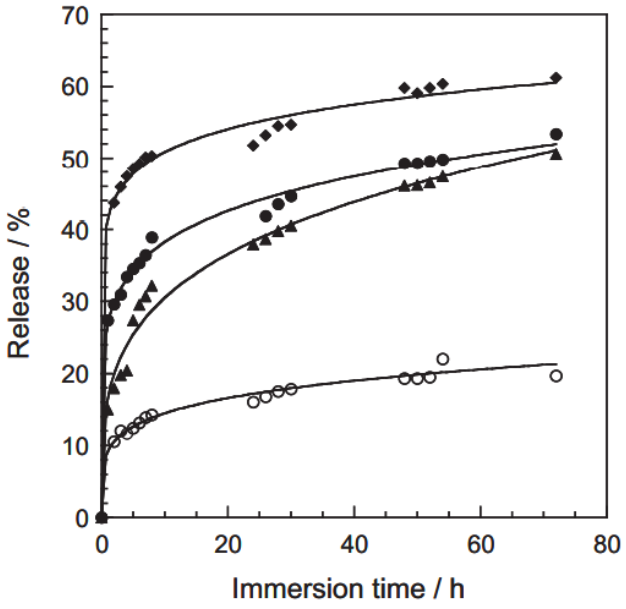

Figure 1.3: Releasing of BTSA from LDH-BTSA in different concentrations of NaCl [38]
(○) 0%; (▲) 0.5%; (●) 1%; (♦) 3%.

The corrosion inhibitor released from modified clay and LDHs have been reported to be favored by higher pH values [44,77]. This could imply that, corrosion process in a neutral media which induces the variation of local interfacial pH could be beneficial in the releasing of inhibitive species from LDHs and confer the self-healing. That is, during corrosion process, the variation of the interfacial local pH could trigger the release of inhibitive species from LDHs. The affinity of OH^- to LDHs scaffold makes pH an influential factor of anion-exchange. The chloride adsorption capacity of LDHs have also been reported to be influenced by pH of the electrolyte [78].

The structure and composition of the LDHs could influence the amount of trapped chloride ions. For example, the larger the interlayer distance, the more chloride binding capacity; the

increase in the divalent to trivalent cation ratio, the less the chloride binding capacity which is attributed to less positive charge and weaker electrostatic interactions [50,67].

The decrease in the aggressiveness of the environment due to the entrapment of chloride ions by LDHs, could mitigate corrosion thereby prolong the service life of the metallic substrate [34,73]. Therefore, LDHs play a double inhibition role, as trap for aggressive species and as a reservoir for corrosion inhibitors [18,33,38]

1.7.2 Self-healing mechanism

Self-healing is the ability of the LDHs coatings to exhibit smart inhibition property against metallic corrosion after damage. It could be due to the inhibitive anions and/or cations releasing from the LDH scaffold. It is interesting to note that, synergistic effect could exist between inhibitors and cations released.

1.7.2.1 Self-healing by inhibitor release from LDHs

LDHs are anion-exchangers and/or reservoirs for corrosion inhibitors. Inhibitor-loaded layered doubled hydroxide is an on-demand releasing system. When they are in contact with aggressive electrolyte, the released inhibitor migrates to the metallic substrate and adsorb to formed chelates with the substrate. These chelates acts as a protective barrier or oxide film which could block either of the anodic or cathodic or both reactions depending on the inhibitor type, thereby protect the substrate from corrosion [18,41]. The presence of the aggressive ions in the electrolyte solution trigger the release of inhibiting anions from the interlayer's gallery of LDH into the electrolyte solution which provide protection and/or self-healing for metallic substrate against corrosion [79]. The anion-exchange reaction by LDHs is an important attribute of LDHs in corrosion protection as its decreases the aggressiveness of the environment and local corrosion rate. The global and local corrosion measurement of inhibitors-loaded LDHs reported in literature is an evident of the self-healing characteristic of LDHs. The corrosion inhibition study of benzoate anion intercalated into Zn-Al LDHs was carried out on Q235 carbon steel immersed in 3.5% NaCl electrolyte solution. The electrochemical impedance spectroscopy (EIS) results revealed improvement in the charge transfer resistance and decrease in the values of the constant phase element parameter Q, of carbon steel due to the control released of benzoate from the LDH gallery and its adsorption on the substrate interface to form a protective film [80]. The decrease in the value of Q, is as a result of decrease in the reactivity at the coating/substrate interface which confers the self-healing effect of LDH. The releasing curves of inhibitive anions

from LDHs usually exhibit an initial rapid increase and then stable plateau [65,71,72]. Surface modification could enhance the releasing of inhibitors from LDHs. Olya *et al* confirmed this by studying the surface decoration of Zn-Al-MoO_4^{2-} LDH with SiO_2. Their study reveals an increase in the releasing ability and inhibition effect of MoO_4^{2-} due to higher loading and controlled releasing of molybdate anions. Therefore surface modification could increase the corrosion inhibitors loading and subsequently increases the releasing ability [81].

1.7.2.2 Self-healing by cations leaching out from LDHs scaffold

When LDH are dispersed into an electrolyte solution, they tend to exhibit partial dissolution to leach out metallic cations into the electrolytes [65]. These cations could play a positive inhibition role along with the released inhibitor or could be beneficial in corrosion protection of the metallic substrate [71,72]. The leaching of Zn^{2+} and Al^{3+} cation have been reported in literature [68]. The leaching of Zn^{2+} from ZnAl-PO_4^{3-} LDH was reported to enhanced corrosion protection performance of silane sol-gel coating which was attributed to synergism between PO_4^{3-} and Zn^{2+} ions [72]. The releasing of Al^{3+} and Zn^{2+} from LDHs was also reported to have significant corrosion inhibition effect on Q235 steel due to the formation of a protective film on the substrate [82]. More research is required on the dissolution of LDHs scaffold and the effect of cations released. The synergistic effect between the released cations and intercalated anions could improve the corrosion protection efficiency.

1.7.3 Labyrinth and physical barrier mechanism

The dispersion of functionalized LDH particles into organic coating matrix could increase the tortuosity of the coating network thereby limit the permeation of water molecules, oxygen and chloride ions. The corrosion protection performance of polymer coating incorporated with Mg-Al LDH/graphene hybrids was reported to significantly improved, compare to the pristine acrylic resin coating. This was attributed to the presence of LDH/graphene which makes the water transport pathways more tortuous (Fig. 1.4) than pristine coating thereby delayed the aggressive species from reaching the coating/substrate interface [45]. LDHs film directly deposited on the substrate could also serve as a physical barrier by preventing the aggressive species contact with the substrate [83].

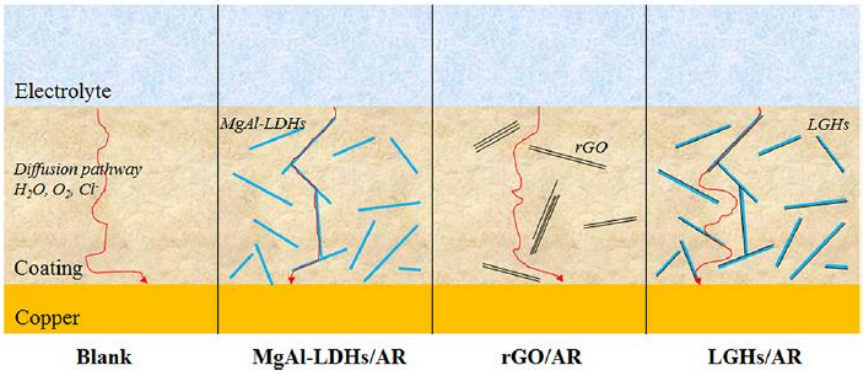

Figure 1.4: Schematic of aggressive species diffusion into the matrix of different coatings [45].

1.7.4 Hydrophobicity mechanism

The intercalated anions could possess hydrophobicity property. This property could be induced into the synthesized LDHs. The water-repellent property and the morphology modification of the intercalated anions increases hydrophobicity which could prevent the diffusion of electrolyte [28,79]. The passive barrier property of the epoxy coatings can be improved by introducing inhibitor loaded LDHs into the epoxy matrix.

The inhibition mechanism of epoxy coating incorporated with inhibitor-loaded LDHs could be summarized as follow:

The presence of inhibitor-loaded LDHs in the epoxy matrix enhanced the passive barrier by increasing the tortuosity of the polymer network thereby delayed the arrival water, oxygen and chloride ion at the coating substrate interface. The releasing of inhibitor out of LDHs scaffold and the entrapment of Cl^- anions into the scaffold based on anion exchange ability of the LDHs, decreases the corrosiveness of the electrolyte.

The self-healing mechanism of epoxy/LDHs coatings is govern by chelates and/or precipitates formation attributed to releasing of inhibitive anions and metallic cations from the LDH scaffold. In our previous study, we observed that the present of Zn^{2+} cations in the electrolyte, protect the carbon steel by the forming some whitish scales-like precipitates (simonkoellite) at the surface. While the presence of EDDS promote complex chelate formation with Fe(II)/Fe(III) [84]. Therefore, precipitation and the chelate formation at the defective sites could healed the coating and stop further corrosion [79] .

1.8 The equilibrium and kinetics study of LDHs for corrosion protection

The isotherms of adsorption are mostly used to study the equilibrium and kinetics of LDHs. The equilibrium isotherms and kinetics of LDHs are usually determined by dispersing a certain amount of LDH into different concentrations of chloride solution.

1.8.1 Equilibrium Study of LDHs

Using equation 1.7, the amount (Q) of chloride uptake by LDH or inhibitor released from LDH at equilibrium can be quantified [28,85–87].

$$Q_e = \frac{(C_i - C_e)V}{m} \quad \text{(eq. 1.7)}$$

Where Q_e (mg g^{-1}) is the amount of chloride uptake or inhibitor released at equilibrium concentration, C_i, and C_e (mg L^{-1}) are initial (t = 0) and equilibrium concentration of chloride or inhibitor in a solution respectively, V (L) is volume of solution, and m (g) is mass of the LDH dispersed in the solution [28,85,87].

Langmuir isotherm (eq. 1.8) and Freundlich isotherm (eq. 1.9) are the general equilibrium models used for the fitting and interpretation of the experimental data [85,86].

$$Q_e = \frac{K_L q_m C_e}{(1 + q_m C_e)} \quad \text{(eq. 1.8)}$$

$$Q_e = K_F C_e^n \quad \text{(eq. 1.9)}$$

K_L is the Langmuir isotherm constant associated to adsorption energy and q_m (mg g^{-1}) is the maximum adsorption or sorption capacity, K_F (L g^{-1}) is the Freundlich isotherm constants and n, is a factor associated to adsorption capacity.

1.8.2 Kinetic study of LDHs

The chloride uptake or inhibitor released kinetics can be studied by varying the exposure time. Using equation 1.10, the amount (Q) of chloride uptake by LDH or inhibitor released from LDH at a given time t (min) can be quantified [28,85–87].

$$Q_t = \frac{(C_i - C_t)V}{m} \quad \text{(eq. 1.10)}$$

Where Q_t (g/g) is the amount of chloride uptake or inhibitor released at a given time (t), C_i, and C_t (g/L) are concentration of chloride or inhibitor in a solution at the initial and given time (t), respectively, V (L) is volume of solution and m (g) is mass of the LDH dispersed in the solution [28,85,87].

The kinetics of LDHs for corrosion protection involved the processes such as uptake of chloride ions by LDH or inhibitor/anion released from LDH. Three stages involved during the kinetics process of LDH which include:

(i) External mass transfer: The boundary layer diffusion between the external surface of the LDH and the surrounding electrolyte.

(ii) Intra-ions transport within the LDH

(iii) Chemisorption: The phase boundaries reaction kinetics, in which the rate of chloride uptake is controlled by bond formation kinetics [28,85,88].

The above kinetic processes can be influenced by chloride ion concentration, pH of solution, amount of LDH dispersed in solution, and temperature. Various models have been employed to explain the mechanism of sorption and desorption from a sorbent [86,88]. The most frequently kinetic models used to describe the uptake of chloride by LDH or the releasing of inhibitors from LDH are namely, first-order kinetics model, pseudo-second-order kinetics model, Elovich equation, and Intraparticle diffusion model. These models are basically employed in solid/liquid sorption or desorption systems for the fitting and interpretation of experimental data [85,87,89].

First-order kinetics model:

$$ln(Q_e - Q_t) = ln(Q_e) - k_1 t \quad \text{(eq. 1.11)}$$

Where Q_e and Q_t (g/g) are amount chloride uptake or inhibitor released at equilibrium and at different times t (h) respectively, k_1 (h) is the first-order model rate constant. Q_e (mg/g) is calculated from Langmuir isotherm equation 1.8. The rate constant k_1 can be determined from a straight-line graph by plotting $\ln(Q_e - Q_t)$ against t.

Pseudo-second-order kinetics model:

$$\frac{t}{Q_t} = \frac{1}{k_2 \times Q_e^2} + \frac{t}{Q_e} \quad \text{(eq. 1.12)}$$

where k_2 (g.mgh^{-1}) is the rate constant, determined from a linear graph by plotting t/Q_t Vs. t.

Elovich equation

$$\frac{dQ_t}{dt} = \alpha exp(-\beta Q_t) \quad \text{(eq. 1.13)}$$

Assuming $\alpha\beta t \gg 1$ and Qt = 0 at t = 0 the equation will become

$$Q_t = \beta In(\alpha\beta) + \beta Int \quad \text{(eq. 1.14)}$$

where α (mg/g.h) and β (g/mg) obtained from the slope and intercept of a straight-line plot of Q_t against Int, are initial adsorption rate and desorption constant respectively.

Intra-particle diffusion model

$$Q_t = k_i t^{1/2} + C_i \quad \text{(eq. 1.15)}$$

k_i (g/mg.$h^{1/2}$) is the intraparticle diffusion rate constant and C_i is intercept obtained from a straight-line plot of Q_t against $t^{1/2}$.

Lv *et al*., studied the uptake of chloride ions by calcined layered double hydroxides (CLDH). The equilibrium isotherms revealed the consistent uptake of chloride ion by CLDH in which the Langmuir isotherm gave a better experimental data fitting than Freundlich isotherm. The influence of the amount of LDH dispersed into the solution, concentration of chloride ion in solution, pH of solution and temperature on the kinetics of chloride uptake by LDH was also studied by using four kinetic models mention earlier. It was found that pseudo-second-order kinetics model best describe the uptake process compared to others. This suggest that the uptake of chloride ion by the CLDH was governed by reaction rate between chloride and CLDH rather than diffusion [85]. The kinetics of imidazole released from LDH was also reported to depend on the concentration of ion in the solution [87]. There are very little research on this topic and most of the available research are not directly on the kinetics released of inhibitor from LDH, however, their results is an insight on the mechanism of chloride ions uptake by LDHs and inhibitors released from LDHs [90–92].

1.9 Corrosion protection application of LDHs

The corrosion protection application of LDHs is versatile owing to their anion-exchange potentials, positively-charged hydroxide layers, wide range of cationic combination, tunability, low cost of production, simplicity methods of synthesis and biocompatibility.

1.9.1 Steel reinforced concrete

Corrosion protection techniques such as stainless steel reinforcement, epoxy coated rebar, corrosion inhibitors, cathodic protection have been developed to enhance corrosion resistance of steel in concrete [93–95]. LDH, due to its anion-exchange characteristic could also present a potential application in corrosion protection of Steel-reinforced concrete. The introduction of calcined layered double hydroxide into a simulated concrete pore solution was report to decrease the amount Cl^- ions concentration and also increase the solution pH [96]. MgAl-NO_2^- LDH in a simulated carbonated concrete pore solution as well as mortar was reported to exhibit a multifunctional corrosion protection of carbon steel. The protection was attributed to decrease in the chloride ions, increase in the pH of concrete solution and releasing of nitrite ions. MgAl-NO_2^- LDH was said to be capable of absorbing Cl^- ions and then releasing NO_2^- and OH^- ions

simultaneously based on anion-exchange characteristic. Therefore, LDH intercalated with Nitrite was proven to improve the corrosion resistance of steel-reinforced concrete [97–101].

1.9.2 Coated system

LDHs either as power or slurry could be incorporated into organic coated systems in an appropriate amount to improve their protection performance. It could also be grown directly on the metal surface as film and then covered by top coatings. Inhibitor-loaded LDHs have been added into epoxy coatings for corrosion protection of carbon steel [13,25,40,102,103].

The incorporation of aminobenzoate intercalated Mg-Al LDH into epoxy coating with proper amount was reported to increases corrosion resistance of epoxy coating. The corrosion protection performance of coatings was in a sequence of 0.5 wt.% LDH > 1 wt.% LDH > neat epoxy > 2 wt.% LDH. The change of the corrosion resistance due to the addition of LDH was attributed to the coating's microstructure variations [104]. Therefore, it is very important to controlled the amount of LDHs addition to avoid the agglomeration and defects occurrence. Karami *et al*, also reported that, the addition of 0.1 wt.% ZnAl-NO_3^- LDH into epoxy formulation caused a rise in the total curing heat thereby shifting the cure state of the coating to an "*excellent zone*". The improvement of the curing was attributed to the Lewis acid catalytic effect of divalent Zn metal which facilitated the epoxy ring opening curing reaction [105]. Zinc-rich epoxy (ZRE) coating incorporated with 2-mercaptobenzothiazole intercalated ZnAl LDH nanocontainers were found to exhibit excellent corrosion protection of carbon steel in 3.5% NaCl. The overall protective performance of the coating was ascribed to the barrier effect from the coating, smart inhibition from the inhibitors and sacrificial cathodic protection from the zinc [40]. Cu-BTA complexes coated MgAl-MoO_4^{2-} LDH was reported to have dual self-healing effect on waterborne epoxy coatings attributed to the controlled release of both BTA and MoO_4^{2-} ions and simultaneous entrapment of chloride ions by the LDH [106]. Su *et al*., studied anti-corrosion performance of epoxy resin incorporated with nitrite intercalated MgAl LDH on carbon steel. The thickness of the epoxy coating was 50 ± 5 μm. Their result reveals a self-healing and long-time active inhibition role of the LDH as confirmed by LEIS, EIS and corrosion product analysis. The lamella structure of the LDH nanosheets contributed to the barrier performance of the coating while the nitrite ion exhibited active anticorrosion role [25]. Rodriguez *et al*., reported a loss in the barriers property of epoxy coating incorporated with unfunc-

tionalized LDHs. However, the functionalization of LDHs with BTA improved the compatibility between the inorganic particles (LDH-BTA) and the epoxy coating. Reasonable barrier and self-healing properties of the coating deposited on ZnMg coated steel over immersion time were maintained [103]. Nguyen *et al*., studied the corrosion protection performance of epoxy coatings on carbon steel. The coatings were incorporated with hydrotalcites intercalated 2-benzothiazolythio-succinic acid (HT-BTSA), benzoate (HT-BZ) and molybdate (HT-MoO4). Their results reveal that, the corrosion protection performance for the solvent free epoxy coating containing HT-BZ at a concentration of 1.5 wt.% was significantly improved. The protection performance of the coating was depended on the degree of dispersion of the hydrotalcite particles in the matrix of the coating and the solubility of the released organic inhibitor in the electrolyte[13,25,102,103].

1.10 Summary and conclusion

This review summarizes the significant contribution of LDHs as corrosion inhibitors reservoir in organic coatings dedicated to corrosion protection. The structure and bonding, formation mechanism, corrosion protection mechanism, thermodynamic and kinetics, and corrosion protection application of LDHs are discussed in this chapter. Among others corrosion inhibitor reservoirs, LDHs have showed promising potentials due to their charged balancing structure, anion-exchanged mechanism, and controlled/on-demand release of the inhibitive species in paralleled with simultaneous capturing of chloride ions. Inhibitor-loaded LDH incorporated into epoxy matrix could provide excellent barrier property and in the same time provide self-healing effect. The enhancement of the barrier property could be attributed to the increasing tortuosity by the LDHs material while the self-healing could be ascribed to active inhibition from the inhibitor. Therefore, LDHs have potential application in the field of corrosion protection and surface engineering. The nature of the hydroxide layers, the type of divalent metallic cations and compatibility between LDHs materials and various organic coatings are important factors to be considered when dispersing LDHs into the coating matrix.

References

[1] D. Dwivedi, K. Lepková, T. Becker, Carbon steel corrosion: a review of key surface properties and characterization methods, RSC Adv. 7 (2017) 4580–4610. https://doi.org/10.1039/C6RA25094G.

[2] O.W. Obot, C.N. Anyakwo, An Investigation of Internal Corrosion of Oil and Gas Transporting Carbon Steel Pipes in the Niger Delta Area of Nigeria, EJERS. 2 (2017) 22. https://doi.org/10.24018/ejers.2017.2.8.374.

[3] B.O. Orisanmi, S.A. Afolalu, O.R. Adetunji, E.Y. Salawu, I.P. Okokpujie, A.A. Abioye, O. Akinyemi, O.P. Abioye, Cost of Corrosion of Metallic Products in Federal University of Agriculture, Abeokuta, International Journal of Applied Engineering. 12 (2017) 14141–14147.

[4] O.S.I. Fayomi, I.G. Akande, S. Odigie, Economic Impact of Corrosion in Oil Sectors and Prevention: An Overview, J. Phys.: Conf. Ser. 1378 (2019) 022037. https://doi.org/10.1088/1742-6596/1378/2/022037.

[5] Y. Cao, D. Zheng, S. Dong, F. Zhang, J. Lin, C. Wang, C. Lin, A Composite Corrosion Inhibitor of MgAl Layered Double Hydroxides Co-Intercalated with Hydroxide and Organic Anions for Carbon Steel in Simulated Carbonated Concrete Pore Solutions, J. Electrochem. Soc. 166 (2019) C3106. https://doi.org/10.1149/2.0141911jes.

[6] A. Jagtap, P.G. Wagle, E. Jagtiani, A.P. More, Layered double hydroxides (LDHs) for coating applications, J Coat Technol Res. 19 (2022) 1009–1032. https://doi.org/10.1007/s11998-022-00624-y.

[7] A.A. Olajire, Recent advances on organic coating system technologies for corrosion protection of offshore metallic structures, Journal of Molecular Liquids. 269 (2018) 572–606. https://doi.org/10.1016/j.molliq.2018.08.053.

[8] C. Gomes, Z. Mir, R. Sampaio, A. Bastos, J. Tedim, F. Maia, C. Rocha, Măą. Ferreira, Use of ZnAl-Layered Double Hydroxide (LDH) to Extend the Service Life of Reinforced Concrete, Materials. 13 (2020) 1769. https://doi.org/10.3390/ma13071769.

[9] M. Attaei, L.M. Calado, Y. Morozov, M.G. Taryba, R.A. Shakoor, R. Kahraman, A.C. Marques, M.F. Montemor, Smart epoxy coating modified with isophorone diisocyanate microcapsules and cerium organophosphate for multilevel corrosion protection of carbon steel, Progress in Organic Coatings. 147 (2020) 105864. https://doi.org/10.1016/j.porgcoat.2020.105864.

[10] N. Granizo, J.M. Vega, D. de la Fuente, B. Chico, M. Morcillo, Ion-exchange pigments in primer paints for anticorrosive protection of steel in atmospheric service: Anion-exchange pigments, Progress in Organic Coatings. 76 (2013) 411–424. https://doi.org/10.1016/j.porgcoat.2012.10.009.

[11] E.J. Ekott, E.J. Akpabio, U.I. Etukudo, Cathodic Protection of Buried Steel Oil Pipelines in Niger Delta, Environmental Research J. 6 (2012) 304–307. https://doi.org/10.3923/erj.2012.304.307.

[12] D.T. Nguyen, H.T.X. To, J. Gervasi, Y. Paint, M. Gonon, M.-G. Olivier, Corrosion inhibition of carbon steel by hydrotalcites modified with different organic carboxylic acids for organic coatings, Progress in Organic Coatings. 124 (2018) 256–266. https://doi.org/10.1016/j.porgcoat.2017.12.006.

[13] D. Nguyen Thuy, H. To Thi Xuan, A. Nicolay, Y. Paint, M.-G. Olivier, Corrosion protection of carbon steel by solvent free epoxy coating containing hydrotalcites intercalated with different organic corrosion inhibitors, Progress in Organic Coatings. 101 (2016) 331–341. https://doi.org/10.1016/j.porgcoat.2016.08.021.

[14] C.-M. Lin, C.-H. Chen, C.-H. Lin, W.C. Su, T.-Y. Juang, Using Dicyclopentadiene-Derived Polyarylates as Epoxy Curing Agents To Achieve High T_g and Low Dielectric Epoxy Thermosets, ACS Omega. 3 (2018) 4295–4305. https://doi.org/10.1021/acsomega.8b00256.

[15] L. Garden, R.A. Pethrick, A dielectric study of water uptake in epoxy resin systems, J. Appl. Polym. Sci. 134 (2017). https://doi.org/10.1002/app.44717.

[16] Y. Elkebir, S. Mallarino, D. Trinh, Săš. Touzain, Effect of physical ageing onto the water uptake in epoxy coatings, Electrochimica Acta. 337 (2020) 135766. https://doi.org/10.1016/j.electacta.2020.135766.

[17] R. Samiee, B. Ramezanzadeh, M. Mahdavian, E. Alibakhshi, G. Bahlakeh, Graphene oxide nano-sheets loading with praseodymium cations: Adsorption-desorption study, quantum mechanics calculations and dual active-barrier effect for smart coatings fabrication, Journal of Industrial and Engineering Chemistry. 78 (2019) 143–154. https://doi.org/10.1016/j.jiec.2019.06.024.

[18] D. Abrantes Leal, F. Wypych, C.E. Bruno Marino, Zinc-Layered Hydroxide Salt Intercalated with Molybdate Anions as a New Smart Nanocontainer for Active Corrosion Protection of Carbon Steel, ACS Appl. Mater. Interfaces. 12 (2020) 19823–19833. https://doi.org/10.1021/acsami.0c02378.

[19] H. Pulikkalparambil, S. Siengchin, J. Parameswaranpillai, Corrosion protective self-healing epoxy resin coatings based on inhibitor and polymeric healing agents encapsulated in organic and inorganic micro and nanocontainers, Nano-Structures & Nano-Objects. 16 (2018) 381–395. https://doi.org/10.1016/j.nanoso.2018.09.010.

[20] F. Zhang, P. Ju, M. Pan, D. Zhang, Y. Huang, G. Li, X. Li, Self-healing mechanisms in smart protective coatings: A review, Corrosion Science. 144 (2018) 74–88. https://doi.org/10.1016/j.corsci.2018.08.005.

[21] M.L. Zheludkevich, D.G. Shchukin, K.A. Yasakau, H. Möhwald, M.G.S. Ferreira, Anticorrosion Coatings with Self-Healing Effect Based on Nanocontainers Impregnated with Corrosion Inhibitor, Chem. Mater. 19 (2007) 402–411. https://doi.org/10.1021/cm062066k.

[22] A.A. Javidparvar, R. Naderi, B. Ramezanzadeh, Manipulating graphene oxide nanocontainer with benzimidazole and cerium ions: Application in epoxy-based nanocomposite for active corrosion protection, Corrosion Science. 165 (2020) 108379. https://doi.org/10.1016/j.corsci.2019.108379.

[23] A.A. Javidparvar, R. Naderi, B. Ramezanzadeh, G. Bahlakeh, Graphene oxide as a pH-sensitive carrier for targeted delivery of eco-friendly corrosion inhibitors in chloride solution: Experimental and theroretical investigations, Journal of Industrial and Engineering Chemistry. 72 (2019) 196–213. https://doi.org/10.1016/j.jiec.2018.12.019.

[24] C. Jing, B. Dong, A. Raza, T. Zhang, Y. Zhang, Corrosion inhibition of layered double hydroxides for metal-based systems, Nano Materials Science. 3 (2021) 47–67. https://doi.org/10.1016/j.nanoms.2020.12.001.

[25] Y. Su, S. Qiu, D. Yang, S. Liu, H. Zhao, L. Wang, Q. Xue, Active anti-corrosion of epoxy coating by nitrite ions intercalated MgAl LDH, Journal of Hazardous Materials. 391 (2020) 122215. https://doi.org/10.1016/j.jhazmat.2020.122215.

[26] I.I. Udoh, H. Shi, E.F. Daniel, J. Li, S. Gu, F. Liu, E.-H. Han, Active anticorrosion and self-healing coatings: A review with focus on multi-action smart coating strategies, Journal of Materials Science & Technology. 116 (2022) 224–237. https://doi.org/10.1016/j.jmst.2021.11.042.

[27] H. Wei, Y. Wang, J. Guo, N.Z. Shen, D. Jiang, X. Zhang, X. Yan, J. Zhu, Q. Wang, L. Shao, H. Lin, S. Wei, Z. Guo, Advanced micro/nanocapsules for self-healing smart anticorrosion coatings, J. Mater. Chem. A. 3 (2014) 469–480. https://doi.org/10.1039/C4TA04791E.

[28] M. Tabish, G. Yasin, M.J. Anjum, M.U. Malik, J. Zhao, Q. Yang, S. Manzoor, H. Murtaza, W.Q. Khan, Reviewing the current status of layered double hydroxide-based smart nanocontainers for corrosion inhibiting applications, Journal of Materials Research and Technology. 10 (2021) 390–421. https://doi.org/10.1016/j.jmrt.2020.12.025.

[29] N. Asadi, R. Naderi, M. Mahdavian, Synergistic effect of imidazole dicarboxylic acid and Zn2+ simultaneously doped in halloysite nanotubes to improve protection of epoxy ester coating, Progress in Organic Coatings. 132 (2019) 29–40. https://doi.org/10.1016/j.porgcoat.2019.03.021.

[30] D. Zhang, H. Zhang, S. Zhao, Z. Li, S. Hou, Electrochemical Impedance Spectroscopy Evaluation of Corrosion Protection of X65 Carbon Steel by Halloysite Nanotube-Filled Epoxy Composite Coatings in 3.5% NaCl Solution, Int. J. Electrochem. Sci. (2019) 4659–4667. https://doi.org/10.20964/2019.05.09.

[31] G. Peng, Q. Qiao, K. Huang, J. Wu, Y. Wang, X. Fu, Z. Zhang, T. Fang, B. Zhang, Y. Huang, X. Li, Ni-Fe-MoO42- LDHs/epoxy resin varnish: A composite coating on carbon steel for long-time and active corrosion protection, Progress in Organic Coatings. 140 (2020) 105514. https://doi.org/10.1016/j.porgcoat.2019.105514.

[32] Y. Cao, D. Zheng, F. Zhang, J. Pan, C. Lin, Layered double hydroxide (LDH) for multifunctionalized corrosion protection of metals: A review, Journal of Materials Science & Technology. 102 (2022) 232–263. https://doi.org/10.1016/j.jmst.2021.05.078.

[33] Y. Cao, D. Zheng, C. Lin, Effect of physical barrier and anion-exchange process of nitrate-intercalated ZnAl layered double hydroxide films grown on Al on corrosion protection, Surface and Coatings Technology. 421 (2021) 127436. https://doi.org/10.1016/j.surfcoat.2021.127436.

[34] A.R. Deip, D.A. Leal, G.H. Sakae, F. Maia, M.A.C. Berton, M.G.S. Ferreira, C.E.B. Marino, Performance of commercial LDH traps for chloride ion in a commercial corrosion protection primer for petrochemical industry, Corrosion Engineering, Science and Technology. 55 (2020) 66–74. https://doi.org/10.1080/1478422X.2019.1671644.

[35] M. Manivannan, S. Rajendran, Ethylenediaminetetraacetic Acid-Zn2+ System as Corrosion Inhibitor for Carbon Steel in Sea Water, Asian J. Chem. 24 (2012) 4713–4716.

[36] K.M. Zohdy, Surface Protection of Carbon Steel in Acidic Solution Using Ethylenediaminetetraacetic Disodium Salt, Int. J. Electrochem. Sci. 10 (2015) 18.

[37] T.T.X. Hang, N.T. Duong, T.A. Truc, T. Hoang, D.T.M. Thanh, S. Daopiset, A. Boonplean, Effects of hydrotalcite intercalated with corrosion inhibitor on cathodic disbonding of epoxy coatings, J Coat Technol Res. 12 (2015) 375–383. https://doi.org/10.1007/s11998-014-9642-3.

[38] T.T.X. Hang, T.A. Truc, N.T. Duong, N. Pébère, M.-G. Olivier, Layered double hydroxides as containers of inhibitors in organic coatings for corrosion protection of carbon steel, Progress in Organic Coatings. 74 (2012) 343–348. https://doi.org/10.1016/j.porgcoat.2011.10.020.

[39] T.T.X. Hang, T.A. Truc, N.T. Duong, P.G. Vu, T. Hoang, Preparation and characterization of nanocontainers of corrosion inhibitor based on layered double hydroxides, Applied Clay Science. 67–68 (2012) 18–25. https://doi.org/10.1016/j.clay.2012.07.004.

[40] H. Hayatdavoudi, M. Rahsepar, Smart inhibition action of layered double hydroxide nanocontainers in zinc-rich epoxy coating for active corrosion protection of carbon steel substrate, Journal of Alloys and Compounds. 711 (2017) 560–567. https://doi.org/10.1016/j.jallcom.2017.04.044.

[41] A.C. Pellanda, A.G.C. Neto, A.R. de Carvalho Jorge, M.A.C. Berton, J.B. Floriano, S. Thomas, P.P. Vijayan, Performance Evaluation of Layered Double Hydroxides Containing Benzotriazole and Nitrogen Oxides as Autonomic Protection Particles against Corrosion, Int. J. Polym. Sci. 2021 (2021) 6630194. https://doi.org/10.1155/2021/6630194.

[42] A. Seniski, R.F. Monteiro, G.T. Carrera, M. d'Orey G.P. Bragança, K.F. Portella, A. Seniski, R.F. Monteiro, G.T. Carrera, M. d'Orey G.P. Bragança, K.F. Portella, The inhibitory and comparative effects of Zn-Al layered double hydroxide microcontainers intercalated with benzotriazole and nitrite for corrosion protection coatings on AISI 1010 carbon steel, Matéria (Rio de Janeiro). 25 (2020). https://doi.org/10.1590/s1517-707620200002.1064.

[43] T.A. Truc, T.T. Thuy, V.K. Oanh, T.T.X. Hang, A.S. Nguyen, N. Caussé, N. Pébère, 8-hydroxyquinoline-modified clay incorporated in an epoxy coating for the corrosion protection of carbon steel, Surfaces and Interfaces. 14 (2019) 26–33. https://doi.org/10.1016/j.surfin.2018.10.007.

[44] T.T.X. Hang, T.A. Truc, M.-G. Olivier, C. Vandermiers, N. Guérit, N. Pébère, Corrosion protection mechanisms of carbon steel by an epoxy resin containing indole-3 butyric acid modified clay, Progress in Organic Coatings. 69 (2010) 410–416. https://doi.org/10.1016/j.porgcoat.2010.08.004.

[45] W. Li, A. Liu, H. Tian, D. Wang, Controlled Release of Nitrate and Molybdate Intercalated in Zn-Al-Layered Double Hydroxide Nanocontainers towards Marine Anticorrosion Applications, Colloid and Interface Science Communications. 24 (2018) 18–23. https://doi.org/10.1016/j.colcom.2018.03.003.

[46] W. Sun, T. Wu, L. Wang, C. Dong, G. Liu, Controlled Preparation of MgAl-Layered Double Hydroxide/Graphene Hybrids and Their Applications for Metal Protection, Ind. Eng. Chem. Res. 58 (2019) 16516–16525. https://doi.org/10.1021/acs.iecr.9b01742.

[47] F.L. Theiss, G.A. Ayoko, R.L. Frost, Synthesis of layered double hydroxides containing Mg2+, Zn2+, Ca2+ and Al3+ layer cations by co-precipitation methods - A review, Applied Surface Science. 383 (2016) 200–213. https://doi.org/10.1016/j.apsusc.2016.04.150.

[48] J. Liu, H. Shi, M. Yu, R. Du, G. Rong, S. Li, Effect of divalent metal ions on durability and anticorrosion performance of layered double hydroxides on anodized 2A12 aluminum alloy, Surface and Coatings Technology. 373 (2019) 56–64. https://doi.org/10.1016/j.surfcoat.2019.05.066.

[49] D. Sokol, A.N. Salak, M.G.S. Ferreira, A. Beganskiene, A. Kareiva, Bi-substituted Mg3Al–CO3 layered double hydroxides, J Sol-Gel Sci Technol. 85 (2018) 221–230. https://doi.org/10.1007/s10971-017-4506-9.

[50] K.-H. Goh, T.-T. Lim, Z. Dong, Application of layered double hydroxides for removal of oxyanions: A review, Water Research. 42 (2008) 1343–1368. https://doi.org/10.1016/j.watres.2007.10.043.

[51] E. Alibakhshi, E. Ghasemi, M. Mahdavian, B. Ramezanzadeh, Mana yasaei, The effect of interlayer spacing on the inhibitor release capability of layered double hydroxide based nanocontainers, Journal of Cleaner Production. 251 (2020) 119676. https://doi.org/10.1016/j.jclepro.2019.119676.

[52] A.V. Besserguenev, A.M. Fogg, R.J. Francis, S.J. Price, D. O'Hare, V.P. Isupov, B.P. Tolochko, Synthesis and Structure of the Gibbsite Intercalation Compounds [$LiAl_2(OH)_6$]X {X = Cl, Br, NO_3} and [$LiAl_2(OH)_6$]Cl·H_2O Using Synchrotron X-ray and Neutron Powder Diffraction, Chem. Mater. 9 (1997) 241–247. https://doi.org/10.1021/cm960316z.

[53] F. Wang, Z. Guo, Facile synthesis of superhydrophobic three-metal-component layered double hydroxide films on aluminum foils for highly improved corrosion inhibition, New J. Chem. 43 (2019) 2289–2298. https://doi.org/10.1039/C8NJ05732J.

[54] L. Wu, X. Ding, Z. Zheng, A. Tang, G. Zhang, A. Atrens, F. Pan, Doublely-doped Mg-Al-Ce-V2O74- LDH composite film on magnesium alloy AZ31 for anticorrosion, Journal of Materials Science & Technology. 64 (2021) 66–72. https://doi.org/10.1016/j.jmst.2019.09.031.

[55] C.A. Johnson, F.P. Glasser, HYDROTALCITE-LIKE MINERALS (M2Al(OH)6(CO3)0.5.XH2O, WHERE M=Mg,Zn,Co,Ni)INTHEENVIRONMENT: SYNTHESIS, CHARACTERIZATION AND THERMODYNAMIC STABILITY, Clays and Clay Minerals. 51 (2003) 1–8. https://doi.org/10.1346/CCMN.2003.510101.

[56] S. Britto, A.V. Radha, N. Ravishankar, P.V. Kamath, Solution decomposition of the layered double hydroxide (LDH) of Zn with Al, Solid State Sciences. 9 (2007) 279–286. https://doi.org/10.1016/j.solidstatesciences.2007.01.002.

[57] R. k. Allada, Thermochemistry and Aqueous Solubilities of Hydrotalcite-Like Solids, Science. 296 (2002) 721–723. https://doi.org/10.1126/science.1069797.

[58] Z. Meng, Y. Zhang, Q. Zhang, X. Chen, L. Liu, S. Komarneni, F. Lv, Novel synthesis of layered double hydroxides (LDHs) from zinc hydroxide, Applied Surface Science. 396 (2017) 799–803. https://doi.org/10.1016/j.apsusc.2016.11.032.

[59] Y. Wang, Y. Zhang, B. Zhou, C. Li, F. Gao, X. Wang, D. Liang, Y. Wei, In-situ observation of the growth behavior of ZnAl layered double hydroxide film using EQCM, Materials & Design. 180 (2019) 107952. https://doi.org/10.1016/j.matdes.2019.107952.

[60] J. Chen, Y. Song, D. Shan, E.-H. Han, Study of the in situ growth mechanism of Mg–Al hydrotalcite conversion film on AZ31 magnesium alloy, Corrosion Science. 63 (2012) 148–158. https://doi.org/10.1016/j.corsci.2012.05.022.

[61] Z.P. Xu, G.Q. (Max) Lu, Hydrothermal Synthesis of Layered Double Hydroxides (LDHs) from Mixed MgO and Al2O3: LDH Formation Mechanism, Chem. Mater. 17 (2005) 1055–1062. https://doi.org/10.1021/cm048085g.

[62] T.L.P. Galvão, C.S. Neves, A.P.F. Caetano, F. Maia, D. Mata, E. Malheiro, M.J. Ferreira, A.C. Bastos, A.N. Salak, J.R.B. Gomes, J. Tedim, M.G.S. Ferreira, Control of crystallite and particle size in the synthesis of layered double hydroxides: Macromolecular insights and a complementary modeling tool, Journal of Colloid and Interface Science. 468 (2016) 86–94. https://doi.org/10.1016/j.jcis.2016.01.038.

[63] A.C. Bouali, E.A. Straumal, M. Serdechnova, D.C.F. Wieland, M. Starykevich, C. Blawert, J.U. Hammel, S.A. Lermontov, M.G.S. Ferreira, M.L. Zheludkevich, Layered double hydroxide based active corrosion protective sealing of plasma electrolytic oxidation/sol-

gel composite coating on AA2024, Applied Surface Science. 494 (2019) 829–840. https://doi.org/10.1016/j.apsusc.2019.07.117.

[64] A. Mikhailau, H. Maltanava, S.K. Poznyak, A.N. Salak, M.L. Zheludkevich, K.A. Yasakau, Măą.G.S. Ferreira, One-step synthesis and growth mechanism of nitrate intercalated ZnAl LDH conversion coatings on zinc, Chem. Commun. 55 (2019) 6878–6881. https://doi.org/10.1039/C9CC02571E.

[65] A.N. Salak, J. Tedim, A.I. Kuznetsova, M.L. Zheludkevich, M.G.S. Ferreira, Anion exchange in Zn–Al layered double hydroxides: In situ X-ray diffraction study, Chemical Physics Letters. 495 (2010) 73–76. https://doi.org/10.1016/j.cplett.2010.06.041.

[66] V. Shkirskiy, P. Keil, H. Hintze-Bruening, F. Leroux, P. Vialat, G. Lefèvre, K. Ogle, P. Volovitch, Factors Affecting MoO_4^{2-} Inhibitor Release from Zn_2Al Based Layered Double Hydroxide and Their Implication in Protecting Hot Dip Galvanized Steel by Means of Organic Coatings, ACS Appl. Mater. Interfaces. 7 (2015) 25180–25192. https://doi.org/10.1021/acsami.5b06702.

[67] K. Hoshino, S. Furuya, R.G. Buchheit, Effect of NO3− Intercalation on Corrosion Resistance of Conversion Coated Zn-Al-CO3 LDHs on Electrogalvanized Steel, J. Electrochem. Soc. 165 (2018) C461. https://doi.org/10.1149/2.0091809jes.

[68] M. Chen, F. Wu, L. Yu, Y. Cai, H. Chen, M. Zhang, Chloride binding capacity of LDHs with various divalent cations and divalent to trivalent cation ratios in different solutions, CrystEngComm. 21 (2019) 6790–6800. https://doi.org/10.1039/C9CE01322A.

[69] M.L. Zheludkevich, S.K. Poznyak, L.M. Rodrigues, D. Raps, T. Hack, L.F. Dick, T. Nunes, M.G.S. Ferreira, Active protection coatings with layered double hydroxide nanocontainers of corrosion inhibitor, Corrosion Science. 52 (2010) 602–611. https://doi.org/10.1016/j.corsci.2009.10.020.

[70] A.V. Radha, P. Vishnu Kamath, C. Shivakumara, Mechanism of the anion exchange reactions of the layered double hydroxides (LDHs) of Ca and Mg with Al, Solid State Sciences. 7 (2005) 1180–1187. https://doi.org/10.1016/j.solidstatesciences.2005.05.004.

[71] T.T.X. Hang, T.A. Truc, N.T. Duong, P.G. Vu, T. Hoang, Preparation and characterization of nanocontainers of corrosion inhibitor based on layered double hydroxides, Applied Clay Science. 67–68 (2012) 18–25. https://doi.org/10.1016/j.clay.2012.07.004.

[72] E. Alibakhshi, E. Ghasemi, M. Mahdavian, B. Ramezanzadeh, S. Farashi, Active corrosion protection of Mg-Al-PO 4 3− LDH nanoparticle in silane primer coated with epoxy on mild steel, Journal of the Taiwan Institute of Chemical Engineers. 75 (2017) 248–262. https://doi.org/10.1016/j.jtice.2017.03.010.

[73] E. Alibakhshi, E. Ghasemi, M. Mahdavian, B. Ramezanzadeh, A comparative study on corrosion inhibitive effect of nitrate and phosphate intercalated Zn-Al- layered double hydroxides (LDHs) nanocontainers incorporated into a hybrid silane layer and their effect on cathodic delamination of epoxy topcoat, Corrosion Science. 115 (2017) 159–174. https://doi.org/10.1016/j.corsci.2016.12.001.

[74] J. Tedim, A. Kuznetsova, A.N. Salak, F. Montemor, D. Snihirova, M. Pilz, M.L. Zheludkevich, M.G.S. Ferreira, Zn–Al layered double hydroxides as chloride nanotraps in active protective coatings, Corrosion Science. 55 (2012) 1–4. https://doi.org/10.1016/j.corsci.2011.10.003.

[75] M.L. Zheludkevich, J. Tedim, M.G.S. Ferreira, "Smart" coatings for active corrosion protection based on multi-functional micro and nanocontainers, Electrochimica Acta. 82 (2012) 314–323. https://doi.org/10.1016/j.electacta.2012.04.095.

[76] Z. Yang, H. Fischer, J. Cerezo, J.M.C. Mol, R. Polder, Modified hydrotalcites for improved corrosion protection of reinforcing steel in concrete – preparation, characterization, and assessment in alkaline chloride solution, Materials and Corrosion. 67 (2016) 721–738. https://doi.org/10.1002/maco.201508618.

[77] S.K. Poznyak, J. Tedim, L.M. Rodrigues, A.N. Salak, M.L. Zheludkevich, L.F.P. Dick, M.G.S. Ferreira, Novel Inorganic Host Layered Double Hydroxides Intercalated with Guest Organic Inhibitors for Anticorrosion Applications, ACS Appl. Mater. Interfaces. 1 (2009) 2353–2362. https://doi.org/10.1021/am900495r.

[78] M.Z. bin Hussein, Z. Zainal, A.H. Yahaya, D.W.V. Foo, Controlled release of a plant growth regulator, α-naphthaleneacetate from the lamella of Zn–Al-layered double hydroxide nanocomposite, Journal of Controlled Release. 82 (2002) 417–427. https://doi.org/10.1016/S0168-3659(02)00172-4.

[79] J. Wei, J. Xu, Y. Mei, Q. Tan, Chloride adsorption on aminobenzoate intercalated layered double hydroxides: Kinetic, thermodynamic and equilibrium studies, Applied Clay Science. 187 (2020) 105495. https://doi.org/10.1016/j.clay.2020.105495.

[80] M. Junaid Anjum, J. Zhao, H. Ali, M. Tabish, H. Murtaza, G. Yasin, M.U. Malik, W.Q. Khan, A Review on Self-Healing Coatings Applied to Mg Alloys and Their Electrochemical Evaluation Techniques, Int. J. Electrochem. Sci. (2020) 3040–3053. https://doi.org/10.20964/2020.04.36.

[81] Y. Wang, D. Zhang, Synthesis, characterization, and controlled release anticorrosion behavior of benzoate intercalated Zn–Al layered double hydroxides, Materials Research Bulletin. 46 (2011) 1963–1968. https://doi.org/10.1016/j.materresbull.2011.07.021.

[82] N. Olya, E. Ghasemi, B. Ramezanzadeh, M. Mahdavian, Synthesis, characterization and protective functioning of surface decorated Zn-Al layered double hydroxide with SiO2 nano-particles, Surface and Coatings Technology. 387 (2020) 125512. https://doi.org/10.1016/j.surfcoat.2020.125512.

[83] M. Miao, J. Wang, W. Hu, Synthesis, characterization and inhibition properties of ZnAlCe layered double hydroxide intercalated with 1-hydroxyethylidene-1,1-diphosphonic acid, Colloids and Surfaces A: Physicochemical and Engineering Aspects. 543 (2018) 144–154. https://doi.org/10.1016/j.colsurfa.2018.01.056.

[84] J. Tedim, A.C. Bastos, S. Kallip, M.L. Zheludkevich, M.G.S. Ferreira, Corrosion protection of AA2024-T3 by LDH conversion films. Analysis of SVET results, Electrochimica Acta. 210 (2016) 215–224. https://doi.org/10.1016/j.electacta.2016.05.134.

[85] G.J. Ayemi, S. Marcelin, S. Therias, F. Leroux, B. Normand, Synergy effect between layer double hydroxide (LDH) and EDDS for corrosion inhibition of carbon steel, Applied Clay Science. 222 (2022) 106497. https://doi.org/10.1016/j.clay.2022.106497.

[86] L. Lv, J. He, M. Wei, D.G. Evans, X. Duan, Uptake of chloride ion from aqueous solution by calcined layered double hydroxides: Equilibrium and kinetic studies, Water Research. 40 (2006) 735–743. https://doi.org/10.1016/j.watres.2005.11.043.

[87] I.M. Ahmed, M.S. Gasser, Adsorption study of anionic reactive dye from aqueous solution to Mg–Fe–CO3 layered double hydroxide (LDH), Applied Surface Science. 259 (2012) 650–656. https://doi.org/10.1016/j.apsusc.2012.07.092.

[88] E.V. Bendinelli, I.V. Aoki, O. Barcia, I.C.P. Margarit-Mattos, Kinetic aspects of Mg-Al layered double hydroxides influencing smart corrosion protective behavior, Materials Chemistry and Physics. 238 (2019) 121883. https://doi.org/10.1016/j.matchemphys.2019.121883.

[89] N.K. Lazaridis, D.D. Asouhidou, Kinetics of sorptive removal of chromium(VI) from aqueous solutions by calcined Mg–Al–CO3 hydrotalcite, Water Research. 37 (2003) 2875–2882. https://doi.org/10.1016/S0043-1354(03)00119-2.

[90] Y. Lu, B. Jiang, L. Fang, F. Ling, J. Gao, F. Wu, X. Zhang, High performance NiFe layered double hydroxide for methyl orange dye and Cr(VI) adsorption, Chemosphere. 152 (2016) 415–422. https://doi.org/10.1016/j.chemosphere.2016.03.015.

[91] X. Gao, L. Lei, D. O'Hare, J. Xie, P. Gao, T. Chang, Intercalation and controlled release properties of vitamin C intercalated layered double hydroxide, Journal of Solid State Chemistry. 203 (2013) 174–180. https://doi.org/10.1016/j.jssc.2013.04.028.

[92] R. Rojas, A.F. Jimenez-Kairuz, R.H. Manzo, C.E. Giacomelli, Release kinetics from LDH-drug hybrids: Effect of layers stacking and drug solubility and polarity, Colloids and Surfaces A: Physicochemical and Engineering Aspects. 463 (2014) 37–43. https://doi.org/10.1016/j.colsurfa.2014.09.031.

[93] F. Khodam, Z. Rezvani, A.R. Amani-Ghadim, Enhanced adsorption of Acid Red 14 by co-assembled LDH/MWCNTs nanohybrid: Optimization, kinetic and isotherm, Journal of Industrial and Engineering Chemistry. 21 (2015) 1286–1294. https://doi.org/10.1016/j.jiec.2014.06.002.

[94] M. Criado, I. Sobrados, J.M. Bastidas, J. Sanz, Steel corrosion in simulated carbonated concrete pore solution its protection using sol–gel coatings, Progress in Organic Coatings. 88 (2015) 228–236. https://doi.org/10.1016/j.porgcoat.2015.06.002.

[95] Y. Zhou, Y. Zuo, The inhibitive mechanisms of nitrite and molybdate anions on initiation and propagation of pitting corrosion for mild steel in chloride solution, Applied Surface Science. 353 (2015) 924–932. https://doi.org/10.1016/j.apsusc.2015.07.037.

[96] R.B. Figueira, C.J.R. Silva, E.V. Pereira, Hot-dip galvanized steel dip-coated with ureasilicate hybrid in simulated concrete pore solution: Assessment of coating morphology and corrosion protection efficiency, Progress in Organic Coatings. 88 (2015) 245–255. https://doi.org/10.1016/j.porgcoat.2015.07.008.

[97] Y. Tang, X. Zhao, L. Niu, Y. Zuo, The adsorbing effect of calcined layered double hydroxide for chloride ions in simulated concrete pore solutions, J. Wuhan Univ. Technol.-Mat. Sci. Edit. 29 (2014) 278–283. https://doi.org/10.1007/s11595-014-0908-5.

[98] Y. Cao, S. Dong, D. Zheng, J. Wang, X. Zhang, R. Du, G. Song, C. Lin, Multifunctional inhibition based on layered double hydroxides to comprehensively control corrosion of carbon steel in concrete, Corrosion Science. 126 (2017) 166–179. https://doi.org/10.1016/j.corsci.2017.06.026.

[99] Y. Tian, C. Wen, G. Wang, P. Deng, W. Mo, Inhibiting property of nitrite intercalated layered double hydroxide for steel reinforcement in contaminated concrete condition, J Appl Electrochem. 50 (2020) 835–849. https://doi.org/10.1007/s10800-020-01439-8.

[100] J. Xu, J. Wei, G. Ma, Q. Tan, Effect of MgAl-NO2 LDHs inhibitor on steel corrosion in chloride-free and contaminated simulated carbonated concrete pore solutions, Corrosion Science. 176 (2020) 108940. https://doi.org/10.1016/j.corsci.2020.108940.

[101] Y. Tian, C. Dong, G. Wang, X. Cheng, X. Li, Zn–Al–NO2 layered double hydroxide as a controlled-release corrosion inhibitor for steel reinforcements, Materials Letters. 236 (2019) 517–520. https://doi.org/10.1016/j.matlet.2018.10.177.

[102] J. Zuo, B. Wu, C. Luo, B. Dong, F. Xing, Preparation of MgAl layered double hydroxides intercalated with nitrite ions and corrosion protection of steel bars in simulated carbonated concrete pore solution, Corrosion Science. 152 (2019) 120–129. https://doi.org/10.1016/j.corsci.2019.03.007.

[103] T.D. Nguyen, A.S. Nguyen, B.A. Tran, K.O. Vu, D.L. Tran, T.T. Phan, N. Scharnagl, M.L. Zheludkevich, T.X.H. To, Molybdate intercalated hydrotalcite/graphene oxide composite as corrosion inhibitor for carbon steel, Surface and Coatings Technology. 399 (2020) 126165. https://doi.org/10.1016/j.surfcoat.2020.126165.

[104] J. Rodriguez, E. Bollen, T.D. Nguyen, A. Portier, Y. Paint, M.-G. Olivier, Incorporation of layered double hydroxides modified with benzotriazole into an epoxy resin for the corrosion protection of Zn-Mg coated steel, Progress in Organic Coatings. 149 (2020) 105894. https://doi.org/10.1016/j.porgcoat.2020.105894.

[105] Y. Mei, J. Xu, L. Jiang, Q. Tan, Enhancing corrosion resistance of epoxy coating on steel reinforcement by aminobenzoate intercalated layered double hydroxides, Progress in Organic Coatings. 134 (2019) 288–296. https://doi.org/10.1016/j.porgcoat.2019.05.023.

[106] Z. Karami, M. Jouyandeh, J.A. Ali, M.R. Ganjali, M. Aghazadeh, S.M.R. Paran, G. Naderi, D. Puglia, M.R. Saeb, Epoxy/layered double hydroxide (LDH) nanocomposites: Synthesis, characterization, and Excellent cure feature of nitrate anion intercalated Zn-Al LDH, Progress in Organic Coatings. 136 (2019) 105218. https://doi.org/10.1016/j.porgcoat.2019.105218.

[107] P. Xie, Y. He, F. Zhong, C. Zhang, C. Chen, H. Li, Y. Liu, Y. Bai, J. Chen, Cu-BTA complexes coated layered double hydroxide for controlled release of corrosion inhibitors in dual self-healing waterborne epoxy coatings, Progress in Organic Coatings. 153 (2021) 106164. https://doi.org/10.1016/j.porgcoat.2021.106164.

Chapter 2 Experimental procedures

This chapter presents the different techniques that were used for the subsequent two chapters of results. The specific techniques for chapter 3, concerning the characterization of the inhibitory properties of Zn_2Al-$EDDS^{4-}$ LDH, and chapter 4, concerning the barrier performance of the coated systems, are presented in the respective chapters.

The synthesis (done at ICCF) and characterization techniques used as well as experimental designs and conditions for each are discussed in details.

2.1 Strategy of investigation

In order to decouple the synergism effects between the barrier effect of the organic coating/matrix and the inhibition role of the LDH nanofillers, a first approach was to synthesized and study the inhibiting behavior of the Zn_2Al-$EDDS^{4-}$ LDH system in chapter 3.

Table 2.1: Characterization techniques

Samples	Characterization Techniques	Outcomes
Zn_2Al-$EDDS^{4-}$ LDH	X-Ray Diffraction (XRD)	Lattice parameters, phase composition, crystal structure, atomic spacing and purity.
		Intercalation of EDDS4- anions, Anion-exchange mechanism
	Scaning Electron Microscopy (SEM)	Morphology
	Inductively coupled plasma-optical emission spectroscopy (ICP-OES)	Quantification of Zn^{2+} and Al^{3+} cations.
Bared carbon steel/ Coated System	Open circuit potential (OCP)	Stationary and non-stationary state of the system
	Electrochemical Impedance Spectrocopy (EIS)	Inhibition mechanism. Electrochemical behavior of bared carbon steel. Determination of dielectric parameters such as capacitance and permittivity in dry condition. Electrochemical behavior of coated system in wet condition.
	Potentiodynamic polarization	Kinetics of electrochemical reactions at the electrolyte/substrate interface. Dertermination of type of inhibition machanism.
	Scaning Electron Microscopy (SEM)	Surface state of bared carbon steel after immersion. Nature of the protective films/oxides formed on bared carbon steel. Understand details inhibition mechanism.

The crystallographic microstructure and composition of the synthesized Zn_2Al-$EDDS^{4-}$ LDH material was characterized. The electrochemical behavior of a bared carbon steel, immersed in a solution containing each constituent element of LDH (zinc and aluminum hydroxides and the EDDS molecule), was evaluated by polarization curves and electrochemical impedance spectroscopy measurements. Finally, in chapter 4, after the elaboration of coatings containing different contents of Zn_2Al-$EDDS^{4-}$ LDH, the barrier effect of the composite coating was quantified by global electrochemical impedance measurements. The electrochemical approach was complemented by physicochemical characterizations. Table 2.1 shows overview characterization techniques in an ordered fashion used for this study with their intentional outcomes for all systems studied.

2.2 Synthesis of $Zn_2Al(OH)_6]^+[EDDS^{4-}]_{0.25}.2H_2O$ LDHs

LDHs could be synthesized as slurry and as powder. The synthesis processes include coprecipitation, ion-exchange, rehydration, hydrothermal etc. The choice of the any synthesis methods depends on the purpose for which the LDH will be used. In this study, coprecipitation route was employed.

Coprecipitation is the most widely and versatile methods used to synthesize powder LDHs materials due to the following reasons: simplicity and fastest method of synthesis. It is usually referring as direct synthesis method because, it involves the direct additions of the corresponding salts solution of the divalent and trivalent cations, and the salts solution of the anion of interest as shown in Figure 2.1a. A global view of the set-up used in this study is showing in Figure 2.1b.

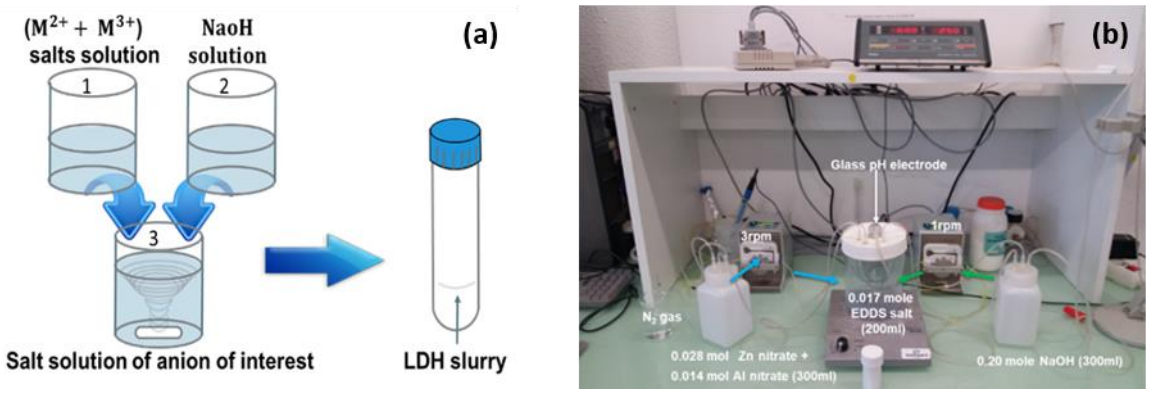

Figure 2.1: Synthesis of LDH by Co-precipitation method

The principle of coprecipitation depends on the precipitation of hexa-aquo complexes in the solution to form a brucite-like structure with uniform distribution of both metallic cations and

interlayers anions [1,2]. Low supersaturation co-precipitation process involves the slow and drop-wise addition of mixed-salts solution of the corresponding divalent and trivalent cations into another solution containing the salt of the desired interlayer anion. To keep constant pH of the synthesis and to also enhance the co-precipitation of the metallic hydroxide, an alkali solution is added simultaneously during this process.

High supersaturation co-precipitation process is similar to the above process. Just a slight difference, were the salts of the anion to be intercalated is prepared in alkaline solution. Therefore, the salts solution of mixed metallic cations is slowly added to the alkaline solution containing the salts of the desired anion. The crystallization nuclei are lager compare to low supersaturation coprecipitation process. Hence less crystalline LHDs are produced by this method. Thermal treatment might be required to increase crystallinity of the LDHs product [3].

The zinc-aluminum LDH intercalated with the anions of ethylenediamine-N,N′-disuccinic acid trisodium salt Zn_2Al-$EDDS^{4-}$ LDH was prepared at room temperature by direct co-precipitation route. The chemical structure of EDDS is shown in Figure 2.2.

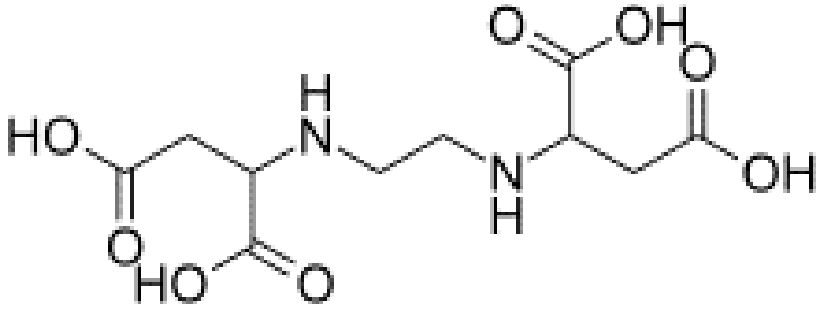

Figure 2.2: Molecular structure of ethylenediamine-N,N'-disuccinic acid.

The synthesis mole ratio of 2:1 for Zn:Al was chosen to obtain a stable Zn_2Al-$EDDS^{4-}$ LDH. 300 mL of a solution containing a mixture 0.028 mol of $Zn(NO_3)_2.6H_2O$ and 0.014 mol of $Al(NO_3)_3.9H_2O$, was gradually added in a dropwise manner at a constant flowrate of 2.5 mL/min to 300 mL solution containing 0.017 mol of trisodium EDDS under slow and then vigorous stirring for 2 hours. Simultaneously, the synthesis pH value of the mixed solutions was kept close to 9 to optimize the co-precipitation of both Al^{3+} and Zn^{2+} to form LDH platelets. Thus, the achieved synthesis pH was 8.7±0.1 by controllable dropwise addition of 300 mL solution containing 0.20 mol of NaOH at the flow rate of 1 mL/min during the co-precipitation reaction [4]. To exclude carbonate anions from the LDH, the experiment was carried out under nitrogen atmosphere. The white precipitate suspension formed at the end of the experiment was

centrifuged at 4500 rpm for about 10 minutes to obtain the slurry of Zn_2Al-$EDDS^{4-}$ LDH particles. The slurry was washed three times with deionized water to removed unreacted elements and part of the sample was dried in an oven at 50°C for 24 hours and then grinded to powder form. Deionized water was used in the rinsing and preparation of aqueous solution procedures to ensure proper purity of the LDHs synthetized.

2.3 Physico-chemical characterization of LDH

2.3.1 Powder X-ray diffraction (XRD)

Powder X-Ray Diffraction (XRD) is a unique analytical technique mostly employed for phase identification of unknown crystalline materials. LDHs as crystalline materials are characterized using this technique in order to evaluate their lattice parameters, phase composition, crystal structure, atomic spacing and purity [5]. Impurities present in the LDH are identified by comparing their powder XRD characteristic diffraction patterns to that of reference patterns.

Crystallinity could influence the dispersibility of LDHs in organic coating matrix and also the releasing kinetics of inhibitor from LDHs. Therefore, it is an important property when considering the application of LDHs as reservoir for corrosion inhibitor. Aside the use of this technique to study the crystal structure of LDHs, XRD have been used to study the successful intercalation of anions, anion-exchange mechanism, and the arrangement of anions in the LDH interlayers [6–8]. The basal $d_{(003)}$ spacing of LDH which corresponds to the inter-layers distance is used to confirm the intercalation of anions. When the interlayer anions are exchange in LDHs, corresponding change in the $d_{(003)}$ spacing is usually observed. This change could suggest the successful intercalation of the new anion into the LDH and/or its adsorption onto the surface of the LDH material [9,10].

The principle of operation is briefly described below and in Figure 2.3.

The cathode ray tube generates X-rays to produce a collimated and monochromatic radiation directed toward the sample. Assuming Bragg's law (eq. 2.1) is satisfied, the bombarded incident (primary) X-rays beam interact with the sample to produce constructive interference diffracted (secondary) X-rays beam which are collected by a detector and the processed as shown in Figure 2.3. The graph of intensity of primary X-ray beam against the diffraction angle is used to characterized the LDHs materials.

$$n\lambda = 2dsin\theta \qquad \text{(eq. 2.1)}$$

where λ = wavelength of electromagnetic radiation, d = inter-lattice distance, θ = diffraction angle, n = an integer)

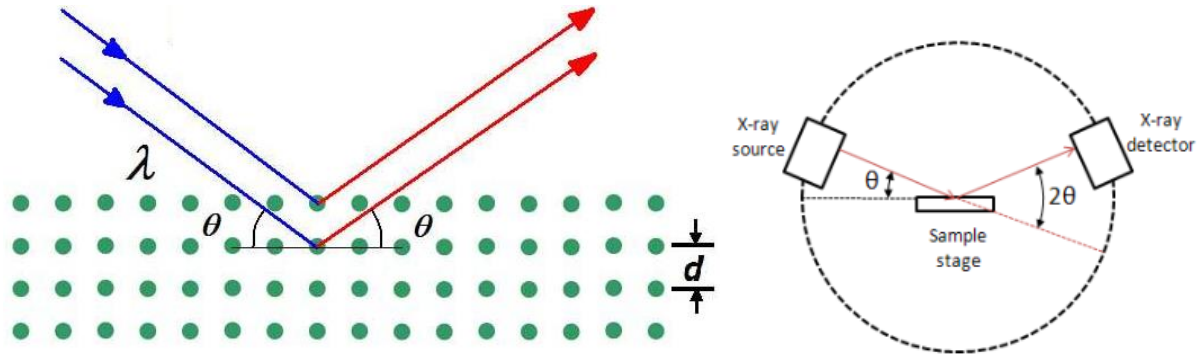

Figure 2.3 Operation principle of X-ray Diffractometer

The anticathode and specific conditions for the analysis of LDH-EDDS powder are specified in Chapter 3.

2.3.2 Scanning electron microscopy (SEM)

The morphology of the LDHs powder was studied by scanning electron microscopy (SEM, VEGA3 TESCAN) at 10 kV electron beam energy (HV), 10 mm working distance (WD) and 7 beam intensity (BI). The powder was first deposited on a conductive carbon adhesive tab and put into a vacuum pump to blow off the dust particle. The powder was then coated with gold (Au) to prevent surface charging, make the surface conductive thereby promote the emission of the secondary electrons, and provide a homogeneous imaging analysis [11]. The SEM observation of the bare carbon steel samples after exposure to electrolyte with or without inhibitive species were also performed using Zeiss SUPRA 55-VP scanning electron microscope (SEM) equipped with a field emission electron gun (FEG). This was done to observe the surface state after immersion, nature of the protective films/oxides formed and to understand in details the inhibition mechanism in the presence and absence of inhibitive species [12].

SEM and FEG-SEM principle of operation is hereby described below.

An electron probe created by the condenser lens system are focused by the objective lens. The probe scan across the sample surface. The high-accelerated-voltage signals of backscattered, secondary and transmitted electrons from the corresponding beam-sample interaction formed the images. The operation principle of FEG-SEM is similar to SEM function. The primary electrons beam liberated from a field emission source are accelerated in a high electrical field gradient within the high vacuum column. These primary electrons are deflected and focused by electronic lenses to produce a narrow scan beam that bombards the sample. Consequently, secondary electrons are emitted from each spot on the sample. The velocity and angle of these

secondary electrons beam relates to the surface morphology of the sample. The secondary electrons are collected by a detector to produce an electronic signal which is amplified and transformed to an image.

2.3.3 Inductively coupled plasma-optical emission spectroscopy (ICP-OES)

Inductively coupled plasma-optical emission spectroscopy (ICP-OES) is a technique to quantify the amount of dissolved species in an extract solution (multi-elements analysis of extract solutions) [13]. From the wavelengths, each element in the sample are identified while the intensities of emission correspond to the concentration of each element present in the sample [14–16]. A diagram showing the basic operational principles of ICP-OES is presented in Figure 2.4.

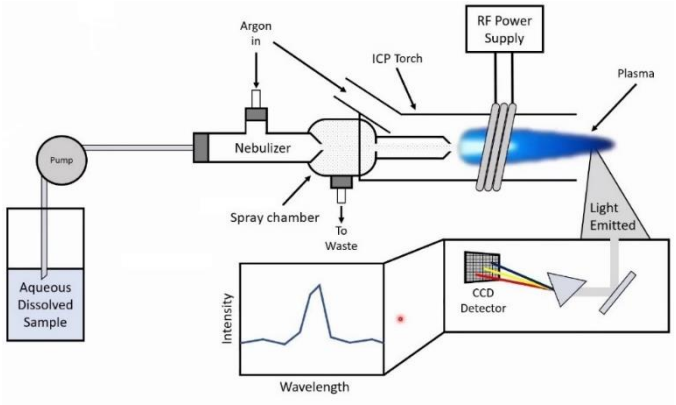

Figure 2.4: Basic operational principles of ICP-OES [15]

2.4 Electrochemical Characterizations

2.4.1. Substrate

The XC38 carbon steel (C = 0.32-0.39, S ≤ 0.035, Mn = 0.5.-0.80, P ≤ 0.035, Si = 0.40 max, Fe balance, in wt.%) was used as a substrate. Bared rods of diameter 1cm^2 and plates with dimensions 100 x 70 x 3 mm^3 were used for Zn_2Al-$EDDS^{4-}$ LDH and coated system respectively.

2.4.2. Electrochemical cells

Electrochemical measurements were performed using a conventional three-electrode set-up in which the working electrode was made of XC38 steel. The different cells used in Chapters 3 and 4 are designed in Figures 2.5 a and b, respectively. The various other specificities of these set-ups will be presented in the dedicated chapters.

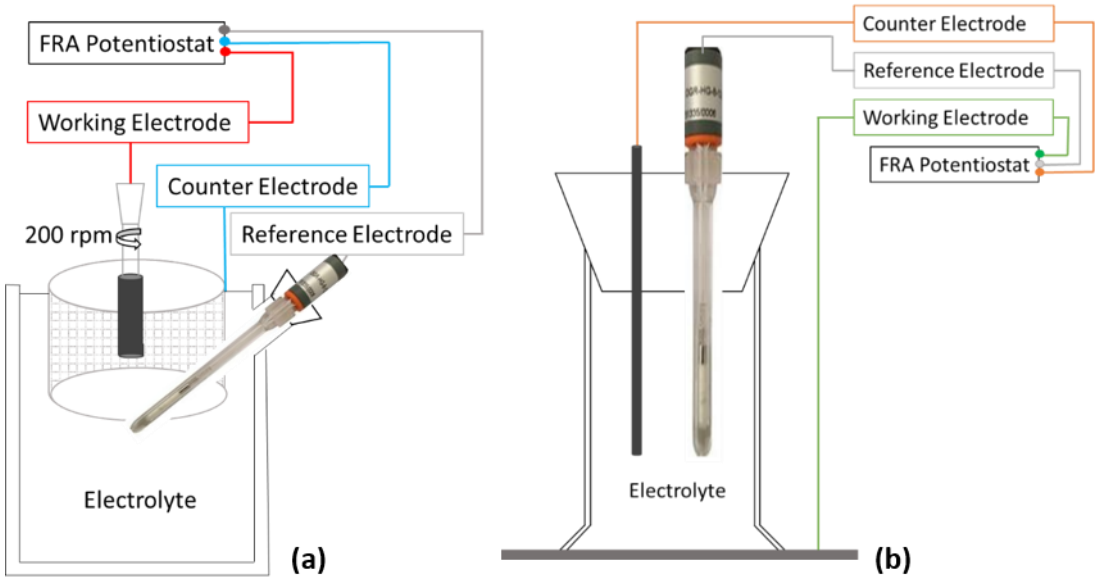

Figure 2.5: Electrochemical set-up for inhibitive study of (a) LDH-EDDS (in chapter 3) and (b) epoxy/LDH-EDDS coated system (in chapter 4).

2.4.3. Electrochemical Techniques

2.4.3.1. Open Circuit Potential (OCP) Measurement

Open circuit potential (OCP) is a mixed-potential at which the cathodic and anodic current densities are equal. During the corrosion potential (E_{corr}) measurement, there is no current flow in the cell, and the potential of the working electrode (WE) is measured with respect to the reference electrode (RE). The evolution of the corrosion potential provides information on the interface between the coated or uncoated carbon steel and the electrolyte. Several cases are possible depending on whether the solution contains an inhibitor or not. If the corrosion potential becomes more positive, this corresponds to a decrease in the activity of the anode sites on the surface of the sample. For the case where the potential becomes more negative, it is important to consider the presence or absence of an inhibitor. Without an inhibitor, and in our case in the presence of Cl^-, this means that the material is corroding. In the presence of an inhibitor, it means a change in the anode/cathode surface ratio which increases and therefore characterizes a cathodic inhibitor [17]. The stability of OCP could signify the uniform corrosion process at meta/electrolyte interface and also the formation of corrosion product which covers the surface of the substrate [18]. The gradual decrease in the OCP after stability could be due to the dissolution of corrosion product which allow the diffusion of corrosive species leading to increase in anodic reaction and causing active corrosion again [19]. While the gradual increase in the

OCP value after stability could be attributed to the formation of a protective layer which drive the potential toward nobler value[20]. The evolution of OCP evaluates the stationary and non-stationary state of the system. The electrochemical measurements are usually carried out at stationary state. Therefore, it is significant in determining the immersion time before launching electrochemical measurements such as EIS, polarization and other techniques [19,21].

2.4.3.2 Polarization curves

The polarization curves are performed by applying a linear potential range on the WE between two chosen potentials. The polarization (current-voltage) curves give the information about kinetics of electrochemical reactions at the electrolyte/substrate interface. For this study, only the anodic polarization curves were obtained from -50 mV vs OCP to +0 V/SCE with a scan rate of 1 mV/s. To ensure reproducibility, all measurements were repeated at least three times.

2.4.3.3 Electrochemical impedance spectroscopy (EIS)

2.4.3.3.1 Principle of EIS

The EIS is considered as one of the most valuable non-destructive techniques used to characterize organic coated system [20,22,23]. It is performed at the stationary state of the system. During the impedance measurements, a sinusoidal low AC potential signal V, is applied to the working electrode and a sinusoidal current signal I, is measured as response to the applied potential excitation. Figure 2.6 represents the principle of EIS.

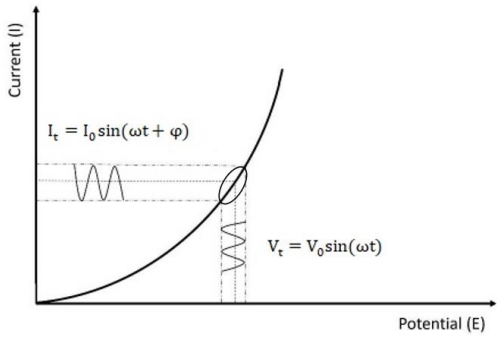

Figure 2.6: Schematic representation of the principle of EIS.

The excitation potential signal (V) as a function of time (t) can be express as:

$$V_t = V_0 \sin(\omega t) \qquad \text{(eq. 2.2)}$$

Where V_0 is the amplitude of the applied sinusoidal potential and ω is the angular frequency ($\omega = 2\pi f$)

In a linear or pseudo-linear system, the system response to V_0 will be a sinusoidal current, I_t, at the same frequency but different amplitude I_0, and shifted in phase (φ) expressed as:

$$I_t = I_0 \sin(\omega t + \varphi) \quad \text{(eq. 2.3)}$$

Consequently, the impedance of the system can be expressed from Ohm's law as:

$$Z = \frac{V_t}{I_t} = \frac{V_0 \sin(\omega t)}{I_0 \sin(\omega t + \varphi)} = Z_0 \frac{\sin(\omega t)}{\sin(\omega t + \varphi)} \quad \text{(eq. 2.4)}$$

The impedance then is expressed as a complex function using Euler's relationship:

$$Z(\omega) = Z_0 \exp(j\omega) = Z_0(\cos\varphi + j\sin\varphi) = Z'(\omega) + Z''(\omega) \quad \text{(eq. 2.5)}$$

$$|Z| = \sqrt{((Z')^2 + (Z'')^2)} \quad \text{(eq. 2.6)}$$

$$\varphi = \tan^{-1}\left(\frac{Z''}{Z'}\right) \quad \text{(eq. 2.7)}$$

Where $|Z|$ is the impedance modulus, Z' and Z'' are the real and imaginary part of the impedance respectively.

2.4.3.3.2 Procedure of impedance diagrams analysis

There are several ways to analyze impedance diagrams, it is imperative to know that this interpretation be based on the knowledge of physical phenomena occurring at the metal/coating/electrolyte interfaces. Hence the importance of the physico-chemical characterizations presented above. This analysis of impedance diagram could be based on mathematical approaches, the use of equivalent electrical circuits and a graphical approach. In this work, we have analyzed graphically the diagrams to extract the parameters of the constant phase element for the fitting procedure using the non-commercial Simad software (developed at the LISE UMR 8235 CNRS, Sorbonne University, Paris), either by the using of equivalent electrical circuits or mathematical models. The graphical analysis will be explained here briefly since it was used for chapters 3 and 4. On the other hand, in chapter 3, the use of electrical equivalent circuits will be detailed, and the use of the power law (mathematical) model will be presented in chapter 4.

The graphical analysis, developed since 2006 [24], allows to extract graphically the parameters of a constant phase element behavior (CPE-non ideal capacitance) and the resistance of the electrolyte. The impedance of CPE is express as in equation 2.8. It is the first step for the analysis of impedance diagrams. At the same time, the good knowledge of the physical phenomena present at the metal/solution interface, allows to be able to propose an equivalent electrical circuit to simulate the reactivity of the system. The values extracted graphically can be used advantageously to guide the adjustment of the experimental data.

$$Z_{CPE} = \frac{1}{(j\omega)^{\alpha} Q} \quad \text{(eq. 2.8)}$$

References

[1] J.J. Bravo-Suárez, E.A. Páez-Mozo, S.T. Oyama, Review of the synthesis of layered double hydroxides: a thermodynamic approach, Quím. Nova. 27 (2004). https://doi.org/10.1590/S0100-40422004000400015.

[2] N. Gerds, V. Katiyar, C.B. Koch, J. Risbo, D. Plackett, H.C.B. Hansen, Synthesis and characterization of laurate-intercalated Mg–Al layered double hydroxide prepared by co-precipitation, Applied Clay Science. 65–66 (2012) 143–151. https://doi.org/10.1016/j.clay.2012.05.003.

[3] A. Rabenau, The Role of Hydrothermal Synthesis in Preparative Chemistry, Angew. Chem. Int. Ed. Engl. 24 (1985) 1026–1040. https://doi.org/10.1002/anie.198510261.

[4] F.L. Theiss, G.A. Ayoko, R.L. Frost, Synthesis of layered double hydroxides containing Mg2+, Zn2+, Ca2+ and Al3+ layer cations by co-precipitation methods - A review, Applied Surface Science. 383 (2016) 200–213. https://doi.org/10.1016/j.apsusc.2016.04.150.

[5] R. Botan, S. de Bona Sartor, X-ray diffraction analysis of layered double hydroxide polymer nanocomposites, in: Layered Double Hydroxide Polymer Nanocomposites, Elsevier, 2020: pp. 205–229. https://doi.org/10.1016/B978-0-08-101903-0.00005-2.

[6] A.N. Salak, J. Tedim, A.I. Kuznetsova, M.L. Zheludkevich, M.G.S. Ferreira, Anion exchange in Zn–Al layered double hydroxides: In situ X-ray diffraction study, Chemical Physics Letters. 495 (2010) 73–76. https://doi.org/10.1016/j.cplett.2010.06.041.

[7] G.J. Ayemi, S. Marcelin, S. Therias, F. Leroux, B. Normand, Synergy effect between layer double hydroxide (LDH) and EDDS for corrosion inhibition of carbon steel, Applied Clay Science. 222 (2022) 106497. https://doi.org/10.1016/j.clay.2022.106497.

[8] M. Serdechnova, A.N. Salak, F.S. Barbosa, D.E.L. Vieira, J. Tedim, M.L. Zheludkevich, M.G.S. Ferreira, Interlayer intercalation and arrangement of 2-mercaptobenzothiazolate and 1,2,3-benzotriazolate anions in layered double hydroxides: In situ X-ray diffraction study, Journal of Solid State Chemistry. 233 (2016) 158–165. https://doi.org/10.1016/j.jssc.2015.10.023.

[9] S.J. Palmer, A. Soisonard, R.L. Frost, Determination of the mechanism(s) for the inclusion of arsenate, vanadate, or molybdate anions into hydrotalcites with variable cationic ratio, Journal of Colloid and Interface Science. 329 (2009) 404–409. https://doi.org/10.1016/j.jcis.2008.09.065.

[10] F.L. Theiss, S.J. Palmer, G.A. Ayoko, R.L. Frost, Sulfate intercalated layered double hydroxides prepared by the reformation effect, J Therm Anal Calorim. 107 (2012) 1123–1128. https://doi.org/10.1007/s10973-011-1369-0.

[11] S.A. Leslie, J.C. Mitchell, REMOVING GOLD COATING FROM SEM SAMPLES, Palaeontology. 50 (2007) 1459–1461. https://doi.org/10.1111/j.1475-4983.2007.00718.x.

[12] M. Manivannan, S. Rajendran, Ethylenediaminetetraacetic Acid-Zn2+ System as Corrosion Inhibitor for Carbon Steel in Sea Water, Asian J. Chem. 24 (2012) 4713–4716.

[13] S. Ghosh, V.L. Prasanna, B. Sowjanya, P. Srivani, M. Alagaraja, D. David, Inductively Coupled Plasma –Optical Emission Spectroscopy: A Review., 3 (n.d.) 11.

[14] P. Su, Sorption of metal ions to wood, pulp and bark materials, Abo Akademi, 2012.

[15] S. Cherevko, K.J.J. Mayrhofer, On-Line Inductively Coupled Plasma Spectrometry in Electrochemistry: Basic Principles and Applications, in: Encyclopedia of Interfacial Chemistry, Elsevier, 2018: pp. 326–335. https://doi.org/10.1016/B978-0-12-409547-2.13292-5.

[16] X. Hou, R.S. Amais, B.T. Jones, G.L. Donati, Inductively Coupled Plasma Optical Emission Spectrometry, Encyclopedia of Analytical Chemistry. (2016) 25.

[17] W. Li, A. Liu, H. Tian, D. Wang, Controlled Release of Nitrate and Molybdate Intercalated in Zn-Al-Layered Double Hydroxide Nanocontainers towards Marine Anticorrosion Applications, Colloid and Interface Science Communications. 24 (2018) 18–23. https://doi.org/10.1016/j.colcom.2018.03.003.

[18] H. Tian, W. Li, B. Hou, D. Wang, Insights into corrosion inhibition behavior of multi-active compounds for X65 pipeline steel in acidic oilfield formation water, Corrosion Science. 117 (2017) 43–58. https://doi.org/10.1016/j.corsci.2017.01.010.

[19] K.M. Deen, R. Ahmad, I.H. Khan, Corrosion Protection Evaluation of Mild Steel Painted Surface by Electrochemical Impedance Spectroscopy, (n.d.) 10.

[20] D.I. Njoku, M. Cui, H. Xiao, B. Shang, Y. Li, Understanding the anticorrosive protective mechanisms of modified epoxy coatings with improved barrier, active and self-healing functionalities: EIS and spectroscopic techniques, Sci Rep. 7 (2017) 15597. https://doi.org/10.1038/s41598-017-15845-0.

[21] Končan Volmajervarna, Steinbücher, Berce, Venturini, Gaberščček, Electrochemical Impedance Spectroscopy Study of Waterborne Epoxy Coating Film Formation, Coatings. 9 (2019) 254. https://doi.org/10.3390/coatings9040254.

[22] J. Kittel, N. Celati, M. Keddam, H. Takenouti, New methods for the study of organic coatings by EIS: New insights into attached and free films, Progress in Organic Coatings. 41 (2001) 93–98. https://doi.org/10.1016/S0300-9440(00)00155-7.

[23] R. Ding, J. Jiang, T. Gui, Study of impedance model and water transport behavior of modified solvent-free epoxy anticorrosion coating by EIS, J Coat Technol Res. 13 (2016) 501–515. https://doi.org/10.1007/s11998-015-9769-x.

[24] M.E. Orazem, N. Pébère, B. Tribollet, Enhanced Graphical Representation of Electrochemical Impedance Data, J. Electrochem. Soc. 153 (2006) B129. https://doi.org/10.1149/1.2168377.

Chapter 3 Synergy effect between layered double hydroxides (LDHs) and Ethylenediamine-N,N'-disuccinic acid (EDDS) for corrosion inhibition of carbon steel

This chapter is based on the original manuscript published in Applied Clay Science with the following reference:

Ayemi, G.J., Marcelin, S., Therias, S., Leroux, F., Normand, B., 2022. Synergy effect between layer double hydroxide (LDH) and EDDS for corrosion inhibition of carbon steel. Applied Clay Science 222, 106497. https://doi.org/10.1016/j.clay.2022.106497

3.1 Introduction

Organic coatings, inhibitors, and cathodic protection among others have been employed for corrosion protection of carbon steel [1–3]. Against environment, organic coatings are chosen for their barrier effect to protect the substrate. However, most organic coatings are prone to water uptake [4,5] which can lead to the substrate corrosion. To compensate this limitation**,** inhibitors can be added into the polymer matrix [6,7] to act with metallic cations from substrate to block the cathodic or anodic or both reactions at the metal/electrolyte interface. Therefore, special attention must be paid to the compatibility between the inhibitors and the organic matrix to ensure the protective character of the new protection system. Smart-coatings are developed to provide "active corrosion protection" for metal substrates [8,9], which confer the so-called "smart properties" of the coatings. A strategy widely used is to develop smart-coating is by incorporating a "guest host" assembly as a corrosion inhibitor reservoir with an ability to respond to an external stimulus [10].

Among these reservoirs, LDH as a promising reservoir for corrosion inhibitors had gained more attention. This is due to its particular chemical structure, which combines tunability and versatility in terms of: - a wide range of combinations between divalent and trivalent cations (Zn-Al, Mg-Al, Ni-Fe, Ni-Al, etc.), - a high anion exchange capacity (release and uptake) and, - a sensitive response to specific stimulus (exchange through mass action law, pH,…) [11–14].

Layered double hydroxides, named also hydrotalcite or anionic clay materials, are lamellar structures. They are composed of positively-charged hydroxide layers of mixed metallic cations, with negatively-charged exchangeable anions and water molecules present within their

interlayer gallery spacing. They have a similar structure to brucite ($Mg(OH)_2$) compounds. Partial substitution between divalent by trivalent cations is charge-balanced by the anions as illustrated by [15,16]. They have a general formula $\left[M^{2+}_{(1-x)}M^{3+}_{x}(OH)_2\right]^{+}\left[A_{x/n}\right]^{n-}.yH_2O$, where M^{2+} and M^{3+} are the divalent (Zn^{2+}, Mg^{2+}, Ca^{2+}, Ni^{2+}, Fe^{2+}, Co^{2+}, Cd^{2+}, etc) and trivalent (Al^{3+}, Cr^{3+}, Fe^{3+}, Co^{3+}, etc) metal cations, respectively, A^{n-} is the exchangeable charge-balancing anion with a valence of n which is located between the interlayer spacing, *x* is the ratio of $[M^{3+}]/([M^{3+}]+[M^{2+}])$ which is usually between $0.25 \leq x \leq 0.33$ range and *y* is number of water molecule [17].

Inhibitor-loaded LDH is an on-demand releasing system with the aim of delivering an inhibitive species to a targeted corrosion sites of the metallic substrate when exposed to electrolyte [2,7]. The inhibitor releasing from LDH is coupled with the simultaneous capturing of chloride ions from electrolyte environment. Therefore, LDH play a double inhibition role as a reservoir for corrosion inhibitor and also as a scavenger to trap aggressive species [18–20]. The following organic inhibitors: ethylenediaminetetraacetic acid (EDTA) [6], Benzothiazolylthio-succinic acid (BTSA) [19,21,22], benzotriazole (BTA) [12,14,23–25], 8-hydroxyquinoline (8-HQ) [14], Indole-3 butyric acid (IBA) [26,27] intercalated into their respective reservoir had been studied to hinder carbon steel corrosion. That is, the inhibitor released from LDH migrates to the metallic substrate, are adsorbed or form a protective barrier or oxide film which could block either or both the anodic or cathodic reactions of corrosion [14,20,28]. Most of the studies were focused only on the releasing ability of LDH but had neglected the solubility of LDH scaffold in the electrolyte solution. There are limited studies on the contribution of each individual components of LDHs and/or synergistic effect between their component on carbon steel corrosion inhibition.

As mentioned earlier, EDTA acts as a corrosion inhibitor for carbon steel. However, it is harmful and should be replaced by another compound. Biodegradable ethylenediamine-N,N′-disuccinic acid (EDDS) has a chemical structure close to the EDTA [29], as chelating agent able to hexadentate thus, it should be a good candidate to protect carbon steel against corrosion. This work is an opportunity to fill this knowledge gap and also to study the efficiency of EDDS, little studied as free inhibitor or intercalated into LDH. This work focusses on the synthesis and characterization of intrinsic properties of Zn_2Al LDH intercalated with organic anion of ethylenediamine-N,N′-disuccinate solution ($EDDS^{4-}$). Co-precipitation process was used for the synthesis of Zn_2Al-$EDDS^{4-}$ LDH.

The crystal structure of the Zn_2Al-$EDDS^{4-}$ LDH was studied using X-ray diffraction (XRD). Scanning Electron Microscopy (SEM) was employed to study the morphology of LDH power and protective layer formed at the surface of the carbon steel substrate after immersion in chloride solution. ICP-OES was used to measure the solubility of zinc and aluminum hydroxides layers. To elucidate the inhibitive mechanism from the Zn_2Al-$EDDS^{4-}$ LDH, the inhibitive effect of each element which includes Zn^{2+}, Al^{3+} and $EDDS^{4-}$ and the synergistic inhibition effect of these components in 0.1M sodium chloride solution was studied by anodic polarization curves and by electrochemical impedance spectroscopy performed at corrosion potential to evaluate their efficiency as carbon steel corrosion inhibitor.

3.2 Experimental

3.2.1 Materials

For reminder LDH were synthetized by using Zinc nitrate hexahydrate $Zn(NO_3)_2.6H_2O$ (98 extra, Acros Organics), aluminum nitrate nonahydrate $Al(NO_3)_3.9H_2O$ (99%, Acros Organics), sodium nitrate $NaNO_3$ (Prolabo), sodium hydroxide NaOH (> 98%, Sigma Aldrich), 35% in water ethylenediamine-N,N′-disuccinic acid trisodium salt solution $C_{10}H_{13}N_2Na_3O_8$ (pKa = 2.4, Sigma Aldrich), and sodium chloride (Sigma Aldrich).

Before each experiment, the carbon steel was mechanically polished with SiC abrasive papers down to 2400 grade, then rinsed with ethanol in ultrasonic bath before air drying.

3.2.2 Analytical characterizations

X-ray diffraction measurements were performed with a Bruker diffractometer (Cu $K_{\alpha'}$ λ=1.5406Å radiation source, Lynx eye detection, 2θ scan range of 5° - 90° in 0.02° scan steps and 184 s count time per step) to characterize the intercalation of EDDS, the crystal structure of LDHs, and to highlight the anion exchange between $EDDS^{4-}$ and Cl^- providing from the electrolyte. The sample for studying the anion exchange between $EDDS^{4-}$ and Cl^- in electrolyte solution was obtained in a powder form, after 72 h of magnetic stirring and dehydration of the neutral chloride solution containing the inhibitive species (0.1 M NaCl+15 g/L Zn_2Al-$EDDS^{4-}$ LDH).

As a reminder, SEM observations were carried out using a VEGA3 TESCAN and a Zeiss Supra 55VP apparatus to observed the morphologies of the Zn_2Al-$EDDS^{4-}$ LDH and the surface state of the carbon steel after immersion in different electrolytes, respectively.

3.2.3 Quantification of hydroxide layers dissolution by ICP-OES

The solubility of Zn_2Al-$EDDS^{4-}$ LDH scaffold in 0.1 M NaCl was studied by an inductively coupled plasma-optical emission spectroscopy (ICP-OES). The principle of the technic is presented in chapter 2.

150 mg of LDH-$EDDS^{4-}$ slurry was added to 10 mL of 0.1M NaCl solution and then magnetically stirred at 300 rpm for 1 h. The mixture was centrifuged at 4500 rpm for 45 mins to obtain a clear extracted solution. The same procedure was repeated up to 72 h. For each extracted solution, the pH was measured using a standard pH meter PHM210 by radiometer analytical. The concentrations of Zn^{2+} and Al^{3+} metallic cations released from the LDH were measured using ICP-OES modelled as iCAP 7400 by thermofischer scientific. The analysis was performed in an axial and radial mode with the glass expansion nebulizer at 0.5 mL/min argon (standard ICP-AES conditions).

3.2.4 Electrochemical characterizations

To evaluate the inhibitive effect of the Zn_2Al-EDDS LDH on carbon steel corrosion, a standard three-electrodes set-up was used. It was constituted by a saturated calomel electrode (SCE) as the reference electrode and a cylindrical platinum grid as the counter electrode. The working electrode was a rotating disk electrode (RDE) with an exposed disk area of 1 cm^2 of the bare carbon steel. The speed of electrode rotation was fixed at 200 rpm. The volume of the electrochemical cell was 100 mL.

The blank electrolyte solution was constituted by 0.1M NaCl solution (pH = 5.8). To investigate the inhibition mechanism, the following inhibitive component were added to the neutral blank chloride solution: 0.02 M $Zn(OH)_2$, 0.01 M $Al(OH)_3$, 0.01 M EDDS, either alone, or mixed, and Zn_2Al-$EDDS^{4-}$ LDH slurry (5 g/L and 15 g/L). The concentrations of the individual component were chosen with respect to the synthesis molar ratio. For each electrolyte, a volume of 100 mL was prepared by magnetic stirring for 72 hours to obtain a clear extract solution, and the pH of the electrolyte solution was measured before carbon steel electrode immersion.

The electrochemical measurements were carried out in a systematic route and were performed using a Biologic SP-300 potentiostat, at room temperature and under a faraday cage. All electrochemical impedance spectroscopy (EIS) measurements were performed using the last defined solution to ensure and control the compounds releasing. After 24 hours of immersion in the last solution, EIS was performed at corrosion potential, using a 10 mV RMS amplitude

sinusoidal perturbation, between 10^5 Hz and 3 mHz and with 8 points per decade. Anodic polarization curves were recorded between from -50 mV vs OCP to +0 V/SCE with a scan rate of 1 mV/s. All measurements were repeated at least three times to ensure the reproducibility. More also, after immersion at the corrosion potential, the surfaces of the carbon steel were observed at macro- and microscopic (by SEM, as earlier mentioned) scale.

3.3 Results and discussion

3.3.1 Characterization of LDH-EDDS^{4-}

From the SEM images, the particles of Zn_2Al-EDDS^{4-} LDH exhibited stacked of agglomerated platelet-like morphology (Fig. 3.1) which is typical of layered double hydroxides [23]. This morphology could be attributed to the nucleation and crystal growth of the LDH particles as a function of the pH value. The observed agglomeration could be due to the initial stages of sheets growth. LDHs are best crystallized at high pH [30,31]. The sample has the typical plate-like morphology of LDH. The LDH particle size is varying and is of the order of a few micrometers.

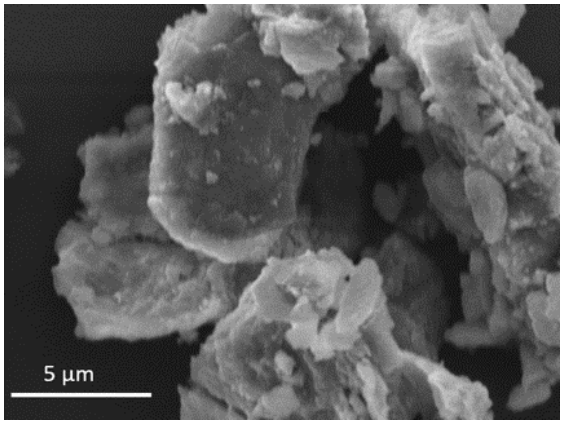

Figure 3.1: SEM micrograph obtained for synthetized Zn_2Al-EDDS^{4-} LDH.

The recorded XRD pattern of the synthesized Zn_2Al-EDDS^{4-} LDH powders is presented in Figure 3.2 and shows diffraction peaks at 2θ angles of 6.33°, 12.78°, 19.16°, 34.40° and 61.07°, corresponding to the reflection by (003), (006), (009), (012) and (110) planes of the LDH crystal structure, respectively. The pattern exhibits nearly symmetric diffraction peaks which suggest that, the synthesized powder is monophasic. The presence of a sharp diffraction reflection peak at (003) confirmed the accommodation of EDDS^{4-} anion into the interlayer galleries of LDH host [6,24,32]. The characteristic diffraction reflections corresponding to R$\bar{3}$m (space group) rhombohedral symmetry were indexed to a hexagonal lattice, generally used to describe LDH crystal structures [6,24]. The anions size and the staking direction of the LDH crystal structure,

determine the basal spacing of the hydroxide layers [24,33,34]. Therefore, using Bragg's law (eq. 3.1), the basal spacing (*d*) was calculated from the most intense reflection (003) position) [35,36]. The $d_{(hkl)}$ values for the diffraction positions (003), (006), and (009) were estimated to be 1.382 nm, 0.691 nm and 0.461 nm respectively, close to that reported for EDTA with 1.462 nm [6], signifying that the Zn_2Al-EDDS LDH has a proper stacking direction order and possess a typical brucite layers structure since d(003)= 2d(006) =3d(009) [6,37]. Equation 3.2, was used to determine the gallery height (*h*) of the LDH by subtracting the cationic inorganic layer thickness (t = 0.471 nm = brucite layer) from the ($d_{(003)}$) value [6,7]. By using equations 3.3 and 3.4, the lattice parameters (*a*, *c*) were estimated from the diffraction reflections (110) and (003), respectively [6,38,39]). The lattice parameter *c*, depends on both the charge and size of the anions [24,37]. The lattice as well as other parameters that characterized crystal structure of the synthesized Zn_2Al-$EDDS^{4-}$ LDH are listed in Table 3.1.

$$d = \frac{n\lambda}{2\sin\theta} \quad \text{(eq. 3.1)}$$

$$h = d - t \quad \text{(eq. 3.2)}$$

$$a = 2d_{(110)} \quad \text{(eq. 3.3)}$$

$$c = 3d_{(003)} \quad \text{(eq. 3.4)}$$

Where, *d*, λ, *t*, *h* and θ are the interlayers basal spacing, wavelength of the incident X-ray beam, layers thickness, gallery height and diffraction angle between the incident X-ray and the reflection crystal plane, in nm and degrees, respectively. The parameter *n* is a constant representing the reflection order, it is usually taken to be 1.

Figure 3.2 (in Red) shows the XRD pattern for Zn_2Al-$EDDS^{4-}$ LDH after exposure to the NaCl solution. Sharp diffraction peaks observed at 2θ angle of 27.4°, 31.7°, 45.5°, 56.5°, 66.2°, 75.3° and 84.1° are ascribed to NaCl structure. The harmonic diffraction peaks of Zn_2Al-$EDDS^{4-}$ LDH after exposure are shifted to higher 2θ values. The peak (003) initially observed at 2θ = 6.4° is shifted to 2 θ = 11.8° giving a basal spacing of d = 0.75 nm, while (006) observed at 2θ = 12.8° is shifted 2θ = 22.9°. After contacting with NaCl, the LDH structure is then modified with a smaller basal spacing of 0.75 nm, value that is similar to chloride LDH reported in the literature [37]. This result suggests the replacement of $EDDS^{4-}$ anion by chloride anion thereby validates the anion-exchange ability of functionalized LDH. Interestingly it shows that even

multiple tethered molecule such as EDDS with its four carboxylate functions, two on each inner-side, is easily released out of LDH host, thanks to a mass action law favoring the uptake of chloride anions.

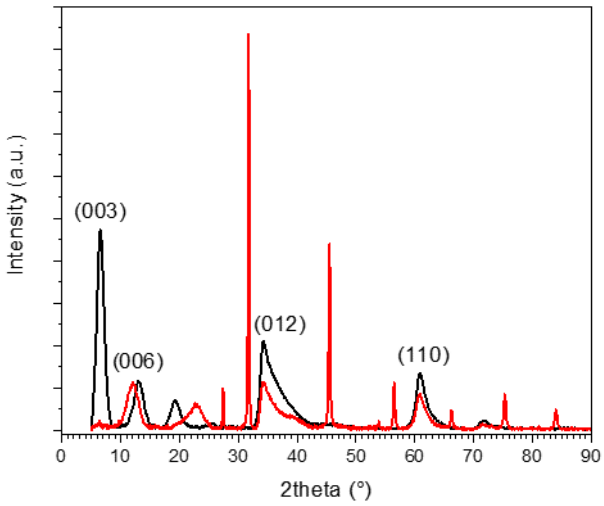

Figure 3.2: XRD patterns for LDHs containing EDDS before (in black) and after exposure (in red) to the neutral chloride solution.

It is generally reported that LDHs release anions from their interlayer space through ion-exchange mechanism, few studies investigate the releasing of the cations composing the sheets. For this purpose, ICP-OES analysis were performed to determine the content of divalent and trivalent metallic cations released from Zn_2Al-EDDS LDH. Table 3.2 reports the concentrations for Zn^{2+} and Al^{3+} as a function of magnetic stirring time in the 0.1M NaCl solution. The pH of all extracted solutions was constant during time and close to the neutrality. The results reveal the presence of zinc and aluminum cations with a significant difference in concentrations (about 42 mg/L and about 0.5 mg/L for Zn^{2+} and Al^{3+}, respectively for the solution extracted after 72 h of stirring) that needs to be further quantified and compare to the initial quantity. Table 3.3 reports the ratio of dissolved cation/initial quantity for Zn^{2+} and Al^{3+}, in weight percent, calculated from the amount of initial LDH structure concerned by the dissolution (150 mg of LDH-EDDS in 10 mL of NaCl solution). The cation concentration measured in solution after the longest time of 72h leads to less than 1% by mass of the initial cation quantity of LDH powder. This explains that it is not significant enough to affect the XRD pattern. Moreover, the dissolved amount is not enough to de-stabilize LDH sheet structure. From Table 3.2, it is interesting to note that, Zn^{2+} cations are no longer released after 24 h. On the other hand, Al^{3+} cations were not significantly dissolved. Such pronounced difference in dissolution between cations results

in LDH material with a ratio Al^{3+}/Zn^{2+} slightly higher than initially, so leaving LDH structure prone to trap even more chlorine anions.

Table 3.1: Basal spacing (*d*), gallery height (*h*) and lattice parameters (*a*, *c*) obtained from Zn_2Al LDH intercalated with $EDDS^{4-}$ anion.

	d (nm)	*h* (nm)	*a* (nm)	*c* (nm)
Zn_2Al-$EDDS^{4-}$ LDH	1.382	0.911	0.303	4.146

Table 3.2: Concentrations of Zn^{2+} and Al^{3+} released during time from Zn_2Al-$EDDS^{4-}$ LDH extracted solutions in exposure in 0.1M NaCl solution

Magnetic Stirring Time (h)	Zn^{2+} (mg/L)	Al^{3+} (mg/L)	pH at 25°C
1	21.1	0.13	6.9
24	49.20	0.14	6.8
72	41.50	0.50	6.7

Table 3.3: Mole and weight of Zn_2Al-$EDDS^{4-}$ LDH, Zn^{2+} and Al^{3+} initially presents in the 150 mg of LDH and ratio between dissolved cation and initial quantity of cation after 72h of magnetic stirring in 10 mL of 0.1M NaCl solution (from Table 3.2).

Chemical species	Mole (n)	Weight (mg)	ratio [dissolved cation/initial quantity] (wt. %)
Zn_2Al-$EDDS^{4-}$ LDH	$0.407\ 10^{-3}$	150	-
Zn^{2+}	$0.814\ 10^{-3}$	53	0.78
Al^{3+}	$0.407\ 10^{-3}$	11	0.045

Therefore, the results validate the fact that, functionalized LDHs do not only released $EDDS^{4-}$ anions (and trap chloride anions), but also a part of zinc cations. These two components could play a role in the inhibition of the carbon steel corrosion, which is investigated in the next section.

3.3.2 Electrochemical behavior of carbon steel in the presence of LDH-EDDS^{4-} and the role of each components

Polarization curves obtained for the carbon steel after 24 h of immersion in the chloride solution and the solution containing the synthetized EDDS-LDH at two different concentrations (5 and 15 g/L) are presented in Figure 3.3. In the presence of Zn_2Al-EDDS^{4-} LDH, the corrosion potential shifts towards more anodic value meanwhile a decrease of the anodic current density values were observed. This trend was emphasized when the functionalized LDH concentration increases. Deip *et al.* observed similar trends from commercially produced Zn-Al layered double hydroxide intercalated with BTA for carbon steel immersed in 35 wt. % NaCl electrolytes [12]. For the highest concentration of LDH-EDDS^{4-}, the anodic domain is characterized by a pseudo-passive plateau between -0.5 and -0.3 V/SCE and the anodic current density is about 10^{-2} A/cm^2. From these observations, it can be concluded that the shift in corrosion potential and the decrease in anodic current densities is due to either the effect of synthesized Zn_2Al-EDDS^{4-} LDH (leading to the presence of EDD^{4-} and Zn^{2+} in the electrolyte) or the decrease in the aggressiveness of the environment as a result of chloride entrapment by LDH, or both.

To validate these facts and discriminate the effect of these species, anodic polarization curves are performed for individual components of LDH alone or mixed using the same protocol as previous. The results are presented in Figures 3.4 and 3.5.

In the presence of EDDS alone, the corrosion potential is shifted to more anodic value (-0.55 V/SCE by comparison with the chloride (blank) solution where the corrosion potential value is about -0.70 V/SCE). The anodic current densities are lower than for the reference result. The shape of the polarization curve in the anodic domain is similar to that of the anodic curve presented in Figure 3.3, for the highest concentration of LDH.

In the presence of zinc hydroxide alone, the electrochemical behavior of the carbon steel is different with a shift to more anodic value of the corrosion potential, and a more decrease in the anodic current density. Moreover, the shape of the polarization curve exhibits a pseudo-passive plateau before a significant increase of the current densities at around -0.35 V/SCE. It should be underlined that the pH in the presence of EDDS is more basic than in the presence of $Zn(OH)_2$. For comparison, the polarization curve obtained in presence of aluminum hydroxide (0.01 M) was similar to the curve obtained in the blank chloride solution. This last result shows that Al^{3+} cations do not modify the reactivity of the carbon steel and thus, the weak released content from LDH does not act in inhibiting the corrosion for carbon steel.

In the presence of both Zn^{2+} cations and $EDDS^{4-}$ anions in the neutral chloride solution (0.1 M), the anodic polarization curve (Figure 3.5) is different compare to when these species are alone (Fig. 3.4). A sharp decrease of the anodic current densities and a plateau defined in a large potential domain where the anodic current density is closed to 10^{-5} A/cm² followed by an increase in current density at -0.15 V/SCE, corresponding to a pitting potential was observed. This result clearly shows the synergy effect between zinc cation and EDDS to inhibit carbon steel corrosion. The polarization curves obtained in presence of Al^{3+} alone (Fig. 3.4) or in mixture with EDDS and zinc hydroxide (Fig. 3.5) confirms its spectator role as the curves were not modified. Thus, the inhibitive properties of the hybrid Zn_2Al-$EDDS^{4-}$ come from the decrease of chloride content by trapping and/or from the synergy between zinc cations and $EDDS^{4-}$ anions. It must be underlined that Al^{3+} doesn't play a role on the corrosion inhibition of carbon steel but needed to stabilize the structure of the LDH.

Figure 3.6 shows the surface states of the carbon steel after 24 h of immersion at corrosion potential in different electrolytes. The Zn_2Al-$EDDS^{4-}$ LDH (5 g/L) limits the dissolution of iron by comparison with the sample immersed in the neutral chloride solution (generalized corrosion), but some corrosion defects are visible. When only Zn^{2+} cations are present in the electrolyte, the sample was protected by the formation of some whitish scales-like precipitates at the surface. The corrosion which appears on the surface of the carbon steel exhibited a spiral form due to hydrodynamics motion of the disk electrode. For EDDS alone in the chloride solution, the surface of the sample looks grey and there were no visible corrosion spots when compare to the sample immersed in LDH solutions. There could be a complexing effect of EDDS with Fe(II) or Fe(III) similar to that of EDTA [29]. However, when Zn^{2+} and EDDS are in mixed in solution, the carbon steel surface was totally protected.

Electrochemical impedance spectroscopy was carried out to obtain more information about the inhibitive mechanism provided by LDH containing EDDS. Figure 3.7 shows the impedance diagrams, in Bode coordinates, obtained for the carbon steel after 24h of immersion at corrosion potential in the neutral aerated chloride solution without inhibitive component and the solution containing Zn_2Al-$EDDS^{4-}$ LDH components for two different concentrations. For the 0.1 M NaCl electrolyte, the impedance diagram was characterized by one single time constant at around 0.3 Hz, attributed to the charge transfer due to the dissolution of iron. When Zn_2Al-$EDDS^{4-}$ LDH was added in the blank electrolyte, the impedance modulus was higher than without and highest for the more concentrated solution. In parallel, the phase diagram shows a sec-

ond time constant at higher frequency, which was described in literature as the chelation between ethylenediamine-N,N'-disuccinic acid molecule and divalent metallic iron cation [38]. The LDH concentration in the electrolyte is an important parameter because the electrochemical response was different when the concentration is higher, the substrate being more resistive to the corrosion phenomena. This result indicates that the synergy effect between Zn^{2+} and $EDDS^{4-}$ ions depends on the LDH concentration in the electrolyte.

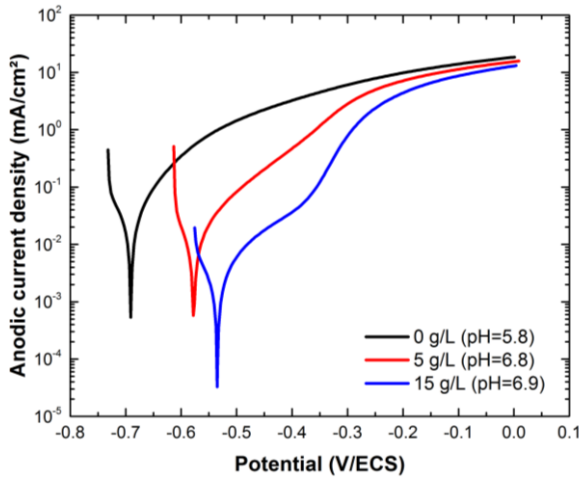

Figure 3.3: Anodic polarization curves obtained for the carbon steel (RDE rotation speed = 200 rpm) after 24 h in the neutral chloride solution and containing different concentrations of Zn_2Al-$EDDS^{4-}$ LDH.

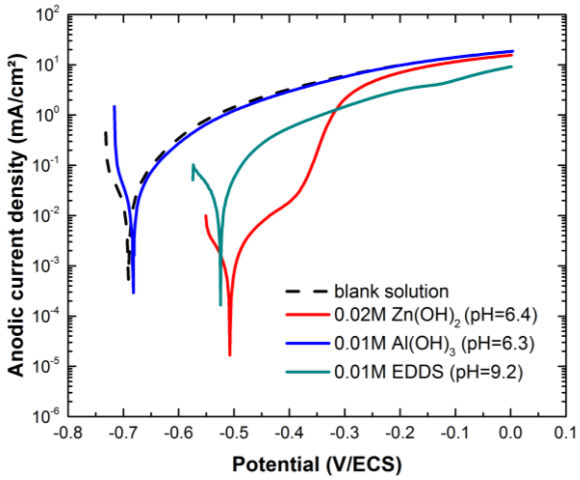

Figure 3.4: Anodic polarization curves for the carbon steel (RDE rotation speed = 200 rpm) obtained after 24 h in the 0.1M NaCl electrolyte containing the components that are part of the synthetized Zn_2Al-$EDDS^{4-}$. The curve in dashed line, obtained in the neutral chloride solution is reported for comparison.

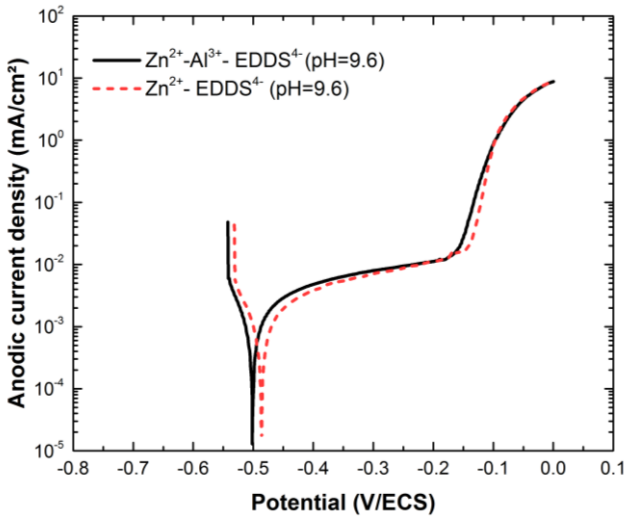

Figure 3.5: Anodic polarization curves obtained for the carbon steel (RDE rotation speed = 200 rpm) after 24 h of immersion in the solution containing the anion couple Zn^{2+} + $EDDS^{4-}$ and with Al^{3+} cations.

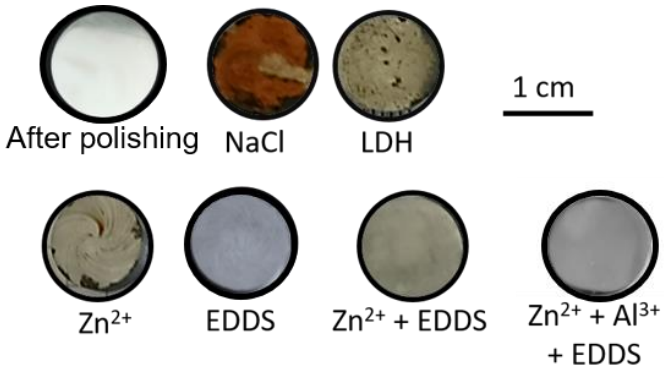

Figure 3.6: Macrographs of the carbon steel sample exposed during 24 h to the neutral chloride solution (RDE rotation speed = 200 rpm) with the addition of components alone or in mixture.

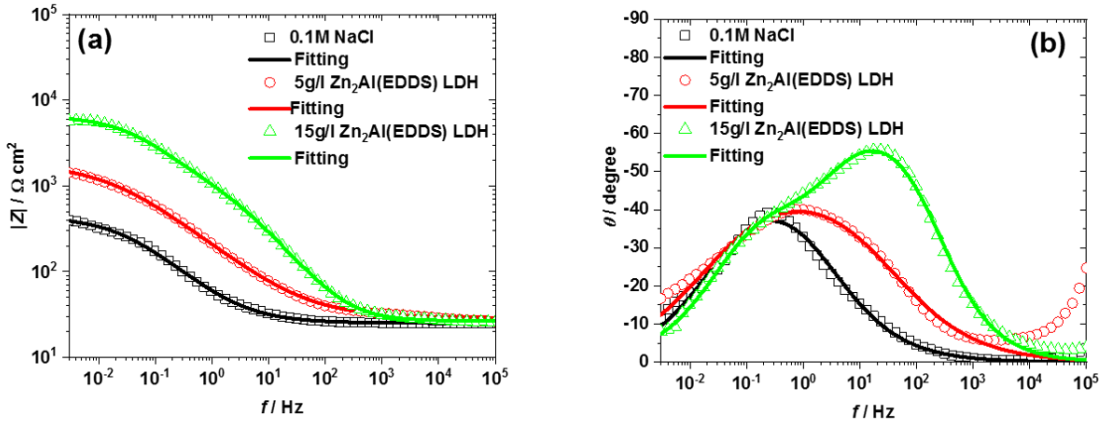

Figure 3.7: Electrochemical impedance diagrams in Bode coordinates: (a) impedance modulus and (b) phase angle *vs* frequency, obtained at corrosion potential for the carbon steel after 24h of immersion in 0.1M NaCl containing Zn_2Al-$EDDS^{4-}$ LDH (RDE rotation speed = 200 rpm). The result obtained without inhibitive components is reported for comparison.

In the same way than the previous result from the potentiodynamic measurements, impedance diagrams are obtained after 24 h of immersion in the chloride solution containing the different components constituting the functionalized LDH, either alone, or in mixture (Fig. 3.8). The shape of impedance diagrams was different for the different electrolytes. In the presence of zinc, the Bode diagram was characterized by two-time constants. By analogy to the previous results, the low frequency time constant can be attributed to the dissolution of iron and the high frequency time constant can be attributed to the precipitation of Zn^{2+} onto the carbon steel surface as described for the galvanized steel. The corrosion of steel could increase the interfacial pH and promote simonkoellite ($Zn_5(OH)_8Cl_2$-H_2O) precipitation [40]. The impedance diagrams in presence of EDDS alone was characterized by a single time constant at medium frequency. This could be attributed to charge transfer by complexing effect of EDDS with divalent or trivalent iron. When both species (Zn and EDDS) are in the electrolyte, the impedance diagram was characterized by two imbricated time constants and the impedance modulus at low frequency was highest. These observations agree with the polarization curves and highlight the beneficial impact of the synergistic effect between zinc and EDDS ions. The impedance diagrams are fitted by using electrical equivalent circuit (Figs. 3.9 a and b) for the one-time constant and two-time constants impedance diagrams respectively, to extract the kinetic characteristics of the metal/electrolyte interface. The high frequency time constant was attributed to the presence of a film (chelate or pseudo-passivation of iron regarding the case) and the low frequency time constant is attributed to the charge transfer related to iron dissolution. The electrolyte resistance (R_e) and the CPE parameters, α and Q are graphically extracted according to

[41], and these values were introduced into the model to guide the fit as hypothesis parameters. The adjustment of the impedance data was performed using a recently available software that employs simplex to fine-tune initial guesses and Levenberg-Marquardt regression to extract parameters (https:///escarxiv.org/kze9x). Table 3.4 reports the fitted parameters as well as the inhibition efficiency obtained from the equation 3.5, where $R_{ct,0}$ and $R_{ct,inh}$ are the charge transfer resistances without and with inhibitive component, respectively [42]:

$$IE\ (\%) = \frac{R_{ct,inh} - R_{ct,0}}{R_{ct,inh}} \qquad \text{(eq. 3.5)}$$

The micrographs of the carbon steel surface after 24 h of immersion at corrosion potential in the different electrolytes, obtained by SEM, are presented in Figure 3.10. The impedance results are discussed regarding to the surface observations.

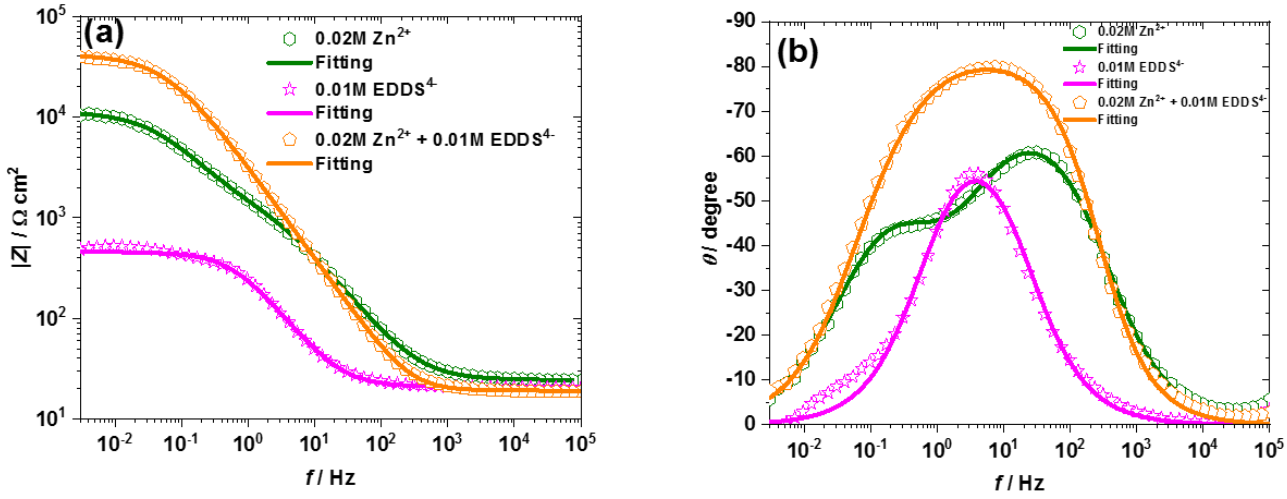

Figure 3.8: Electrochemical Bode impedance diagrams obtained at corrosion potential for the carbon steel after 24h of immersion in the neutral chloride solution (rotation speed = 200 rpm) containing 0.02M Zn^{2+} or/and 0.01M $EDDS^{4-}$ ions.

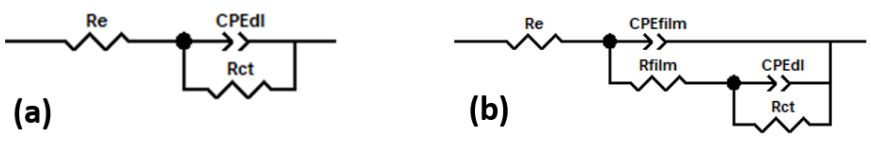

Figure 3.9: Electrical equivalent circuits used to fit the impedance diagrams characterized by: (a) one single-time constant and (b) two well defined or not well dissociated time constants.

Table 3.4: Impedance parameters obtained from the fitting procedure using electrical equivalent circuits presented in Figure 9 and the Levenberg-Marquardt regression (https:///es-carxiv.org/kze9x).

Electrolyte	Model used	Re / Ω cm^2	α_{film}	Q_{film} / Ω^{-1} cm^{-2} s$^{\alpha}$	R_{film} / Ω cm^2	α_{dl}	Q_{dl} / Ω^{-1} cm^{-2} s$^{\alpha}$	R_{ct} / Ω cm^2	IE / %
Blank solution (0.1 M NaCl)	Fig. 9a	25 ± 0.1	-	-	-	0.63 ± 0.004	7.12 10^{-3} ± 5.8 10^{-5}	418 ± 5	-
Blank + LDH-EDDS^{4-} (5 g/L)	Fig. 9a	29 ± 0.2	-	-	-	0.55 ± 0.003	1.80 10^{-3} 1.4 10^{-5}	1789 ± 25	77
Blank + LDH-EDDS^{4-} (15 g/L)	Fig. 9b	27 ± 0.1	0.77 ± 0.004	1.32 10^{-4} ± 3.5 10^{-6}	1223 ± 71	0.62 ± 0.013	3.57 10^{-4} ± 1.0 10^{-5}	5392 ± 127	92
Blank + Zn^{2+}	Fig. 9b	25 ± 0.1	0.81 ± 0.003	7.79 10^{-5} ± 1.3 10^{-6}	1657 ± 48	0.73 ± 0.008	2.17 10^{-4} ± 2.6 10^{-6}	9707 ± 106	95
Blank + EDDS^{4-}	Fig. 9a	21 ± 0.1				0.84 ± 0.005	7.75 10^{-4} ± 1.5 10^{-5}	473 ± 4	11
Blank + Zn^{2+} + EDDS^{4-}	Fig. 9b	19 ± 0.1	0.91 ± 0.002	5.65 10^{-5} ± 7.3 10^{-7}	20642 ± 2970	0.62 ± 0.063	6.69 10^{-5} ± 2.4 10^{-5}	21568 ± 3450	98

The electrochemical behavior of carbon steel is different when either $Zn(OH)_2$, or EDDS is added to the neutral chloride solution (Fig. 3.8). In the presence of Zn^{2+}, a contribution of the impedance response was attributed to the presence of a film leading to the high charge transfer resistance (about 10^4 Ω cm^2, Table 3.4). The SEM micrographs revealed the presence of the passive zinc-based film and some precipitation at the surface of carbon steel which could be described as Simonkolleite ($Zn_5(OH)_8Cl_2.H_2O$) precipitates (Fig. 3.10a). The surface modification must be due to the dissolution of iron which induces the interfacial pH thereby promote simonkolleite precipitation [40]. This proposed mechanism agrees with the polarization curve in Figure 3.4. Moreover, the inhibition efficiency as high as 95 % (Table 3.4) explained by the beneficial impact of Zn^{2+} precipitation on the surface of carbon steel similar to the cutting edge protection of galvanized steel [43].

In the presence of EDDS alone in the 0.1 M NaCl solution, the charge transfer resistance value was low and in the same order of magnitude with that of 0.1 M NaCl electrolyte (around 400-500 Ω cm^2, Table 3.4). The carbon steel surface state was characterized by the presence of pits of about 20 µm of diameter and the selective attack of iron cation due to its complexes with EDDS^{4-} anions (Figs. 3.10 b and c), respectively. The lowest inhibition efficiency equal to 11% could be attributed to the localized corrosion due to the effect of chlorides ions.

When both Zn^{2+} and EDDS^{4-} are in mixture, the carbon steel surface was fully protected (Fig. 3.10 d) with no evidences of corrosion. From the impedance parameters reported in Table 3.4, the film resistance which was attributed to the pseudo-passivation of iron and the chelate between Fe^{2+} ions and EDDS^{4-}, was about ten times higher than for the electrolyte containing only

Zn^{2+} alone and, the charge transfer resistance was twice higher. The synergy mechanism was attributed to the adsorption of $EDDS^{4-}$ together with a modification of the interfacial pH in presence of Zn^{2+}. The inhibition efficiency, reported in Table 3.4, equal to 98 % is the result of the concomitant effect between both components acting in synergy in terms of their efficiency.

The concentration of Zn_2Al-$EDDS^{4-}$ LDH in the electrolyte has a direct effect on the electrochemical behavior of the carbon steel with the appearance of higher impedance modulus for higher content of LDH (15 g/L). The higher the content in solution, the higher the exchange between intercalated $EDDS^{4-}$ anions and Cl^- anions from the electrolyte. The corrosiveness of solution decreases due the entrapment of chloride by the LDH scavenger while the complex formation between $EDDS^{4-}$ anions and Fe^{2+} cations promote protective film formation thereby enhance corrosion protection. The SEM micrograph obtained for a protected surface at the lower concentration of hybrid LDH (5 g/L) (Fig. 3.10 f) shows two types of surface state most presumably coming from Zn-based films and the formation of complexes between EDDS molecules and the iron. In comparison to Figure 3.10 a, the spider web shaped network must come from Zn-based films while coarser, whiter (under electron beam so more insulating) lumps seem to come from EDDS(Fe) complexes. From the impedance diagrams (Fig. 3.7) and the associated refined parameters (Table 3.4), it clearly shows that the efficiency of the synthetized Zn_2Al-$EDDS^{4-}$ LDH depends on its concentration in the electrolyte.

The inhibition mechanism from Zn_2Al-$EDDS^{4-}$ LDH could be explained by:

(i) Zn_2Al-$EDDS^{4-}$ LDH promotes the decrease of the corrosiveness of the electrolyte by exchange between Cl^- and $EDDS^{4-}$ out of the LDH cargo,

(ii) the release of EDDS induces corrosion inhibition by a complexing effect with Fe^{2+}, while such increase in anodic dissolution induces an increase in zinc (II) reduction which should modify the interfacial pH.

(iii) These phenomena promote the precipitation of the simonkoellite or LDH on the surface, and the adhesion of the corrosion products should be due to the mixture between Fe(II) or Fe(III)-EDDS complex and LDH or simonkoellite, surface analysis are in progress to validate this assumption.

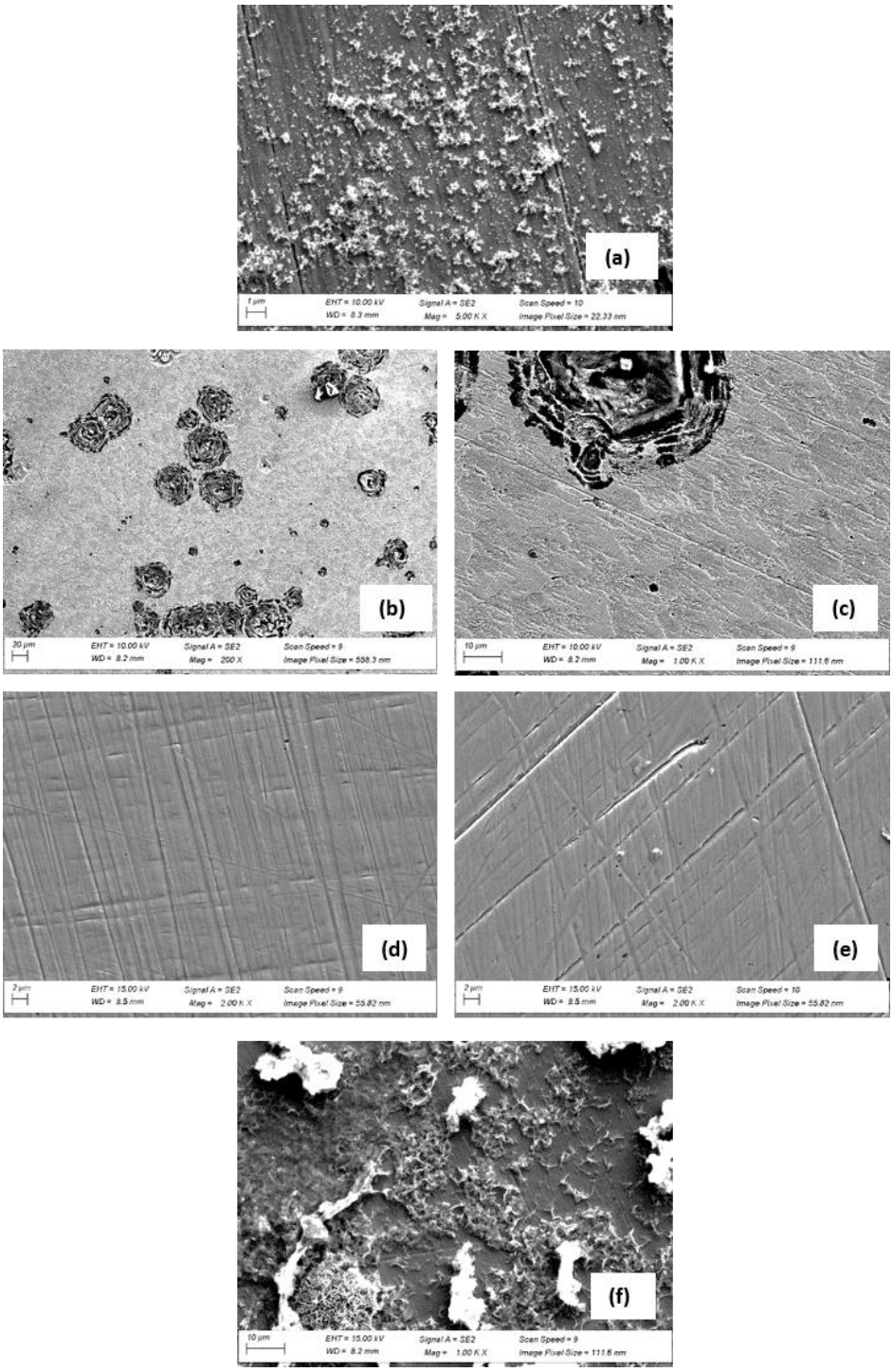

Figure 3.10: SEM micrographs of the carbon steel after 24 h of immersion in the neutral chloride solution (200 rpm) containing: (a) 0.02 M of $Zn(OH)_2$ (pH = 6.4), (b) and (c) 0.01 M of EDDS at different magnifications (pH = 9.2), (d) 0.02 M of $Zn(OH)_2$ + 0.01 M EDDS (pH = 9.6) and (e) 0.02 M $Zn(OH)_2$ + 0.01 M EDDS + 0.01 M $Al(OH)_3$ (pH = 9.6) and (f) 5 g/L of Zn_2Al-$EDDS^{4-}$ LDH (pH = 6.8).

3.4 Conclusion

This work focuses on understanding the mechanism of inhibition of carbon steel in presence of a host/guest-based inhibitor. Selected hybrid $[Zn_2Al(OH)_6]^+[EDDS^{4-}]_{0.25}.2H_2O$ LDH is found to inhibit effectively exhibit corrosion protection that is not only due to anion-exchange mechanism but also a partial and rather selective solubility of the LDH scaffold leading to the presence of zinc in solution. A synergy effect between zinc hydroxide and EDDS was clearly identified. From the electrochemical results some important points can be summarized below:

- Trapping effect of chloride by anion exchange with intercalated EDDS in the LDH cargo inducing a decreasing of aggressiveness of the electrolyte,

- Releasing of both $EDDS^{4-}$ and Zn^{2+} ions from LDH scaffold due to its partial solubility,

- Synergy effect between $EDDS^{4-}$ and Zn^{2+} explained by a competitive effect between the adsorption of EDDS and the buffering effect from the Zn^{2+} precipitation on carbon steel surface,

- Al^{3+} has no role in inhibiting corrosion of carbon steel.

This chapter has demonstrated the effectiveness of the inhibition provided by the Zn_2Al-$EDDS^{4-}$ LDH material. The next chapter will identify the effectiveness this material in an epoxy matrix.

References

[1] E.J. Ekott, E.J. Akpabio, U.I. Etukudo, Cathodic Protection of Buried Steel Oil Pipelines in Niger Delta, Environmental Research J. 6 (2012) 304–307. https://doi.org/10.3923/erj.2012.304.307.

[2] D.T. Nguyen, H.T.X. To, J. Gervasi, Y. Paint, M. Gonon, M.-G. Olivier, Corrosion inhibition of carbon steel by hydrotalcites modified with different organic carboxylic acids for organic coatings, Progress in Organic Coatings. 124 (2018) 256–266. https://doi.org/10.1016/j.porgcoat.2017.12.006.

[3] O.W. Obot, C.N. Anyakwo, An Investigation of Internal Corrosion of Oil and Gas Transporting Carbon Steel Pipes in the Niger Delta Area of Nigeria, EJERS. 2 (2017) 22. https://doi.org/10.24018/ejers.2017.2.8.374.

[4] L. Garden, R.A. Pethrick, A dielectric study of water uptake in epoxy resin systems, J. Appl. Polym. Sci. 134 (2017). https://doi.org/10.1002/app.44717.

[5] S. Morsch, S. Lyon, P. Greensmith, S.D. Smith, S.R. Gibbon, Mapping water uptake in organic coatings using AFM-IR, Faraday Discuss. 180 (2015) 527–542. https://doi.org/10.1039/C4FD00229F.

[6] T. Stimpfling, F. Leroux, H. Hintze-Bruening, Unraveling EDTA corrosion inhibition when interleaved into Layered Double Hydroxide epoxy filler system coated onto aluminum AA 2024, Applied Clay Science. 83–84 (2013) 32–41. https://doi.org/10.1016/j.clay.2013.08.005.

[7] T. Stimpfling, F. Leroux, H. Hintze-Bruening, Phosphate-Based Organic Molecules Interleaved with Layered Double Hydroxide: Unraveling the Roles of Host Cations and the Guest-Inhibiting Effect in Aluminum Corrosion Protection, Eur. J. Inorg. Chem. 2012 (2012) 5396–5404. https://doi.org/10.1002/ejic.201200504.

[8] Y. Cao, D. Zheng, F. Zhang, J. Pan, C. Lin, Layered double hydroxide (LDH) for multifunctionalized corrosion protection of metals: A review, Journal of Materials Science & Technology. 102 (2022) 232–263. https://doi.org/10.1016/j.jmst.2021.05.078.

[9] M.L. Zheludkevich, J. Tedim, M.G.S. Ferreira, “Smart” coatings for active corrosion protection based on multi-functional micro and nanocontainers, Electrochimica Acta. 82 (2012) 314–323. https://doi.org/10.1016/j.electacta.2012.04.095.

[10] G. Zhang, L. Wu, A. Tang, X. Ding, B. Jiang, A. Atrens, F. Pan, Smart epoxy coating containing zeolites loaded with Ce on a plasma electrolytic oxidation coating on Mg alloy

AZ31 for active corrosion protection, Progress in Organic Coatings. 132 (2019) 144–147. https://doi.org/10.1016/j.porgcoat.2019.03.046.

[11] N. Bakhtaoui, O. Benali, E. Mazario, F.J. Recio, P. Herrasti, Layered double hydroxides intercalated with methyl orange as a controlled-release corrosion inhibitor for iron in chloride media, Nano Express. 2 (2021) 010017. https://doi.org/10.1088/2632-959X/abe2b6.

[12] A.R. Deip, D.A. Leal, G.H. Sakae, F. Maia, M.A.C. Berton, M.G.S. Ferreira, C.E.B. Marino, Performance of commercial LDH traps for chloride ion in a commercial corrosion protection primer for petrochemical industry, Corrosion Engineering, Science and Technology. 55 (2020) 66–74. https://doi.org/10.1080/1478422X.2019.1671644.

[13] G. Peng, Q. Qiao, K. Huang, J. Wu, Y. Wang, X. Fu, Z. Zhang, T. Fang, B. Zhang, Y. Huang, X. Li, Ni-Fe-MoO42- LDHs/epoxy resin varnish: A composite coating on carbon steel for long-time and active corrosion protection, Progress in Organic Coatings. 140 (2020) 105514. https://doi.org/10.1016/j.porgcoat.2019.105514.

[14] T.A. Truc, T.T. Thuy, V.K. Oanh, T.T.X. Hang, A.S. Nguyen, N. Caussé, N. Pébère, 8-hydroxyquinoline-modified clay incorporated in an epoxy coating for the corrosion protection of carbon steel, Surfaces and Interfaces. 14 (2019) 26–33. https://doi.org/10.1016/j.surfin.2018.10.007.

[15] E. Alibakhshi, E. Ghasemi, M. Mahdavian, B. Ramezanzadeh, Fabrication and characterization of layered double hydroxide/silane nanocomposite coatings for protection of mild steel, Journal of the Taiwan Institute of Chemical Engineers. 80 (2017) 924–934. https://doi.org/10.1016/j.jtice.2017.08.015.

[16] E. Alibakhshi, E. Ghasemi, M. Mahdavian, B. Ramezanzadeh, A comparative study on corrosion inhibitive effect of nitrate and phosphate intercalated Zn-Al- layered double hydroxides (LDHs) nanocontainers incorporated into a hybrid silane layer and their effect on cathodic delamination of epoxy topcoat, Corrosion Science. 115 (2017) 159–174. https://doi.org/10.1016/j.corsci.2016.12.001.

[17] A. Liu, X. Ju, H. Tian, H. Yang, W. Li, Direct synthesis of layered double hydroxides monolayer nanosheets for co-assembly of nanobrick wall hybrid film with excellent corrosion resistance, Applied Surface Science. 493 (2019) 239–249. https://doi.org/10.1016/j.apsusc.2019.06.295.

[18] Y. Cao, D. Zheng, C. Lin, Effect of physical barrier and anion-exchange process of nitrate-intercalated ZnAl layered double hydroxide films grown on Al on corrosion protection, Surface and Coatings Technology. 421 (2021) 127436. https://doi.org/10.1016/j.surfcoat.2021.127436.

[19] T.T.X. Hang, T.A. Truc, N.T. Duong, P.G. Vu, T. Hoang, Preparation and characterization of nanocontainers of corrosion inhibitor based on layered double hydroxides, Applied Clay Science. 67–68 (2012) 18–25. https://doi.org/10.1016/j.clay.2012.07.004.

[20] D. Abrantes Leal, F. Wypych, C.E. Bruno Marino, Zinc-Layered Hydroxide Salt Intercalated with Molybdate Anions as a New Smart Nanocontainer for Active Corrosion Protection of Carbon Steel, ACS Appl. Mater. Interfaces. 12 (2020) 19823–19833. https://doi.org/10.1021/acsami.0c02378.

[21] T.T.X. Hang, N.T. Duong, T.A. Truc, T. Hoang, D.T.M. Thanh, S. Daopiset, A. Boonplean, Effects of hydrotalcite intercalated with corrosion inhibitor on cathodic disbonding of epoxy coatings, J Coat Technol Res. 12 (2015) 375–383. https://doi.org/10.1007/s11998-014-9642-3.

[22] D. Nguyen Thuy, H. To Thi Xuan, A. Nicolay, Y. Paint, M.-G. Olivier, Corrosion protection of carbon steel by solvent free epoxy coating containing hydrotalcites intercalated with different organic corrosion inhibitors, Progress in Organic Coatings. 101 (2016) 331–341. https://doi.org/10.1016/j.porgcoat.2016.08.021.

[23] J. Rodriguez, E. Bollen, T.D. Nguyen, A. Portier, Y. Paint, M.-G. Olivier, Incorporation of layered double hydroxides modified with benzotriazole into an epoxy resin for the corrosion protection of Zn-Mg coated steel, Progress in Organic Coatings. 149 (2020) 105894. https://doi.org/10.1016/j.porgcoat.2020.105894.

[24] M. Serdechnova, A.N. Salak, F.S. Barbosa, D.E.L. Vieira, J. Tedim, M.L. Zheludkevich, M.G.S. Ferreira, Interlayer intercalation and arrangement of 2-mercaptobenzothiazolate and 1,2,3-benzotriazolate anions in layered double hydroxides: In situ X-ray diffraction study, Journal of Solid State Chemistry. 233 (2016) 158–165. https://doi.org/10.1016/j.jssc.2015.10.023.

[25] A. Seniski, R.F. Monteiro, G.T. Carrera, M. d'Orey G.P. Bragança, K.F. Portella, The inhibitory and comparative effects of Zn-Al layered double hydroxide microcontainers intercalated with benzotriazole and nitrite for corrosion protection coatings on AISI 1010 carbon steel, Revista Matéria (Rio de Janeiro). 25 (2020). https://doi.org/10.1590/s1517-707620200002.1064.

[26] Trinh Anh Truc, To Thi Xuan Hang, Vu Ke Oanh, E. Dantras, C. Lacabanne, D. Oquab, N. Pébère, Incorporation of an indole-3 butyric acid modified clay in epoxy resin for corrosion protection of carbon steel, Surface and Coatings Technology. 202 (2008) 4945–4951. https://doi.org/10.1016/j.surfcoat.2008.04.092.

[27] T.T.X. Hang, T.A. Truc, M.-G. Olivier, C. Vandermiers, N. Guérit, N. Pébère, Corrosion protection mechanisms of carbon steel by an epoxy resin containing indole-3 butyric acid modified clay, Progress in Organic Coatings. 69 (2010) 410–416. https://doi.org/10.1016/j.porgcoat.2010.08.004.

[28] Y. Sui, X. Liu, S. Bai, X. Li, Z. Sun, Phosphate loaded layered double hydroxides for active corrosion protection of carbon steel, Corrosion Engineering, Science and Technology. (2021) 1–8. https://doi.org/10.1080/1478422X.2021.1976086.

[29] S. Metsärinne, T. Tuhkanen, R. Aksela, Photodegradation of ethylenediaminetetraacetic acid (EDTA) and ethylenediamine disuccinic acid (EDDS) within natural UV radiation range, Chemosphere. 45 (2001) 949–955. https://doi.org/10.1016/S0045-6535(01)00022-4.

[30] E. Alibakhshi, E. Ghasemi, M. Mahdavian, B. Ramezanzadeh, Mana yasaei, The effect of interlayer spacing on the inhibitor release capability of layered double hydroxide based nanocontainers, Journal of Cleaner Production. 251 (2020) 119676. https://doi.org/10.1016/j.jclepro.2019.119676.

[31] H.S. Panda, R. Srivastava, D. Bahadur, Synthesis and in situ mechanism of nuclei growth of layered double hydroxides, Bull Mater Sci. 34 (2011) 1599–1604. https://doi.org/10.1007/s12034-011-0364-1.

[32] Y. Cao, S. Dong, D. Zheng, J. Wang, X. Zhang, R. Du, G. Song, C. Lin, Multifunctional inhibition based on layered double hydroxides to comprehensively control corrosion of carbon steel in concrete, Corrosion Science. 126 (2017) 166–179. https://doi.org/10.1016/j.corsci.2017.06.026.

[33] S. Chhetri, P. Samanta, N. Murmu, T. Kuila, Anticorrosion Properties of Epoxy Composite Coating Reinforced by Molybdate-Intercalated Functionalized Layered Double Hydroxide, J. Compos. Sci. 3 (2019) 11. https://doi.org/10.3390/jcs3010011.

[34] Y. Wang, D. Zhang, Synthesis, characterization, and controlled release anticorrosion behavior of benzoate intercalated Zn–Al layered double hydroxides, Materials Research Bulletin. 46 (2011) 1963–1968. https://doi.org/10.1016/j.materresbull.2011.07.021.

[35] W. Li, A. Liu, H. Tian, D. Wang, Controlled Release of Nitrate and Molybdate Intercalated in Zn-Al-Layered Double Hydroxide Nanocontainers towards Marine Anticorrosion Applications, Colloid and Interface Science Communications. 24 (2018) 18–23. https://doi.org/10.1016/j.colcom.2018.03.003.

[36] Y. Mei, J. Xu, L. Jiang, Q. Tan, Enhancing corrosion resistance of epoxy coating on steel reinforcement by aminobenzoate intercalated layered double hydroxides, Progress in Organic Coatings. 134 (2019) 288–296. https://doi.org/10.1016/j.porgcoat.2019.05.023.

[37] A. Ennadi, A. Legrouri, A. De Roy, J.P. Besse, X-Ray Diffraction Pattern Simulation for Thermally Treated [Zn–Al–Cl] Layered Double Hydroxide, Journal of Solid State Chemistry. 152 (2000) 568–572. https://doi.org/10.1006/jssc.2000.8740.

[38] S. Jaber, M. Leremboure, V. Thery, A.-M. Delort, G. Mailhot, Mechanism of photochemical degradation of Fe(III)-EDDS complex, Journal of Photochemistry and Photobiology A: Chemistry. 399 (2020) 112646. https://doi.org/10.1016/j.jphotochem.2020.112646.

[39] M. Zhou, L. Yan, H. Ling, Y. Diao, X. Pang, Y. Wang, K. Gao, Design and fabrication of enhanced corrosion resistance Zn-Al layered double hydroxides films based anion-exchange mechanism on magnesium alloys, Applied Surface Science. 404 (2017) 246–253. https://doi.org/10.1016/j.apsusc.2017.01.161.

[40] J.D. Yoo, K. Ogle, P. Volovitch, The effect of synthetic zinc corrosion products on corrosion of electrogalvanized steel. II. Zinc reactivity and galvanic coupling zinc/steel in presence of zinc corrosion products, Corrosion Science. 83 (2014) 32–37. https://doi.org/10.1016/j.corsci.2013.12.024.

[41] M.E. Orazem, N. Pébère, B. Tribollet, Enhanced Graphical Representation of Electrochemical Impedance Data, J. Electrochem. Soc. 153 (2006) B129. https://doi.org/10.1149/1.2168377.

[42] M. Outirite, M. Lagrenée, M. Lebrini, M. Traisnel, C. Jama, H. Vezin, F. Bentiss, ac impedance, X-ray photoelectron spectroscopy and density functional theory studies of 3,5-bis(n-pyridyl)-1,2,4-oxadiazoles as efficient corrosion inhibitors for carbon steel surface in hydrochloric acid solution, Electrochimica Acta. 55 (2010) 1670–1681. https://doi.org/10.1016/j.electacta.2009.10.048.

[43] R.M. Souto, B. Normand, H. Takenouti, M. Keddam, Self-healing processes in coil-coated cladding studied by the scanning vibrating electrode, Electrochimica Acta. 55 (2010) 4551–4557. https://doi.org/10.1016/j.electacta.2010.03.008.

Chapter 4: Electrochemical investigation of barrier properties of epoxy coatings containing layered double hydroxides $[Zn_2Al(OH)_6]^+[EDDS]^{4-}0.25.2H_2O$ dedicated to carbon steel corrosion protection

4.1 Introduction

Using of self-healing epoxy coating is one of the most effective methods of carbon steel corrosion protection [1–4]. Recently, so called "smart" coatings are design by incorporating a "guest host" assembly as a corrosion inhibitor reservoir with an ability to respond to certain external stimuli such as changes in local pH, temperature and wet environment [5,6]. Examples of reservoirs that have been incorporated into epoxy coatings to protect carbon steel are polymeric capsules, halloysite, and recently hydrotalcites and more generally layered double hydroxides (LDHs) [7–10].

LDHs have shown a promising potential for the development of smart corrosion inhibition system [11–14]. The protective agents (inhibitors) are usually loaded into the reservoir (LDH) [15]. The inhibitor-loaded LDH is then incorporated into organic coating matrix. Dormant without stimuli, *i.e.* without breaking the coating, such active fraction is able to react with aggressive chloride ions which diffuse through the coating micropores towards the metal/coating interface. The inhibitors are then released from the LDH interlayer galleries, thus impeding the corrosion process. In the same time, LDHs scaffold are able to capture corrosive ions, thus providing an active protection for the substrate via the action of inhibitor as well as to decrease the whole corrosiveness in the vicinity of the diffusive path [16–18].

Several organic inhibitors can be intercalated into LDHs for corrosion protection of carbon steel. However, as far as sustainability is concerned, it is necessary to consider the environmental friendliness of an inhibitor before its intercalation. In our recent publication, we studied a new combination of LDH by replacing EDTA with EDDS for the first time into the interlayer gallery of ZnAl hydroxides layers, $[Zn_2Al(OH)_6]^+[EDDS]^{4-}0.25.2H_2O$, ($Zn_2Al$-$EDDS^{4-}$) LDH. The corrosion inhibition mechanism of Zn_2Al-$EDDS^{4-}$ LDH on XC38 carbon was sum-

marized as: (i) the entrapment of chloride by anion-exchange of LDH-EDDS decreases the aggressiveness of the electrolyte, (ii) both $EDDS^{4-}$ and Zn^{2+} ions are released from Zn_2Al-$EDDS^{4-}$ LDH scaffold due to its partial solubility and (iii) synergistic effect existed between $EDDS^{4-}$ and Zn^{2+} ions [19].

The dispersion of functionalized LDH particles into organic coating provides labyrinth effect which increases the tortuosity of the polymer network [20]. Such passive phenomenon is usually found to limit or delay the diffusion of water and/or arrival of the aggressive species at the coating/substrate interface. On the other hand, if the LDH is not well-dispersed into the epoxy network and LDH particles agglomerate due to high amount, it could cause early degradation of the coated system mostly from incompatible phase separation between filler and polymer creating porous defects [16].

This study deals with the characterization of the barrier properties offered by the Zn_2Al-$EDDS^{4-}$ LDH in an epoxy matrix for different concentrations (0 %, 0.25 %, 0.75 % and 1.25 %) in LDH-EDDS. The aim is to determine the best coating formulation and the optimum concentration of LDH-EDDS needed for a long-term protection against the corrosion of XC38 carbon steel. The epoxy/LDH-EDDS coatings were elaborated on XC38 using bar coater method. The barrier properties were studied using mainly electrochemical impedance spectroscopy (EIS) to characterize the barrier properties of coating (global measurements). The analysis of EIS data were improved by graphical analysis [21,22] and by a model which was able to describe the resistivity profiles along the coating thickness [23–25]. This approach allows to give a physical meaning to the non-ideal capacitive behavior generally observed from experimental data.

4.2 Experimental

4.2.1 Preparation of epoxy incorporated EDDS-LDH coatings deposited on XC38 carbon steel

The compositions of the carbon steel substrate are detailed in chapter 2. Plates with dimensions 100 x70 x 3 mm^3 was used as a substrate. The carbon steel plates were sand blasted to a roughness of about 3µm and have been ultrasonically degreased with ethanol prior to the coating deposition to promote adhesion of the coating to the substrate.

Epoxy and epoxy/ Zn_2Al-$EDDS^{4-}$ coatings were prepared using an epoxy resin: bisphenol A diglycidyl ether (DGEBA) from Huntsmann (Araldite GZ7071X75) in xylene (at 75%) and a

polyamidoamine hardener as the curing agent, from Huntsmann (Aradur 423XW60) in xylene/n-butanol 4:1 (at 60%) solution.

Different percentage weight concentrations (0.25 %, 0.75 %, and 1.25 %) of Zn_2Al-$EDDS^{4-}$ LDH grounded to a powder form were mixed with epoxy resin. These concentrations were chosen to determine the best coating formulation and the optimum amount of Zn_2Al-$EDDS^{4-}$ LDH needed for better corrosion protection of XC38 carbon steel. The amine curing agent was then added with the amine/epoxy ratio equal to 1.1. The mixed coating formulation was deposited on XC38 plates using bar coater presented on the Figure 4.1. The curing protocols were as follows: *(i)* 24 h at room temperature in the bar coater chamber, to allow slow evaporation of solvent; *(ii)* 1h at 80 °C in the oven, was the real curing step; and *(iii)* 2h at 100 °C under vacuum, to ensure maximum curing without early degradation of the coatings. The particle dispersion was checked by SEM, and particle aggregates of less than 10 µm were observed. Epoxy coating without Zn_2Al-$EDDS^{4-}$ LDH was also produced as reference. The resulting coatings were: Epoxy/amine + 0 % Zn_2Al-$EDDS^{4-}$ LDH, Epoxy/amine + 0.25 % Zn_2Al-$EDDS^{4-}$ LDH, Epoxy/amine + 0.75 % Zn_2Al-$EDDS^{4-}$ LDH, and Epoxy/amine + 1.25 % Zn_2Al-$EDDS^{4-}$ LDH which will be subsequently referred to as 0 %, 0.25 %, 0.75 % and 1.25 % coating, respectively. The expected coating thicknesses were 80 µm. The measured dry thicknesses using a profilometer showed that the thicknesses were not homogeneous on the steel plates. The thicknesses of 80 µm ± 5 µm were reached on a surfaces of a few cm² in the center of the samples. The thicknesses of coatings were not homogeneous which was attributed to non-flattened carbon steel surface and probably the deposition technique used.

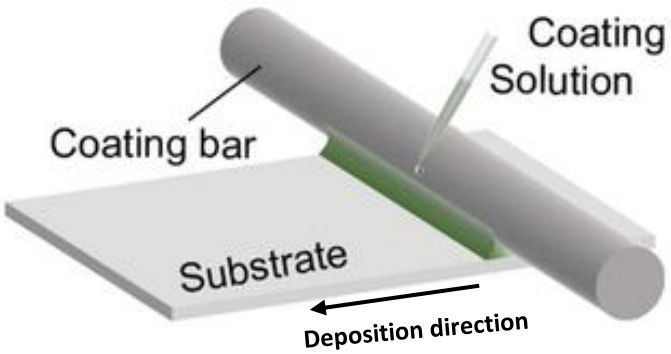

Figure 4.1: Coating deposition by bar coating method

4.2.2 Analytical characterizations

In addition to the scanning electron microscopy described above, differential scanning calorimetry (DSC) measurement was used to determine the glass transition temperature (T_g) of epoxy coatings before immersion. DSC was performed using a Mettler Toledo DSC3+ device at a rate of 15 °C.min^{-1} in the range -20°C to 100°C under air flow. T_g values were measured during the second heating ramp at the inflexion point of the thermogram.

4.2.3 Electrochemical impedance measurements

The electrochemical measurements were performed using two cell configurations: carbon steel/coating/mercury (dry condition) and carbon steel/coating/0.1 M NaCl solution (wet condition). In both cases, the coated carbon-steel plate was used as the working electrode. For the dry condition, the electrochemical cell was filled with mercury due to its highly nonwetting property [26]. The working electrode had an exposed area of 3 cm², and the platinum wire used as the counter and reference electrode was dipped in mercury to ensure electrical contact. A potentiostat/galvanostat (Biologic SP-300) was used to measure the impedance for this configuration. The impedance diagrams were obtained using a DC bias of 0 V over the frequency range of 10^4 Hz to 0.1 Hz with 8 points per decade and 50 mV RMS peak-to-peak sinusoidal perturbation amplitude. For the wet condition, a three-electrode cell was used. Two different types of masks providing from GAMRY were used to delimit the analysis area to 15 cm² or 3 cm² (the exposure area is the area where the coating thickness is homogeneous). The reference electrode was saturated calomel electrode (SCE), and a graphite bar with a large surface was used as the counter electrode. Both electrochemical set-ups were placed in a Faraday cage. A potentiostat/galvanostat (Gamry Reference 600) was used to measure the impedance for the carbon steel/coating/electrolyte configuration. The impedance diagrams were obtained under potentiostatic conditions at the corrosion potential over the frequency range of 105 Hz to 3 mHz with 8 points per decade and 15 mV RMS peak-to-peak sinusoidal perturbation amplitude. All the impedance measurements were performed at room temperature. For the wet condition, the impedance of the coatings was measured for exposure times ranging from 2 hours to 21 days. The solution was aerated and stagnant during the experimentation. For reproducibility, all measurements were repeated at least three times. The impedance diagrams were analyzed using non-commercial software developed at the LISE UMR CNRS 8235, Paris.

4.3 Results and discussion

4.3.1 Dielectric properties of coating under dry condition

The electrochemical impedance was measured in the dry condition to determine the parameters associated with the dielectric properties of the coating. To evaluate the water uptake of these different coatings, these parameters will be taken into account [26–28]. Figure 4.2 shows the impedance diagrams obtained for different amounts of LDH in organic matrix. Regardless the content of additive in the epoxy matrix, the phase angle is close to -90° between 10 kHz and 100 Hz. For lower frequencies, a slight distribution of the time constant was attributed to the surface roughness [25].

In parallel, the impedance modulus at lowest frequency was high and close to 10^{11} Ω cm². The results indicate that the coating/mercury interface can be considered as a pure capacitance.

The complex capacitance is given in equation 4.1. Figure 4.2 shows the complex capacitances in a Cole-Cole plot for the four samples. The capacitance of the dry coatings was extracted by graphical method (C_∞ indicated in Fig. 4.2) [22,29] and is reported in the table 1.

$$C(\omega) = \frac{1}{j\omega(Z-R_e)} \qquad \text{(eq.4.1)}$$

with, ω the angular frequency ($\omega=2\pi f$), Z the impedance of the coating, and R_e the electrolyte resistance. From the figure 4.2, the electrochemical behavior of the coated sample can be considered as a pure capacitive behavior. Thus, the real part of the capacitance determined in high frequency (C_∞) range allows to obtained the permittivity of the coating by using the equation 4.2.

$$C = \frac{\varepsilon_c \varepsilon_0}{\delta} \qquad \text{(eq.4.2)}$$

with ε_c the permittivity of the dry coating, ε_0 the vacuum permittivity, and δ the coating thickness.

The obtained capacitance and permittivity values are reported in the table 4.1. The values of the dry coatings obtained are closed to the ones reported in literature [30,31]. Regardless of Zn_2Al-$EDDS^{4-}$ LDH content, the capacitance values of the coatings are on the order of 3 to 5 10^{-11} F cm^{-2}, leading to permittivity values of the order of 3 and 4. Note that the T_g are not depending on the content in Zn_2Al-$EDDS^{4-}$ LDH as the values were between 54°C and 57°C (Table 4.1). These values concern organic matrix only which have been submitted to the curing protocols. Since the T_g depends on the cure temperature [27]. These closed values characterize that organic matrix are chemically equivalent whatever the presence of LDH.

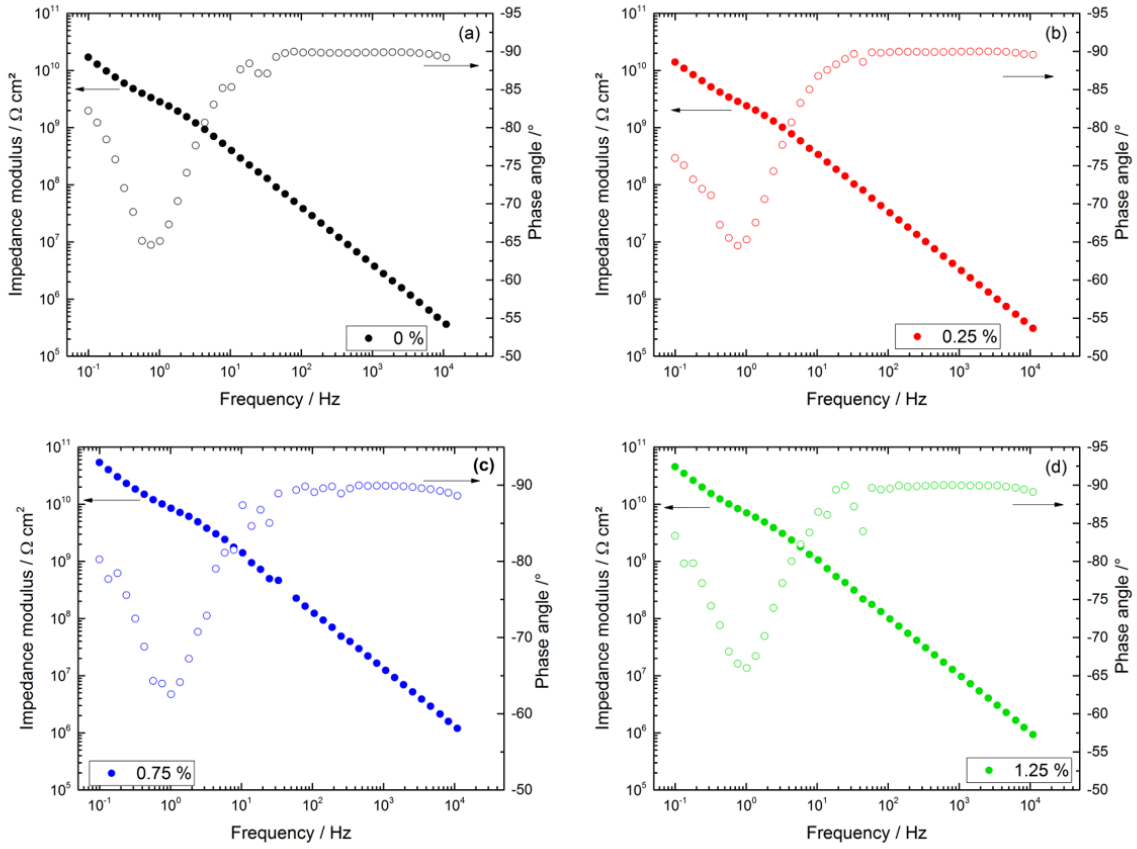

Figure 4.2: Electrochemical impedance diagrams obtained in dry conditions for the four samples with different contents of LDH: (a) 0 %, (b) 0.25 %, (c) 0.75 % and (d) 1.25 %.

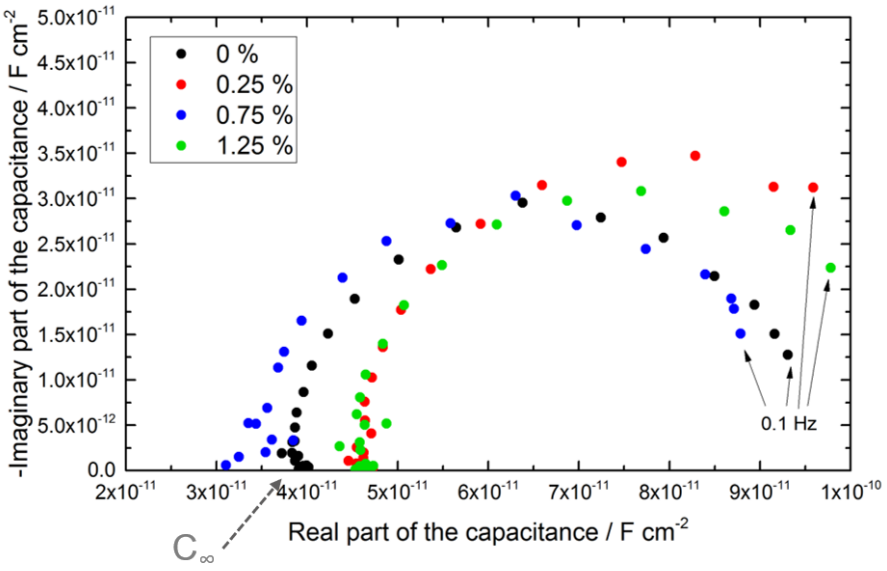

Figure 4.3: Cole-Cole plot obtained from the impedance measurements in Figure 1 representing the complex capacitance of the imaginary part as a function of the real part of the capacitance. An example of the C∞ value obtained by the intersection with the real axis is given.

Table 4.1: Parameters obtained in dry conditions for the different samples

Coatings	C_∞ / 10^{-11} F cm^{-2} *graphically determined from (fig. 4.3)*	ε_C *calculated from (eq.4.2)*	T_g / °C
0 %	3.90	3.5	57
0.25 %	4.63	4.2	57
0.75 %	3.54	3.2	57
1.25 %	3.07	2.8	54

4.3.2 Evaluation of the barrier properties of coatings under wet conditions

The four coated samples were immersed in the 0.1 M NaCl solution and the impedance was measured. Figure 4.4 presents the value of the impedance modulus at 3 mHz during time. This value was representative of the corrosion resistance of the coated carbon steel [32]. The evolutions are not the same for all samples. Some of the tests were stopped whenever corrosion signs are noticed, except for the reference coating which was removed after longer immersion times with the 0.75% LDH containing coating. This monitored immersion test was carried out in order to select the best candidate to protect the carbon steel against corrosion. It is interesting to underline that the value of the impedance modulus at low-frequency was not the same for all coatings at the initial time of immersion. For both 0.25% and 0.75% LDH-containing coatings, $|Z|_{3mHz}$ was around 10^{11} Ω cm^2 for the first 2 to 3 days of measurement. For the former coating, this value drastically decreases from 3 days of immersion to reach the same value as for 1.25% LDH-containing coating (≈ 5.10^7 Ω cm^2) whereas for the later coating, the value slowly decreases and reaches 10^{10} Ω cm^2 after 21 days of immersion. For the coating containing 1.25% Zn_2Al-$EDDS^{4-}$ LDH, the low-frequency impedance modulus value was the lowest from the beginning of the immersion (but relatively close to that of the free LDH coating) and decreases continuously during the 3 days of immersion, indicating defects in the epoxy matrix and a loss of protection giving rise to a corrosion process underneath the coating [10,33].

Figure 4.5 shows the macrographs of the samples after immersion in the neutral chloride solution. Some blisters and/or whitish spots were observed for all samples which could suggest water uptake. For the coating without Zn_2Al-$EDDS^{4-}$ LDH (Fig. 4.5 a), there were numerous spots of blisters uniformly distributed all over the entire immersed surface, suggesting some water uptake from the damaged coating. Some reddish-brown spots emphasizing the presence

of the corrosion process are also visible. From results and observations presented in Figures 4.4 and 4.5, for this coating free of Zn_2Al-$EDDS^{4-}$ LDH, the electrolyte diffuses easily through its thickness without any hindrance causing de-bonding, and consequently early degradation of coating barrier properties [34,35].

When Zn_2Al-$EDDS^{4-}$ LDH is incorporated into the epoxy coating, the surface state is different compared to the coating without Zn_2Al-$EDDS^{4-}$ LDH. Whitish precipitates are observed which could be attributed to the interaction between the electrolyte and the LDH themselves. For 0.25 % LDH-containing coating (Fig. 4.5 b), the whitish spots were less than that of the LDH free-coating, suggesting weaker interactions between epoxy and electrolyte. It is interesting to observe that the whitish spots are distributed randomly compared to the reference. This suggest that the presence of 0.25 % Zn_2Al-$EDDS^{4-}$ LDH limits the diffusion of electrolyte to some extent and acts locally as inhibitive specie. However, reddish-brown corrosion spots were also observed and attributed to insufficient amount of Zn_2Al-$EDDS^{4-}$ LDH, which could explain the decrease in the impedance modulus after 3 days of immersion [36].

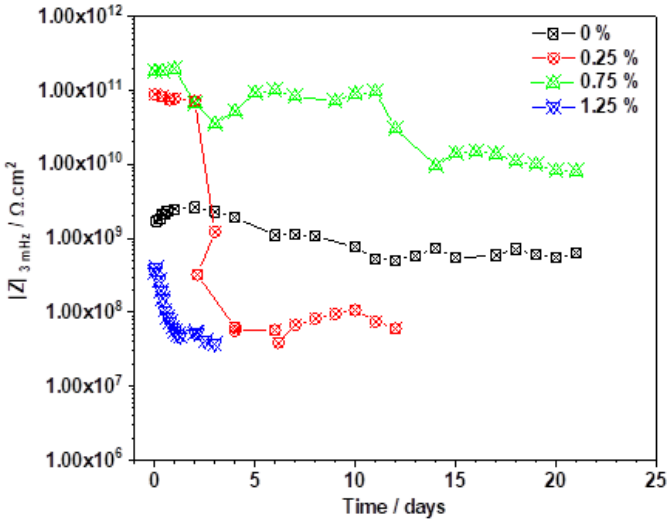

Figure 4.4: Impedance modulus at 3 mHz for epoxy coated carbon steel with or without Zn_2Al-$EDDS^{4-}$ LDH as a function of immersion time in the neutral chloride electrolyte.

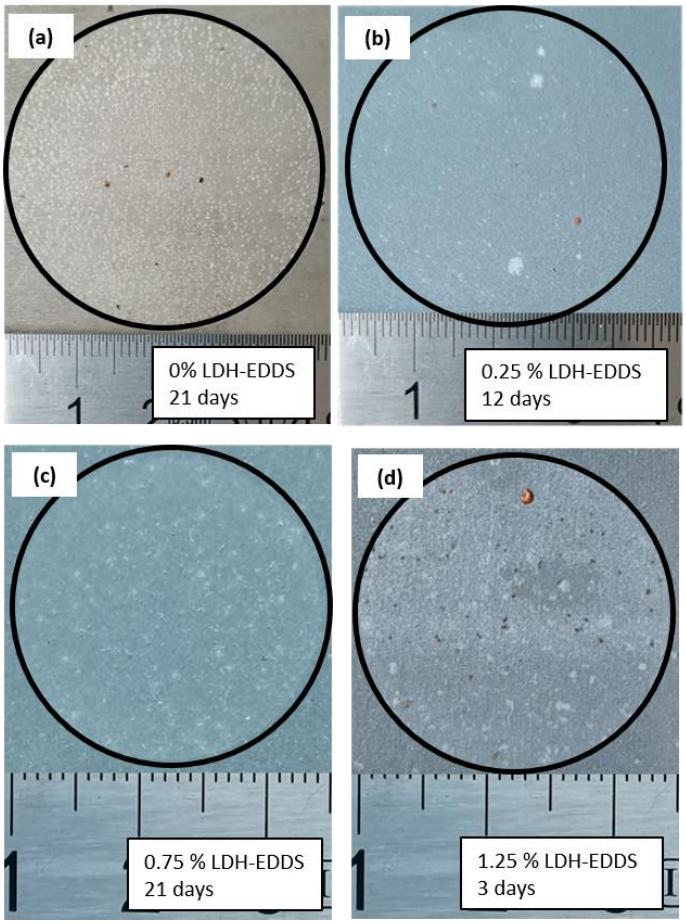

Figure 4.5: Macrographs of samples immersed in 0.1M NaCl electrolyte obtained after: (a) 21 days for the reference coating, (b) 12 days for the 0.25 % LDH-containing coating, (c) 21 days for the 0.75 % LDH -containing coating and (d) 3 days for the 1.25 % LDH-containing coating. The black circle marks the surface in contact with the aqueous solution.

The presence of 0.75% Zn_2Al-$EDDS^{4-}$ LDH gave the highest impedance modulus values after 21 days of immersion, with no colored visible corrosion spots, except some whitish spots (Fig. 4.5 c). This coating demonstrates superior protection in agreement with its impedance modulus which could be attributed to optimum amount of Zn_2Al-$EDDS^{4-}$ LDH [37]. The surface state of the coated sample containing the higher content of Zn_2Al-$EDDS^{4-}$ LDH is characterized by some black spots of corrosion signatures and a large reddish-brown corrosion product (Fig. 4.5 d). This suggest that 1.25 % Zn_2Al-$EDDS^{4-}$ LDH concentration could cause severe corrosion instead of protection [36]. That could be attributed to Zn_2Al-$EDDS^{4-}$ LDH particles agglomerating together and creating more defects [16]. In addition, higher concentration of Zn_2Al-$EDDS^{4-}$ LDH could lead to excessive leaching of EDDS which could cause osmotic pressure and blistering [33,37]. From these results, the best candidate is the coating loaded with 0.75% of Zn_2Al-$EDDS^{4-}$ LDH.

Impedance diagrams obtained for both coated systems immersed in 0.1 M NaCl solution as a function of immersion time are presented in Figure 4.6 using Bode coordinates. The shape of the impedance diagrams at high frequency range indicates a Constant-Phase-Element (CPE) behavior, which is defined by a constant phase angle $|\phi| < 90°$ [38]. The frequency range attributed to the CPE behavior is larger for the sample loaded with LDH (Fig. 4.6 b) compare to the LDH-free sample (Fig. 4.6 a). It is interesting to note that the high frequency part of the impedance diagrams remained superimposable with immersion time for both samples. The impedance measurement in low frequency range was not stationary for the sample containing LDH for immersion time less than 21 days. After this time, the shape of the phase as a function of the frequency was similar to that of the LDH-free sample for shorter immersion times. In parallel, the impedance modulus at low frequency was relatively high for the sample with 0.75% Zn_2Al-$EDDS^{4-}$ LDH ($\approx 10^{11}$-10^{10} Ω cm²) by comparison with the LDH-free coated plate ($\approx 10^9$ Ω cm²), indicating the highest barrier properties for the coating loaded with LDH. The low frequency part of the Bode diagrams was attributed to the carbon steel/electrolyte interface. For epoxy systems, the presence of a Constant-Phase-Element (CPE) was attributed to the presence of pores and/or free volume in the macromolecular network, which lead to hydration of the coating via permeation of the electrolyte through the epoxy matrix. Two types of pores are generally considered: those that are as deep as the coating thickness, where the penetrating electrolyte reaches the substrate/coating interface, and those that are less deep [24,39] called "short pores" by Musiani *et al.* [24]. They proposed a model to assess the local electrolyte volume fraction in different elemental layers of the coating for "short pores". In the present study, the value of the CPE exponent, graphically determined [21], remained at 0.98 during the entire immersion for the free and 0.75%-containing LDH samples. This indicates that the barrier properties of the epoxy are high, but with the observation of the surface states, there are open pores when the coating does not contain LDH.

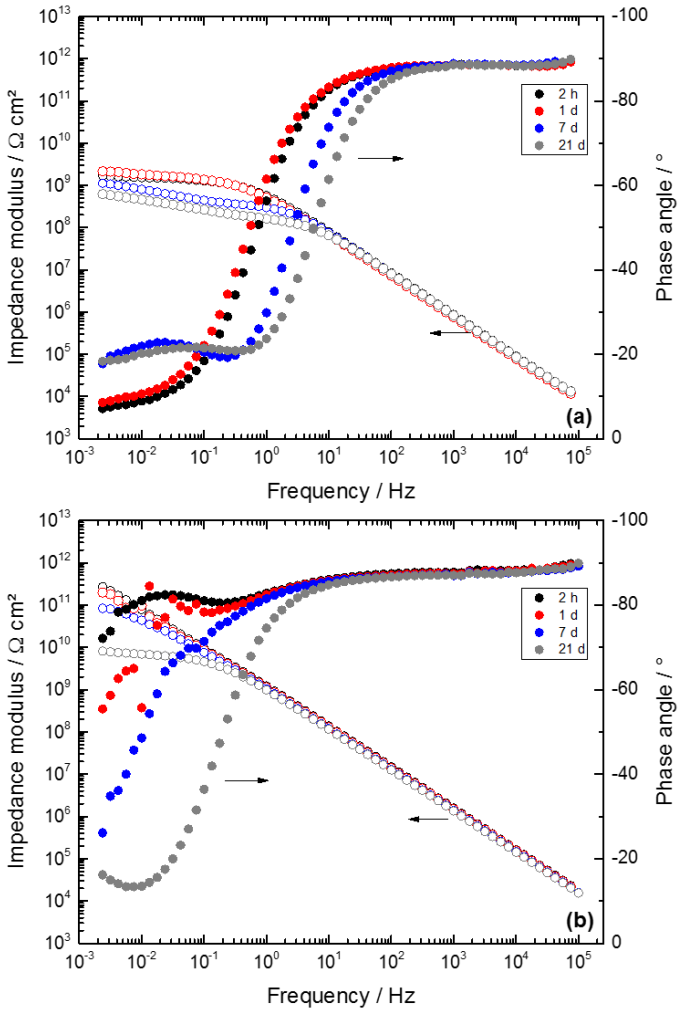

Figure 4.6: Bode impedance diagrams obtained during time for: (a) the LDH-free and (b) the 0.75%-LDH sample in the 0.1M NaCl solution.

In others studies, the CPE behavior observed for conventional epoxy coatings had been attributed to a normal distribution of the properties explained by a power law distribution of the resistivity along the coating thickness. The power law model (PLM) proposed by Hirschorn *et al*. [40,41] had been successfully used for analysis of impedance diagrams for epoxy coatings [24,25,31,39,42]. Table 4.2 summarizes the representative parameters obtained for both coatings using the PLM. The impedance data were fitted by PLM from 10^5 Hz to 0.1 Hz. The CPE parameter α was graphically determined from the phase vs frequency representation on the plateau in high frequency range ($\alpha = -\varphi / 90°$, [21]). The capacitance was graphically determined using the Cole-Cole plot, and finally the permittivity of the coating was determined using equation 4.2, with the same procedure as before for the data obtained in dry condition. The

resistivity at the interface between the carbon steel and epoxy coatings (ρ_0) was determined by the fitting with Simad software provided by LISE CNRS Paris.

The resistivity at the epoxy coating/electrolyte interface (ρ_δ) was determined using equation 4.3, where the capacitance is defined as [40]:

$$C = gQ(\rho_\delta \varepsilon \varepsilon_0)^{(1-\alpha)} \quad \text{(eq. 4.3)}$$

Here,

$$Q = \frac{(\varepsilon \varepsilon_0)^\alpha}{g \delta \rho_\delta^{1-\alpha}} \quad \text{(eq. 4.4)}$$

And the function g, depending on α value, allows to adjust the model, is given by:

$$g = 1 + 2.88 \left(\frac{1}{1-\alpha}\right)^{-2.375} \quad \text{(eq. 4.5)}$$

α and Q are the CPE parameters, ε is the permittivity of the coating, and ε_0 is the vacuum permittivity. The parameters δ and ω are the coating thickness and the angular frequency, respectively. The swelling by the water uptake is neglected. Thus, the thicknesses δ used to obtain the resistivity profiles are equal to 80 µm. Figure 4.7 shows a good agreement between the experimental and fitted impedance diagrams. Figure 4.8 presents the resistivity distribution obtained for both coated samples, showing that the dielectric properties of the coatings were only affected for a very small layer thickness: ≈ 20 µm and ≈ 30 µm for LDH-free coating and 0.75%-containing coating, respectively. This distribution was attributed to the roughness of the coating. The length of the plateau corresponding to a resistivity equal to ρ_0 doesn't vary with immersion time. However, for the coating without LDH, the value of the limit resistivity is decreasing with time, indicating a decrease of the barrier properties of the epoxy coating (Fig. 4.8 a). When Zn_2Al-$EDDS^{4-}$ LDH are present in the epoxy matrix, the resistivity ρ_0 remained high and evolves slowly with time (Fig. 4.8 b), indicating higher barrier properties than the LDH-free epoxy coating, in agreement with the impedance diagrams in Figure 4.6. The ρ_δ was higher in presence of LDH probably due to the Zn_2Al-$EDDS^{4-}$ LDH leaching [20]. From resistivities, the frequency domain of application of the model is defined by the characteristic frequencies f_0 and f_δ [40,41]:

$$f_0 = \frac{1}{2\pi \rho_0 \varepsilon \varepsilon_0} \quad \text{(eq. 4.6)}$$

and

$$f_\delta = \frac{1}{2\pi \rho_\delta \varepsilon \varepsilon_0} \quad \text{(eq. 4.7)}$$

It appears that the PLM was valid for the domain of frequencies between almost 10^5 Hz and 0.1 Hz. These results clearly indicate that the PLM could be used to analyze the CPE behavior observed for these two coatings. This conclusion reinforces the idea that the CPE behavior observed for both coatings can be attributed to their barrier properties.

Table 4.2: Parameters obtained by graphical method, calculation and by fitting procedure.

Coating	Time	α_c [21]	Q_c /10^{-10} Ω^{-1} cm^{-2} s$^{\alpha}$ [21]	C_∞ /10^{-10} F cm^{-2} from (4.1)	ε_C from (4.2)	ρ_δ 10^5 Ω cm from (4.4)	α_c by fitting	ρ_δ / 10^5 Ω cm by fitting	ρ_0 / 10^{11} Ω cm by fitting	f_δ / 10^5 Hz from (4.7)	f_0 /Hz from (4.6)
0 %	2 h	0.98	2.13	1.61	14.55	6.33	0.98	6.88	1.65	1.8	0.75
	1 d	0.98	2.50	1.81	16.36	0.66	0.98	1.13	1.82	9.7	0.60
	7 d	0.98	2.30	1.77	16.00	1.43	0.98	1.12	0.49	10.0	2.29
	21 d	0.98	2.27	1.61	14.55	2.62	0.98	1.12	0.26	11.0	1.10
0.75 %	2 h	0.98	1.19 10	0.92	8.31	33.3	0.97	59.2	19.7	0.37	0.11
	1 d	0.98	1.25	0.97	8.77	39.9	0.97	47.6	18.2	0.43	0.11
	7 d	0.98	1.31	1.01	9.13	27.5	0.97	36.4	16.1	0.54	0.38
	21 d	0.98	1.34	1.03	9.31	23.0	0.97	29.9	7.44	0.65	0.26

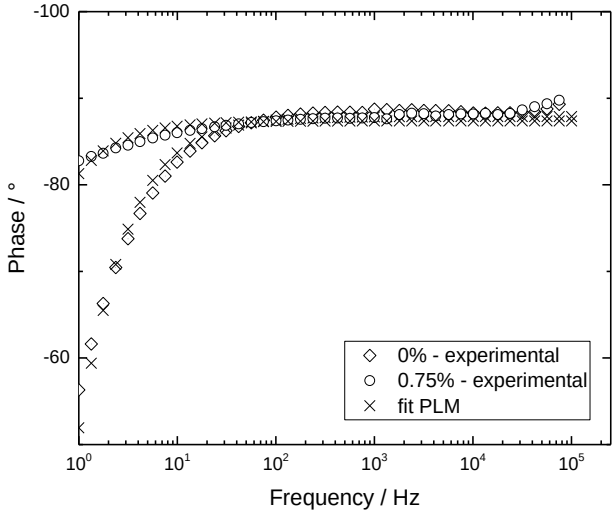

Figure 4.7: Fit result from power law model for experimental high frequency part of the impedance diagrams obtained after 2 h of immersion for both coatings.

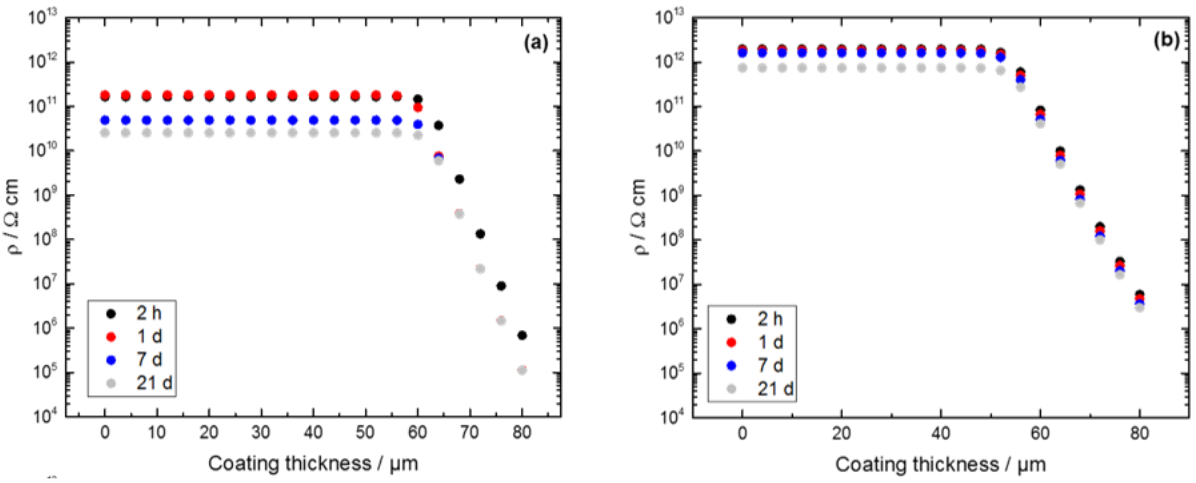

Figure 4.8: Resistivity distribution in the coatings thicknesses according to a power law: (a) epoxy coating without LDH and (b) with 0.75% of Zn_2Al-$EDDS^{4-}$ LDH.

In order to quantify the water uptake for both coatings, a linear relationship proposed by Nguyen *et al.* [26] was used:

$$\varepsilon_\omega = \varepsilon_c - \varepsilon_c \emptyset + \varepsilon_{water} \emptyset \qquad \text{(eq. 4.8)}$$

With ε_ω, ε_c and ε_{water}, the permittivity of the coating after immersion in the electrolyte (calculated from the graphical capacitance value using equation 4.2), the permittivity of the dry coating (reported in Table 1) and the permittivity of water (78.5 at 25°C), respectively. The volume fraction of water in the coating is Φ. Figure 4.9 shows the sorption kinetics for both coatings. The swelling of both coatings was assumed to be negligible. Thus, the coating thicknesses were assumed to be constant during the entire immersion. The water absorption is immediate for the free LDH epoxy coating and does not vary with the immersion time. A water-uptake of 15% is very high for epoxy coating and is attributed to the presence of porosities probably due to the coating preparation. In presence of LDH in the epoxy matrix, the water uptake is different. It is progressively increasing during the first hours then, for longer times, the evolution is slowed down to stabilize at 8.5 %. This last behavior was related to the presence of LDH which seal the porosities and therefore limits water sorption [36]. These results agree with the macrographs

of the samples after immersion in the chloride sodium solution (Fig. 3), the distributivity profiles which showed the higher barrier properties offered by the presence of Zn_2Al-$EDDS^{4-}$ LDH in the coating (Fig. 8).

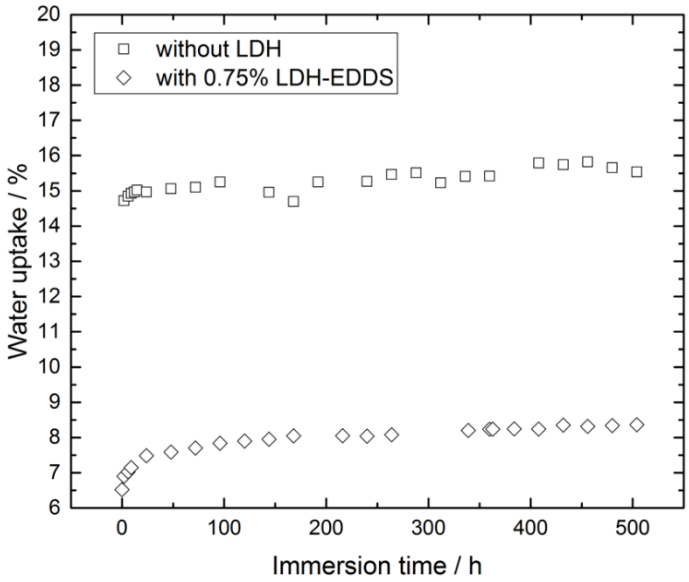

Figure 4.9: Water uptake obtained by impedance analysis using the linear relationship (eq. 4.8).

4.4 Conclusion

In this work, epoxy systems containing double hydroxide layers $[Zn_2Al(OH)_6]^+[EDDS]^{4-}0.25.2H_2O$ were developed as anticorrosive coatings for XC38 carbon steel. The water-barrier properties of these new materials were evaluated using electrochemical impedance measurements performed in a neutral chloride solution. The thicknesses of the coatings were not homogeneous on all the surfaces of the carbon steel plates and some defects were visible. Nevertheless, by selecting the test surface, it was shown that the electrochemical behaviors of the samples were different allowing the content in LDH. The best candidate was the 0.75 % LDH-containing coating, for which the barrier properties were compared to the refer-

ence sample (without LDH). The power law model was used and the obtained resistivity profiles showed a higher resistivity at the carbon steel/coating and coating/electrolyte interfaces during time for the coating loaded with 0.75% Zn_2Al-$EDDS^{4-}$ LDH by comparison with the free LDH coating. The higher resistivities were attributed to the presence of Zn_2Al-$EDDS^{4-}$ LDH which occupy the porosities to delay diffusion of water as well as acting locally as inhibitive pigment due to releasing of Zn^{2+} cations and $EDDS^{4-}$ anions. These results are promising even if the surface states of the different samples present defects due to a preparation that could be improved.

The contribution of LDH to inhibit the dissolution of iron is interesting and should be further investigated with local electrochemical measurements.

References

[1] M. Attaei, L.M. Calado, Y. Morozov, M.G. Taryba, R.A. Shakoor, R. Kahraman, A.C. Marques, M.F. Montemor, Smart epoxy coating modified with isophorone diisocyanate microcapsules and cerium organophosphate for multilevel corrosion protection of carbon steel, Progress in Organic Coatings. 147 (2020) 105864. https://doi.org/10.1016/j.porgcoat.2020.105864.

[2] X. Liu, C. Gu, Z. Wen, B. Hou, Improvement of active corrosion protection of carbon steel by water-based epoxy coating with smart CeO_2 nanocontainers, Progress in Organic Coatings. 115 (2018) 195–204. https://doi.org/10.1016/j.porgcoat.2017.10.015.

[3] M.F. Montemor, Functional and smart coatings for corrosion protection: A review of recent advances, Surface and Coatings Technology. 258 (2014) 17–37. https://doi.org/10.1016/j.surfcoat.2014.06.031.

[4] T. Liu, D. Zhang, L. Ma, Y. Huang, X. Hao, H. Terryn, A. Mol, X. Li, Smart protective coatings with self-sensing and active corrosion protection dual functionality from pH-sensitive calcium carbonate microcontainers, Corrosion Science. 200 (2022) 110254. https://doi.org/10.1016/j.corsci.2022.110254.

[5] Y. Su, S. Qiu, D. Yang, S. Liu, H. Zhao, L. Wang, Q. Xue, Active anti-corrosion of epoxy coating by nitrite ions intercalated MgAl LDH, Journal of Hazardous Materials. 391 (2020) 122215. https://doi.org/10.1016/j.jhazmat.2020.122215.

[6] I.I. Udoh, H. Shi, E.F. Daniel, J. Li, S. Gu, F. Liu, E.-H. Han, Active anticorrosion and self-healing coatings: A review with focus on multi-action smart coating strategies, Journal of Materials Science & Technology. 116 (2022) 224–237. https://doi.org/10.1016/j.jmst.2021.11.042.

[7] D.T. Nguyen, H.T.X. To, J. Gervasi, Y. Paint, M. Gonon, M.-G. Olivier, Corrosion inhibition of carbon steel by hydrotalcites modified with different organic carboxylic acids for organic coatings, Progress in Organic Coatings. 124 (2018) 256–266. https://doi.org/10.1016/j.porgcoat.2017.12.006.

[8] N. Asadi, R. Naderi, M. Mahdavian, Synergistic effect of imidazole dicarboxylic acid and Zn2+ simultaneously doped in halloysite nanotubes to improve protection of epoxy ester coating, Progress in Organic Coatings. 132 (2019) 29–40. https://doi.org/10.1016/j.porgcoat.2019.03.021.

[9] D. Zhang, H. Zhang, S. Zhao, Z. Li, S. Hou, Electrochemical Impedance Spectroscopy Evaluation of Corrosion Protection of X65 Carbon Steel by Halloysite Nanotube-Filled

Epoxy Composite Coatings in 3.5% NaCl Solution, Int. J. Electrochem. Sci. (2019) 4659–4667. https://doi.org/10.20964/2019.05.09.

[10] G. Peng, Q. Qiao, K. Huang, J. Wu, Y. Wang, X. Fu, Z. Zhang, T. Fang, B. Zhang, Y. Huang, X. Li, Ni-Fe-MoO_4^{2-} LDHs/epoxy resin varnish: A composite coating on carbon steel for long-time and active corrosion protection, Progress in Organic Coatings. 140 (2020) 105514. https://doi.org/10.1016/j.porgcoat.2019.105514.

[11] N. Bakhtaoui, O. Benali, E. Mazario, F.J. Recio, P. Herrasti, Layered double hydroxides intercalated with methyl orange as a controlled-release corrosion inhibitor for iron in chloride media, Nano Express. 2 (2021) 010017. https://doi.org/10.1088/2632-959X/abe2b6.

[12] A.R. Deip, D.A. Leal, G.H. Sakae, F. Maia, M.A.C. Berton, M.G.S. Ferreira, C.E.B. Marino, Performance of commercial LDH traps for chloride ion in a commercial corrosion protection primer for petrochemical industry, Corrosion Engineering, Science and Technology. 55 (2020) 66–74. https://doi.org/10.1080/1478422X.2019.1671644.

[13] M.L. Zheludkevich, J. Tedim, M.G.S. Ferreira, "Smart" coatings for active corrosion protection based on multi-functional micro and nanocontainers, Electrochimica Acta. 82 (2012) 314–323. https://doi.org/10.1016/j.electacta.2012.04.095.

[14] M.L. Zheludkevich, S.K. Poznyak, L.M. Rodrigues, D. Raps, T. Hack, L.F. Dick, T. Nunes, M.G.S. Ferreira, Active protection coatings with layered double hydroxide nanocontainers of corrosion inhibitor, Corrosion Science. 52 (2010) 602–611. https://doi.org/10.1016/j.corsci.2009.10.020.

[15] M.L. Zheludkevich, D.G. Shchukin, K.A. Yasakau, H. Möhwald, M.G.S. Ferreira, Anticorrosion Coatings with Self-Healing Effect Based on Nanocontainers Impregnated with Corrosion Inhibitor, Chem. Mater. 19 (2007) 402–411. https://doi.org/10.1021/cm062066k.

[16] Y. Cao, D. Zheng, F. Zhang, J. Pan, C. Lin, Layered double hydroxide (LDH) for multifunctionalized corrosion protection of metals: A review, Journal of Materials Science & Technology. 102 (2022) 232–263. https://doi.org/10.1016/j.jmst.2021.05.078.

[17] Y. Cao, D. Zheng, C. Lin, Effect of physical barrier and anion-exchange process of nitrate-intercalated ZnAl layered double hydroxide films grown on Al on corrosion protection, Surface and Coatings Technology. 421 (2021) 127436. https://doi.org/10.1016/j.surfcoat.2021.127436.

[18] M. Tabish, G. Yasin, M.J. Anjum, M.U. Malik, J. Zhao, Q. Yang, S. Manzoor, H. Murtaza, W.Q. Khan, Reviewing the current status of layered double hydroxide-based smart

nanocontainers for corrosion inhibiting applications, Journal of Materials Research and Technology. 10 (2021) 390–421. https://doi.org/10.1016/j.jmrt.2020.12.025.

[19] G.J. Ayemi, S. Marcelin, S. Therias, F. Leroux, B. Normand, Synergy effect between layer double hydroxide (LDH) and EDDS for corrosion inhibition of carbon steel, Applied Clay Science. 222 (2022) 106497. https://doi.org/10.1016/j.clay.2022.106497.

[20] W. Sun, T. Wu, L. Wang, C. Dong, G. Liu, Controlled Preparation of MgAl-Layered Double Hydroxide/Graphene Hybrids and Their Applications for Metal Protection, Ind. Eng. Chem. Res. 58 (2019) 16516–16525. https://doi.org/10.1021/acs.iecr.9b01742.

[21] M.E. Orazem, N. Pébère, B. Tribollet, Enhanced Graphical Representation of Electrochemical Impedance Data, J. Electrochem. Soc. 153 (2006) B129. https://doi.org/10.1149/1.2168377.

[22] M. Benoit, C. Bataillon, B. Gwinner, F. Miserque, M.E. Orazem, C.M. Sánchez-Sánchez, B. Tribollet, V. Vivier, Comparison of different methods for measuring the passive film thickness on metals, Electrochimica Acta. 201 (2016) 340–347. https://doi.org/10.1016/j.electacta.2015.12.173.

[23] S. Marcelin, Z. Zhang, B. Ter-Ovanessian, B. Normand, Relationship between the Resistivity Profiles Obtained from the Power Law Model and the Physico-Chemical Properties of Passive Films, J. Electrochem. Soc. 168 (2021) 021503. https://doi.org/10.1149/1945-7111/abde84.

[24] M. Musiani, M.E. Orazem, N. Pébère, B. Tribollet, V. Vivier, Determination of resistivity profiles in anti-corrosion coatings from constant-phase-element parameters, Progress in Organic Coatings. 77 (2014) 2076–2083. https://doi.org/10.1016/j.porgcoat.2013.12.013.

[25] A.S. Nguyen, M. Musiani, M.E. Orazem, N. Pébère, B. Tribollet, V. Vivier, Impedance analysis of the distributed resistivity of coatings in dry and wet conditions, Electrochimica Acta. 179 (2015) 452–459. https://doi.org/10.1016/j.electacta.2015.02.109.

[26] A.S. Nguyen, N. Causse, M. Musiani, M.E. Orazem, N. Pébère, B. Tribollet, V. Vivier, Determination of water uptake in organic coatings deposited on 2024 aluminium alloy: Comparison between impedance measurements and gravimetry, Progress in Organic Coatings. 112 (2017) 93–100. https://doi.org/10.1016/j.porgcoat.2017.07.004.

[27] L. Garden, R.A. Pethrick, A dielectric study of water uptake in epoxy resin systems, J. Appl. Polym. Sci. 134 (2017). https://doi.org/10.1002/app.44717.

[28] B. Normand, H. Takenouti, M. Keddam, H. Liao, G. Monteil, C. Coddet, Electrochemical impedance spectroscopy and dielectric properties of polymer: application to PEEK

thermally sprayed coating, Electrochimica Acta. 49 (2004) 2981–2986. https://doi.org/10.1016/j.electacta.2004.01.057.

[29] S. Chakri, I. Frateur, M.E. Orazem, E.M.M. Sutter, T.T.M. Tran, B. Tribollet, V. Vivier, Improved EIS Analysis of the Electrochemical Behaviour of Carbon Steel in Alkaline Solution, Electrochimica Acta. 246 (2017) 924–930. https://doi.org/10.1016/j.electacta.2017.06.096.

[30] G. Bouvet, D.D. Nguyen, S. Mallarino, S. Touzain, Analysis of the non-ideal capacitive behaviour for high impedance organic coatings, Progress in Organic Coatings. 77 (2014) 2045–2053. https://doi.org/10.1016/j.porgcoat.2014.02.008.

[31] A.S. Nguyen, M. Musiani, M.E. Orazem, N. Pébère, B. Tribollet, V. Vivier, Impedance study of the influence of chromates on the properties of waterborne coatings deposited on 2024 aluminium alloy, Corrosion Science. 109 (2016) 174–181. https://doi.org/10.1016/j.corsci.2016.03.030.

[32] N. Wang, X. Diao, J. Zhang, P. Kang, Corrosion Resistance of Waterborne Epoxy Coatings by Incorporation of Dopamine Treated Mesoporous-TiO_2 Particles, Coatings. 8 (2018) 209. https://doi.org/10.3390/coatings8060209.

[33] M. Yeganeh, N. Asadi, M. Omidi, M. Mahdavian, An investigation on the corrosion behavior of the epoxy coating embedded with mesoporous silica nanocontainer loaded by sulfamethazine inhibitor, Progress in Organic Coatings. 128 (2019) 75–81. https://doi.org/10.1016/j.porgcoat.2018.12.022.

[34] Q. Le Thu, H. Takenouti, S. Touzain, EIS characterization of thick flawed organic coatings aged under cathodic protection in seawater, Electrochimica Acta. 51 (2006) 2491–2502. https://doi.org/10.1016/j.electacta.2005.07.049.

[35] S. Duval, M. Keddam, M. Sfaira, A. Srhiri, H. Takenouti, Electrochemical Impedance Spectroscopy of Epoxy-Vinyl Coating in Aqueous Medium Analyzed by Dipolar Relaxation of Polymer, J. Electrochem. Soc. 149 (2002) B520. https://doi.org/10.1149/1.1512667.

[36] A. Jagtap, P.G. Wagle, E. Jagtiani, A.P. More, Layered double hydroxides (LDHs) for coating applications, J Coat Technol Res. 19 (2022) 1009–1032. https://doi.org/10.1007/s11998-022-00624-y.

[37] N. Wang, H. Gao, J. Zhang, L. Li, X. Fan, X. Diao, Anticorrosive waterborne epoxy (EP) coatings based on sodium tripolyphosphate-pillared layered double hydroxides (STPP-LDHs), Progress in Organic Coatings. 135 (2019) 74–81. https://doi.org/10.1016/j.porgcoat.2019.04.055.

[38] M. Mahdavian, M.M. Attar, Another approach in analysis of paint coatings with EIS measurement: Phase angle at high frequencies, Corrosion Science. 48 (2006) 4152–4157. https://doi.org/10.1016/j.corsci.2006.03.012.

[39] S. Amand, M. Musiani, M.E. Orazem, N. Pébère, B. Tribollet, V. Vivier, Constant-phase-element behavior caused by inhomogeneous water uptake in anti-corrosion coatings, Electrochimica Acta. 87 (2013) 693–700. https://doi.org/10.1016/j.electacta.2012.09.061.

[40] B. Hirschorn, M.E. Orazem, B. Tribollet, V. Vivier, I. Frateur, M. Musiani, Constant-Phase-Element Behavior Caused by Resistivity Distributions in Films, I. Theory, Journal of The Electrochemical Society. 157 (2010) C452–C457.

[41] B. Hirschorn, M.E. Orazem, B. Tribollet, V. Vivier, I. Frateur, M. Musiani, Constant-phase-element behavior caused by resistivity distributions in films, II. Applications, Journal of The Electrochemical Society. 157 (2010) C458–C463.

[42] Y.-M. Chen, A.S. Nguyen, M.E. Orazem, B. Tribollet, N. Pébère, M. Musiani, V. Vivier, Identification of Resistivity Distributions in Dielectric Layers by Measurement Model Analysis of Impedance Spectroscopy, Electrochimica Acta. 219 (2016) 312–320. https://doi.org/10.1016/j.electacta.2016.09.136.

General conclusion, and Perspectives

The objective of this work was to formulate composite organic coatings for corrosion protection of carbon steel. It was chosen to study layered double hydroxides (LDH) as a potential reservoir of corrosion inhibitor and then incorporated this material into organic coatings. It was thus an opportunity to collaborate with the Institute of Chemistry Clermont-Ferrand for the synthesis of LDHs and the deposition of coating on the carbon steel substrate. This work was realized, thanks to the contribution of characterization techniques, generally used in material science. It was also appropriate to use electrochemical techniques most especially electrochemical impedance spectroscopy which allowed a better understanding of the inhibition mechanism provided by LDHs and the barrier behavior of organic composite coatings. It is recalled here, as a conclusion of this work, the contribution of the techniques and the significant results obtained. This state will then allow to propose some perspectives.

The first objective of this work was to understand the corrosion inhibition mechanism of XC38 carbon steel offer by zinc-aluminum LDH intercalated with EDDS. The analytical characterization of the ZnAl-$EDDS^{4-}$ LDH power was done by XRD, and ICP-OES; Surface observation of the LDH powder, and carbon steel after immersion was carried out by SEM; the electrochemical behavior of carbon steel immersed in 0.1M NaCl solution containing different inhibitive species was studies by polarization curves and EIS.

The powder XRD pattern showed a nearly symmetric diffraction peaks and a sharp diffraction reflection peak at (003) which confirmed that, the synthesized powder is monophasic and a successfully intercalation of EDDS (inhibitor) into the interlayer galleries of LDH (reservoir) respectively, to produce a hybrid Zn_2Al-$EDDS^{4-}$ LDH. Additionally, the XRD pattern also revealed the anion-exchange potential of the Zn_2Al-$EDDS^{4-}$ LDH in the chloride environment. The SEM observation of the Zn_2Al-$EDDS^{4-}$ LDH power exhibited stacked of agglomerated platelet-like morphology as a typical characteristic of LDH.

The ICP-OES revealed the partial solubility of Zn_2Al-$EDDS^{4-}$ LDH scaffold in 0.1 M NaCl to release Zn^{2+} and Al^{3+} metallic cations. The inhibition role of these cations was studied by electrochemical measurements.

The polarization curves showed that Zn_2Al-$EDDS^{4-}$ LDH acts as an anodic inhibitor. To discriminate the contribution each of the element (Zn^{2+} or Al^{3+} or $EDDS^{4-}$) constituting the functionalized Zn_2Al-$EDDS^{4-}$ LDH, these elements were studied alone or in combination. The polarization curves showed a synergistic effect between Zn^{2+} and $EDDS^{4-}$ in anodic domain. EIS was performed to obtain further information about the inhibitive mechanism provided by

$Zn_2Al\text{-}EDDS^{4-}$ LDH and similar trends of results were observed as for polarization curves. In the absence of inhibitive species, the impedance modulus value at low-frequency was the lowest and the diagram was characterized by one single time constant attributed to charge transfer. When $Zn_2Al\text{-}EDDS^{4-}$ LDH are in solution, the impedance modulus at low frequency increases, with highest value for higher amount of $Zn_2Al\text{-}EDDS^{4-}$ LDH. For the higher amount, phase diagram shows a second time constant at higher frequency, attributed to the chelate formation due to the effect of $Zn_2Al\text{-}EDDS^{4-}$ LDH. When Zn^{2+} are in solution, impedance diagram was characterized by two-time constants with low frequency time constant attributed to charge transfer due to the dissolution of iron and the high frequency time constant attributed to the protective film formation. The impedance diagram was characterized by a single time constant at medium frequency in presence of EDDS alone which was attributed to charge transfer. However, when Zn^{2+} and $EDDS^{4-}$ are both in the solution, the impedance modulus at low frequency was the highest and the impedance diagram was characterized by two imbricated time constants. The EIS results agree with the polarization curves and highlight the beneficial synergistic effect between Zn^{2+} and $EDDS^{4-}$ ions.

The SEM micrographs of carbon steel after 24 h of immersion in chloride solution containing different inhibitive species (alone or in combination), confirmed the presence of a protective film attributed to the precipitation of simonkoellite ($Zn_5(OH)_8Cl_2\text{-}H_2O$) and/or Zn^{2+} onto the carbon steel surface as described for the galvanized steel. The carbon steel surface was fully protected when $EDDS^{4-}$ and Zn^{2+} are in solution attributed to the synergism. Therefore, the protection of XC38 carbon offer by $Zn_2Al\text{-}EDDS^{4-}$ LDH, comes from the contribution of $EDDS^{4-}$ anion and Zn^{2+} cation.

The second objective of this work was to developed smart epoxy coating incorporated with different concentrations of previously studied $Zn_2Al\text{-}EDDS^{4-}$ LDH to determine the optimum concentration needed for the best corrosion protection. The goal was to supplement passive barrier of the epoxy coating with active inhibition for the long-term corrosion protection of XC38 carbon steel. The properties investigated are: glass transition temperature (T_g) by DSC; barrier performance properties of the coating by EIS (global measurements); water uptake assessment from EIS data; self-healing properties by LEIS (local measurements).

The T_g values for all coatings before immersion were between 54°C to 57°C. The closeness of these values was attributed to the fact the coatings were produced using the same curing protocols since the T_g is dependent on the cure temperature.

The EIS was performed in both dry and wet condition. The capacitance (C_c) for the dry coatings were graphically determined from the dry impedance data and the permittivity (ε_c) was calculated. The results showed lower capacitance and permittivity values for the coatings loaded with Zn_2Al-$EDDS^{4-}$ LDH and the values decreases with increase in the amount of Zn_2Al-$EDDS^{4-}$ LDH in the coating suggesting the modification of the coatings network. The results obtained from wet condition EIS showed that the coating loaded with 0.75% Zn_2Al-$EDDS^{4-}$ LDH demonstrates a superior protection performance compare to 0% Zn_2Al-$EDDS^{4-}$ LDH coatings as the impedance at the low frequency was significantly higher for the former coating than the later coating. The water uptake for the coating loaded with 0.75 % Zn_2Al-$EDDS^{4-}$ LDH was about 8.5 % compare to 15 % for 0 % Zn_2Al-$EDDS^{4-}$ LDH coating. The resistivity profiles also emphasized that the presence of 0.75 % in LDH modifies the resistivity of the coating by comparison with the reference coating. These results suggest that the presence of Zn_2Al-$EDDS^{4-}$ LDH block and/or limit the diffusion of water and delayed the arrival of aggressive species at the coating/substrate interface.

This research allows us to synthesis Zn_2Al-$EDDS^{4-}$ LDH for the corrosion protection of bared carbon steel for the first time, developed smart epoxy coatings loaded with the LDH material, and methodology for the characterization of these kind of coatings, which have proven to be efficient for corrosion protection of carbon steel. In other to demonstrate the opportunity of our methodology, this work proposed a prospect for the use of these coatings in corrosion protection of carbon steel for various surface engineering application.

Based on the present research, the following perspectives can be proposed for future research:

It would be interesting to study physico-chemical mechanism of $EDDS^{4-}$ and Zn^{2+}/carbon steel interaction and effects of solution/interfacial chemistry upon $EDDS^{4-}/Zn^{2+}$ release/Cl^- entrapment, EDDS/carbon steel interaction as well as the surface coverage of the inhibitive species. These will give better understanding of the corrosion inhibition mechanism of carbon steel by these elements.

Electrochemical assessment of inhibition reversibility. This could be achieved by immersing the substrate into a fresh blank solution (e.g 0.1M NaCl) after the initial immersion in the solution containing an inhibitive species. This will help to determine if the initial protection provided by inhibitive species is either maintain, decreases or increases.

Characterization of corrosion product to determine its composition. This will help to determine the role of carbon steel substrate (oxide) surface chemistry and microstructure.

It could be interesting to use various rotation speeds for the rotating disc electrode to see an effect of diffusion of species at the electrolyte/carbon steel interface.

This thesis was based on Zn-Al LDH; however, it could be interested to explore other cationic combinations such as Zn-Fe to compare with Zn-Al combination. Since EDDS formed a complex chelate with iron, the Al^{3+} could be replace with Fe^{3+}, may be a better protection and/or synergistic effect could be observed.

Since Al^{3+} did not play any inhibition role, it would be interesting to try Zn Layered Single Hydroxide (LSH) with EDDS to compare the results with LDH since inhibitor could also be adsorbed at the surface of the hydroxides layers.

The contribution of LDH to inhibit the dissolution of iron is interesting and should be further investigated with local electrochemical measurements to validate the self-healing properties of coatings with/without LDHs.

Fourier transform infra-red (FT-IR) could be used to study the chemical structure/bonding, degree of crosslinking, of the epoxy coatings (before or after immersion) to understand the influence of LDH content.

Electrochemical impedance is very sensitive to variations in thickness. The thickness of the coatings produced in this study were not homogeneous. There could be need for improvement on the preparation and deposition of coatings.

To conclude definitely with prospect, it would be required to validate the efficiency of coating with long term inhibition.

FOLIO ADMINISTRATIF

THESE DE L'INSA LYON, MEMBRE DE L'UNIVERSITE DE LYON

NOM : **AYEMI** DATE de SOUTENANCE : **03/07/2023**
(Avec précision du nom de jeune fille, le cas échéant)

Prénoms: **Gata Joseph**

TITRE: **Methodology for development of smart epoxy coatings incorporated with Ethylenediamine-N, N'-disuccinic acid (EDDS) layered double hydroxides (LDHs) for corrosion protection of XC38 carbon steel**

NATURE : **Doctora**t Numéro d'ordre : **2023ISAL0038**

Ecole doctorale : **Matériaux de Lyon - ED 34**

Spécialité : **Science et génie des matériaux**

RESUME :
Les hydroxydes doubles stratifiés (LDH) sont des candidats intéressants comme réservoirs d'inhibiteurs de corrosion pour la protection des métaux. En effet, ces espèces présentent une forte capacité à libérer l'inhibiteur contenu entre leurs lamelles d'hydroxyde, et selon le principe de l'échange d'anions, elles permettent simultanément la capture d'espèces agressives telles que l'ion chlorure présent dans la solution. En raison de leurs propriétés susmentionnées, ils représentent des charges intéressantes qui peuvent être incorporées dans la matrice des revêtements époxy pour améliorer les propriétés de barrière. La conception d'un système intelligent d'inhibition de la corrosion utilisant ce matériau, pourrait augmenter de manière significative la durabilité et l'efficacité du système revêtu en fournissant une protection active contre la corrosion.
L'objectif de cette thèse est d'étudier l'efficacité du système LDH Zn-Al comme réservoir intelligent d'acide éthylènediamine-N,N'-disuccinique (EDDS). Les $[Zn_2Al(OH)_6]^+$ $[EDDS]^{4-}{}_{0.25}$ $2H_2O$ HDL (Zn_2Al-$EDDS^{4-}$ HDL) sont ensuite incorporés dans la matrice d'un revêtement époxy pour une protection active contre la corrosion de l'acier au carbone XC38 en milieu chlorure de sodium. L'EDDS est une molécule non toxique et biodégradable est intéressante à utiliser comme inhibiteur pour remplacer l'acide éthylènediaminetétraacétique (EDTA), qui est nocif et non respectueux de l'environnement. De plus, l'$EDDS^{4-}$ a la capacité de former des complexes stables avec les ions métalliques du fer, qui est le principal composant de l'acier au carbone pour apporter une protection du substrat et peu interagir en synergie avec d'autres inhibiteurs de corrosion. La première partie des résultats, présente une méthodologie de caractérisation de l'efficacité du Zn_2Al-$EDDS^{4-}$ HDL essentiellement basée sur des mesures électrochimiques. Cette partie permet de mettre en évidence un effet synergique entre les anions $EDDS^{4-}$ et les cations Zn^{2+} constituant le squelette du LDH. La deuxième partie des résultats est consacrée à la caractérisation de revêtements époxy contenant différentes quantités de Zn_2Al-$EDDS^{4-}$ HDL afin de déterminer la teneur optimale nécessaire pour obtenir de meilleures propriétés de protection contre la corrosion. Le meilleur revêtement candidat est ensuite sélectionné pour une caractérisation plus poussée en termes d'absorption d'eau et de propriétés barrière. L'étude est menée en utilisant des techniques électrochimiques, telles que le tracé des courbes courant-potentiel, la spectroscopie d'impédance électrochimique (SIE). Les données d'impédance du système revêtu obtenues par SIE sont interprétées en détail à l'aide d'une méthode graphique améliorée et par l'utilisation du modèle en loi de puissance qui permet d'obtenir des profils de résistivité dans l'épaisseur des revêtements. Ces résultats permettent une meilleure compréhension des différentes prises en eau lorsque le revêtement des HDL que lorsqu'il n'en contient pas.

Mots-clés : Inhibition de la corrosion, acier au carbone, revêtement époxy, hydroxydes doubles stratifiés (LDH), spectroscopie d'impédance électrochimique (SIE)..

Laboratoire (s) de recherche : **MATEIS UMR5510**

Directeur de thèse : **NORMAND Bernard**

Président de jury : **PEBERE Nadine**

Composition du jury :

MOL Arjan (Rapporteur)

ZHELUDKEVICH Mikhail (Rapporteur)

THERIAS Sandrine (Examinatrice)

MARCELIN Sabrina (Co-directrice de thèse)